DEVELOPMENT OF COOPERATIVE AND COORDINATED CONTROL FOR DISTRIBUTED GENERATION

JOSÉ ALBERTO CUNHA BARROS

DISSERTATION SUBMITTED ON THE EXTENT OF THE

MASTER OF SCIENCE COURSE IN ELECTRICAL AND COMPUTER ENGINEERING

SPECIALIZATION AREA OF POWER SYSTEMS

UNDER THE SUPERVISION OF:

PROFESSOR DOCTOR HÉLDER FILIPE DUARTE LEITE

(THE JURY PRESIDENT, **PROFESSOR DOCTOR ANTÓNIO MACHADO E MOURA**)

FACULTY OF ENGINEERING OF THE UNIVERSITY OF PORTO

DEPARTMENT OF ELECTRICAL AND COMPUTER ENGINEERING

RUA ROBERTO FRIAS, S/N, 4200-465 PORTO, PORTUGAL

MARCH 2008

“Para ser grande, sê inteiro: nada
Teu exagera ou exclui.
Sê todo em cada coisa. Põe quanto és
No mínimo que fazes.
Assim em cada lago a lua toda
Brilha, porque alta vive”.

Ricardo Reis

Abstract

The climate change has been causing severe effects in the global environment which will, in a near future, cause social and economical problems worldwide, if nothing is done to reduce its impacts. To limit the impacts of climate change, it was celebrated, at the end of 1997, the Kyoto Protocol, where quantified limits for the emission of greenhouse effect gases (such as CO_2) during the period 2008-2012 had been established. To reach the objectives proposed by the various governments who signed the Kyoto Protocol, one of the main areas to perform changes is the electric energy production.

Therefore, in terms of energy production, many governments are supporting its production from renewable sources, such as wind and biomass, with the objective of reducing the dependence of the fossil fuels, which are environmentally harmful. For a massive penetration of energy production from renewable sources in the next few years, it must be integrated in the distribution networks – the Distributed Generation (DG). However, this massive integration of distributed generation without planning may be an issue in the near future for the distribution system operators.

This work has the main objective of proposing a contribution for the planning of the distributed generation integration, in terms of active power. This contribution will be done by means of the adaption and cooperation of the DG's involved: wind and biomass energy plants. For simulations purposes in this extent, it will be used the transient electromagnetic program PSCAD/EMTDC®.

Resumo

As alterações climáticas têm vindo a causar efeitos severos no ambiente global e irão, num futuro próximo, causar problemas sociais e económicos à escala mundial, se nada for feito para reduzir o seu impacto. Com o objectivo de conter as alterações climáticas, foi celebrado, no final de 1997, o Protocolo de Quioto, onde foram estabelecidos limites quantificados para a emissão de gases com efeito de estufa (como o CO_2) durante o período 2008-2012. Com o fim de atingir os objectivos propostos pelos vários governos no âmbito to Protocolo de Quioto, uma das áreas principais onde deverão existir alterações é na produção de energia eléctrica.

Assim, em termos de produção de energia eléctrica, muitos governos têm apoiado a sua produção através de fontes renováveis, como o vento e a biomassa, com o objectivo de reduzir a dependência dos combustíveis fósseis, ambientalmente danosos. Para uma penetração massiva de produção de energia a partir de fontes renováveis, ela deverá ser integrada nas redes de distribuição – produção dispersa. No entanto, esta penetração massiva de produção dispersa sem planeamento associado poderá igualmente vir a ser um problema, num futuro próximo, para os operadores de distribuição.

Este trabalho tem o objectivo principal de propor uma contribuição para o planeamento da integração de produção dispersa, em termos de potência activa. Esta contribuição será efectuada por meio da adaptação e cooperação das centrais de produção dispersa envolvidas neste trabalho: central de produção eólica e central de produção de energia a partir de biomassa. Para efeitos de simulação neste trabalho será utilizado o programa de transitórios electromagnéticos PSCAD/EMTDC®.

Preface

The effects in global environment caused by the denominated climate change will, at short term, cause social and economical problems worldwide, if nothing is done to reduce its impact.

In terms of energy production, many governments around the world are supporting energy production from renewable sources, such as wind and biomass, with the objective of reducing the emission of greenhouse effect gases from this activity and, hence, decrease the effects of energy production in the climate change.

Since a great part of the integration of this renewable energy production will be done in the distribution networks, measures have to be taken to ensure its planned and coordinated control. Therefore, this work is intended to contribute for the planning of the distributed generation integration, in terms of active power.

The present work has the following objectives:

- Study both intermittent and non-intermittent renewable distributed generation (DG) technologies and integrate them in a typical grid-connected distribution network. In this work, the intermittent energy plant considered is the wind energy plant and the non-intermittent energy plant is the biomass energy plant;
- Develop algorithms in which the DG's considered adapt and cooperate to provide predictable active power output at the primary distribution substation;
- Determinate and quantify the advantages of obtaining a predictable active power output at the primary distribution substation.

Chapter Contents

Chapter 1 introduces the motivation behind this work. The climate change concern and how it increased the importance of distributed generation, namely renewable distributed generation, is discussed in this chapter. At last, are detailed some investigation works about the combination of renewable generation plants.

Chapter 2 overviews the wind energy production technology. The main types of aerogenerators are presented, with a closer focus on the conventional induction generator and the doubly-fed induction generator (DFIG), which will be used for simulation purposes in Chapters 5 and 6, respectively.

Chapter 3 details the steam turbine based-synchronous generation technology, which is the technology behind the biomass energy plant considered in this work for simulation purposes in Chapters 5 and 6.

Chapter 4 describes two meta-heuristic-based algorithms used to tune the rotor side converter's proportional-integral (PI) controllers of the doubly-fed induction generator introduced in Chapter 2. The two meta-heuristics used are: Particle Swarm Optimization and Evolutionary Particle Swarm Optimization. The obtained PI controller tunings will be used in the DFIG-based wind energy plant of Chapter 6.

Chapter 5 details an adaptive control of distributed generation to provide predictable active power output at the primary distribution substation. In this chapter is detailed an algorithm that, by acting only at the biomass energy plant, aims to predict the active power output from the aggregation of wind and biomass energy at the primary distribution substation of a typical distribution network.

Chapter 6 explains a cooperative control of distributed generation to provide predictable active power output at the primary distribution substation. This algorithm acts at a hierarchically superior level and both at the biomass and wind energy plants, with the objective of predicting the active power output at the primary distribution substation of a typical distribution network.

Chapter 7 presents the main conclusions of this work. In this chapter are as well suggested some future work on this area.

Acknowledgments

Many difficulties and drawbacks have emerged during the conception of this dissertation and, now that it is completed, I must recall everybody who helped me, in different ways, to overcome them.

I want, at first, to thank God as He was a major source of strength during the creation of this dissertation, in good and bad times.

Next, I would like to express my gratitude to my supervisor, Prof. Doctor Hélder Leite. His guidance, expertise, friendship and presence whenever I needed were essential for this work to get done successfully.

Very special thanks go to Prof. Doctor Maciel Barbosa, who was extremely kind with me when I required his help. I would also like to thank Prof. Doctor João Peças Lopes and Prof. Doctor Lobo Pereira for their advice and vast knowledge which allowed me to increase considerably the quality of this work.

Also an acknowledgement for all my family, for the support they provided me all my life and, in particular, during the writing of this dissertation. This acknowledgment is, above all, for my parents, for their example, and my brothers and sister, for their understanding.

I must also acknowledge my girlfriend, Joana, who encouraged me for all this time when I needed. In fact, her presence and love were fundamental for me to get this dissertation done. From the bottom of my heart, thank you very much indeed.

I don’t want to miss the opportunity to say thanks to all my friends, in particular to Emanuel, Gustavo, Pedro and Vasco for their support and for “being there” all the time.

At last, I want to thank Bruno, for its companionship, and José António, for all the help provided, and both for the good moments we spent during the writing of this dissertation.

Index

Table and Figure Index

Tables

Figures

Chapter 1 – Literature Review

1.1 – Introduction

This chapter presents the motivation behind this work. The climate change has been causing severe effects in the global environment which will, in a near future, cause social and economical problems worldwide, if nothing is done to reduce its impacts. In an effort to reduce the impacts of the climate change, many governments are taking measures to control the emission of greenhouse effect gases, such as CO_2.

In terms of electric energy production, many governments are supporting its production from renewable sources, such as wind and biomass, with the objective of reducing the dependence of the fossil fuels and therefore decrease the CO_2 emissions. For a massive penetration of energy production from renewable sources in the next few years, it must be integrated in the distribution networks. Therefore, this production is called distributed generation (DG). However, this massive integration of distributed generation without planning may be an issue in the near future for the distribution system operators.

This work has the main objective of proposing a contribution for the planning of the distributed generation integration, in terms of active power. This contribution will be done by means of the adaption and cooperation of the DG's involved: wind and biomass energy plants.

In a first part of this chapter, it will be introduced the main lines behind the denominated climate change. It will follow the introduction of the Distributed Generation concept and how it has been evolving over the years. Afterwards, it will be shown a first and global look over wind and biomass energy production technologies. Next, an overview of cooperative control of distributed generation will be presented. This chapter ends with some headlines about combined control of renewable energy sources in the specialized literature, with a closer focus on wind and biomass energy production.

1.2 – Climate Change

Climate change is, nowadays, the most serious environmental problem worldwide, with impact in the Present and Future Societies [PNAC, 2002]. The increased amount of greenhouse effect gases in the atmosphere has been causing the increase of Earth's temperature. The increase of Earth's temperature conduces to severe effects in the global environment. This problem was formally recognized, in a worldwide level, by the creation of the Intergovernmental Panel on Climate Change (IPCC) in 1988, with the signature of the Framework Convention on Climate Change in 1992, at the Earth Summit in Rio de Janeiro and, more recently, with the Kyoto Protocol in 1997 [*idem*].

Reports from the Intergovernmental Panel on Climate Change say that since 1861 the Earth's temperature rose significantly (approximately 0.6 ºC). During the twentieth century, according to the same source, the sea level rose, in mean values, from 10 to 20 cm. Furthermore, the 1990's (1990-1999) was the warmest decade since there is stored data (i.e., since 1861). The main implications of climate change worldwide, if no concrete actions would be made, may be [IPCC, 2001]:

• Changes in several physical (e.g., glacier retreat or reduction of the ice present in rivers, lakes and seas) and biological systems (e.g., population decrease of many animal and plant species, anticipation of reproduction or flowering of plants);

• Increase of the occurrence of extreme dry and wet seasons as well as other extreme weather conditions (intense precipitation, strong winds, etc);

• Increased risk of extinction of several species of animals and plants;

• Increased vulnerability of infrastructures, productive and leisure systems associated to human activities (agriculture, fishing, industry, services, etc.);

• Increased risk of social conflicts and migrations due to the consecutive occurrence of extreme weather conditions or degradation of water and soil resources;

Earth's mean temperature results from the equilibrium between the solar radiation flux which arrives to its surface and the infrared radiation flux sent to

the space. Solar energy, after passing the atmosphere, arrives to the Earth's surface mostly under the form of short wavelength radiation, warming the Earth's surface. Earth reflects part of this energy under the form of great wavelength radiation, or infrared radiation, which is absorbed by the water vapour, carbon dioxide and other greenhouse effect gases present in the atmosphere. These gases allow the occurrence of many processes responsible for the Earth's temperature rise. The emission of greenhouse effect gases resultant of the human activities increase the capacity of the atmosphere to absorb infrared radiation, altering the form the climate maintains the balance between the energy that arrives and the one that leaves the Earth.

The greenhouse effect gases, representing less than 1% of the gases present in the atmosphere (that is mainly composed by nitrogen and oxygen), control the energy flows in the atmosphere through the absorption of infrared radiation. The human activities affect this balance through the increased emissions of greenhouse effect gases and with the interferences in the natural removal of these gases (e.g.: through deforestation).

The first identified gases as responsible for the increase of the greenhouse effect, integrated in the Kyoto Protocol, are: the carbon dioxide (CO_2), the methane (CH_4) and the nitrous oxide (N_2O). More recently, other gases were considered to induce greenhouse effect (also included in this Protocol), the halogen compounds: HFC or hydrofluorocarbons, PFC or perfluorocarbons and SF_6 or sulphur hexafluoride. These halogen compounds have been contributing to the aggravation of the global warm. HFC and PFC were introduced to be alternative products to the responsible substances for the destruction of the ozone layer (CFC or chlorofluorocarbons), while SF6, the gas with more potential of global warming, is very used in the energy transmission and distribution systems.

TABLE 1.1

GREENHOUSE EFFECT GASES – INCREASE OF CONCENTRATIONS, CONTRIBUTION FOR GLOBAL WARMING AND MAIN EMISSION SOURCES [PNAC, 2002]

Greenhouse Effect Gases	Concentration increase since 1750 (%)	Contribution for global warming (%)	Main emission sources
CO2	31	60	Fossil fuels, deforestation and soil destruction
CH4	151	20	Energy production and consumption, agriculture activities, landfills and polluted water
N2O	17	6	Fertilizers, acid production, biomass and fossil fuel combustion
Halogen compounds (HFC, PFC e SF6)	-	14	Industry, refrigeration, energy transmission and distribution, propellants, spumes, solvents

Finally, the ozone (O_3), present in the stratosphere and in the troposphere, it is also considered an important greenhouse effect gas. However, its contribution for the greenhouse effect is, at the moment, difficult to evaluate on account of its space and time distribution variations [PNAC, 2002].

The estimates of CO_2 emissions, main contributor for the global warming, associated to the world consumption of fossil fuels, show the strong increase occurred in the last 100 years, mainly since the period after the Second World War. According to the Energy International Agency [EIA, 2001], the industrialized countries, with about 20% of the world population, contributed in 1999 to 51% of the total emissions of CO_2, being the electrical energy production one of the main factors for this contribution. On the other hand, the developing countries present, at the moment, values relatively low of emissions of CO_2, *per capita*. However, forecasts of strong increase in energy consumption at the developing countries appoint for an equally strong increase of greenhouse effect gases emissions during the twenty first century.

In this context, it was celebrated, at the end of 1997, the called Kyoto Protocol. Portugal, jointly with all of the state-members of the European Union, signed the Kyoto Protocol. In this extent, the state-members established an agreement of shared responsibility for the collective reduction of 8% of the greenhouse effect gases in the period 2008-2012, relatively to the emissions verified in 1990. With this agreement, Portugal committed to not increase more than 27% the greenhouse effect gas emissions verified in 1990, in the first period of execution of the Kyoto Protocol (2008-2012) [PNALE, 2006]. In parallel, some European community directives appeared with the objective of

forcing the state-members to limit the use of fossil fuels [European Parliament, 2001].

The energy production is responsible, in Portugal, for about 30% of the emissions of CO_2 for the atmosphere [PNALE, 2006]. Therefore, the Portuguese Government defined, on the extent of the Kyoto Protocol, the commitment of reaching a share of 39% of the total electricity consumption produced from renewable sources of energy, i.e., with reduced impact in global warming, until 2010. To fulfil the established goals, the following measures are being adopted [European Commission, 2006]:

- Implementation of fixed repurchase tariffs in kWh for photovoltaic solar energy production, waves energy production, small hydroelectric energy production, wind energy production, residual forest biomass energy production, urban residues energy production and biogas energy production;
- Adoption of procedures for public contests, in 2005 and 2006, for the construction of wind and biomass energy facilities;
- Possibility of obtaining investment subsidies up to 40% of the investment;
- Availability of fiscal reductions for investors;
- On the extent of the bio-fuels, total or partial exemption of circulation tax until a value established annually, and total exemption of ISP – tax on the petrol products.

Recently, the Portuguese Government revised, by its initiative and over the extent of the Kyoto Protocol, the goal of 39% of total electricity consumption produced from renewable sources of energy until 2010 for 45 % [Assembly of the Republic, 2007].

1.3 – Distributed Generation: Definition

Distributed Generation (DG) typically refers to the production connected to the distribution networks [cf. Ackerman et al. 2001; Dondi, 2002; Jenkins et al., 2000]. In this generation is included the named renewable energy production (wind, biomass, wave and photovoltaic solar energy production,

among others), combined cycle generation, cogeneration, micro-generation, fuel cells, among other production forms of smaller expression. However, neither a universally accepted definition for distributed generation nor what distinguishes it from the called centralized generation exists at the moment.

The International Conference of Electricity Distributors (CIRED), based on a questionnaire sent to some of their members of several countries, tried to harmonize the concept of distributed generation [CIRED, 1999].

The International Council on Large Electric Systems (CIGRE) has a working group in the field of the distributed generation. This working group defined as distributed generation all the generation with production capacity between 50 and 100 MW, typically connected to the distribution networks and that is not planned or dispatched in a centralized way [cf. in CIRED, 1999].

The Institute of Electrical and Electronics Engineers (IEEE) [cf. in Dondi et al., 2002] defined distributed generation as energy production through plants significantly smaller than the great generation plants, allowing the interconnection with the networks at any point of the power system.

Dondi and collaborators [2002] defined distributed generation as small energy production or storage plants (with typical production capacity from less than 1 kW to some dozens of MW), that are not part of a great generation plant and are located close to the loads. The inclusion, by these authors, of storage infrastructures is not very common in the definition of distributed generation.

Ackermann and collaborators [2001] defined distributed generation in terms of connection and location consonant to the energy production capacity, connected directly to the distribution networks. Other authors, as Pepermans and collaborators [2005], share the definition proposed by Ackermann and collaborators.

In summary, there are some points, accepted by the generality of the investigators, which characterize the concept of distributed generation [Jenkins et al., 2000]:

- Non-centralized planning and dispatch;
- Energy production capacity typically low (from 50 to 100 MW, according to the majority of the authors);
- Connection to the distribution networks.

The new challenges for the contemporary societies in what concerns to climate change, as well as subjects linked with new politics of economic and social development, putted the distributed generation in the spotlight. Thus, the core incentives for the increased penetration of distributed generation are [*idem*]:

- The reduction of the emission of greenhouse effect gases via the energy production (mainly CO_2);
- Growing difficulty in locating new high-capacity centralized energy production plants – planning problems, public opinion, etc;
- Small time of construction, low cost of initial investment and shorter amortization of investment periods, due to the present governmental financial incentives;
- Cultural subjects – political and cultural will to develop energy production technologies with lower rate of emissions of CO_2.

Therefore, the development of new distributed generation technologies, such as from renewable sources, is having a growing commercial attention.

1.4 – Wind Energy Technology: an Overview

1.4.1 – Motivation for its Development

Wind energy is the energy that comes from the wind, or in other words, from the air in movement. It is considered a renewable energy, because it is obtained through a natural source (the wind), capable of regenerating, and, therefore, virtually inexhaustible [ADENE / INETI, 2001]. Wind energy is also considered an intermittent energy source, given the relative difficulty of forecasting its power production, because of its unpredictable nature.

A vital incentive for the wind energy development in the seventies of the twentieth century was the rising of the petroleum prices and the concern as for its future shortage. At the moment, the major reason behind the use of the wind energy production technology to produce electrical energy consists in the need of the CO_2 emissions reduction and, thus, in the wind energy potential to limit

the effects of the climate change. In 1997, the European Commission, in the "White Book" on the Renewable Energy Resources, determined that in 2010, 12% of the electrical energy consumption in the European Union should come from renewable energy sources.

Wind energy was always considered essential part in the objectives of supplying energy from renewable sources, with an installed production capacity increase at World level from 2.5 GW in 1995 to 40 GW in 2010 (foreseen). In 2000, Germany had 45% of the European total production capacity of wind energy, followed by Denmark and Spain, with approximately 18% [Burton et al., 2001].

1.4.2 – Integration Problems

The progressive increase wind power integration in the networks has been leading to the emergence of wind farms with very high installed capacities per plant or per farm. It is important to emphasize this production type has been substituting conventional production systems forcing, necessarily, to alterations in the planning and operation procedures of the electric power systems [Fox et al., 2007; Djapic et al., 2007].

As a matter of fact, despite the penetration of wind power production and other forms of distributed generation can decentralize great amounts of energy that would be produced by great centralized generation units and what it means in technical-economical terms, there are concerns with the safety of the electric power systems. These concerns are connected with the uncertainty associated to the wind power production, due to the intermittence of the primary source, with the behaviour of these new production ways in the case of perturbation in the networks and with the possibility of supplying ancillary services [DTI, 2004].

1.5 – Biomass Energy Technology: An Overview

1.5.1 – Motivation for its Development

The production of energy from biomass (that from now on will be called simply as biomass energy) is also a form to produce renewable energy. The biomass burn provokes the carbon dioxide liberation in the atmosphere, but as this compound had been previously absorbed by the plants which gave it origin, the balance of CO_2 emissions is considered null. Biomass energy is a non-intermittent form of energy, i.e., predictable, of average production capacity.

Biomass energy can use a wide range of technologies and of fuel sources. The size of biomass energy plant is limited by the transport capacity and feedstock storage. It is not expectable the size of a biomass energy plant pass 30 to 50 MW [DTI, 2004]. The renewable resources represent presently about 20% of the total energy supply in the world, being about 14% of these coming of biomass [ADENE/INETI, 2001].

1.5.2 – Biomass Conversion Processes

Through the photosynthesis, plants capture energy from the sun and transform it in chemical energy. This energy can be converted in the following forms of energy: electricity, fuel or heat. The organic sources that are used to produce energy using this process are called biomass. Are also included in this classification the agriculture-cattle, agriculture-industrial and urban residues. Thus, these organic sources may be divided in three great groups:

a) Solid biomass;
b) Gaseous bio-fuels;
c) Liquid bio-fuels.

Solid biomass has as source the products and residues of the agriculture (including vegetable and animal substances), the residues from forest and

related industries, and the biodegradable part of the industrial and urban residues.

The gaseous bio-fuels (biogas) have origin in the agriculture-cattle residues, of the agriculture-industry and urban (mud of domestic residues treatment stations) residues and furthermore in the Urban Solid Residues landfills. Gaseous bio-fuels result of the anaerobic biological degradation of the organic matter contained in the residues previously referred and are constituted by a mixture of methane (CH_4) in percentages that vary between 50% and 70%, being the remaining essentially carbon dioxide (CO_2) [ADENE/INETI, 2001].

The liquid bio-fuels, with use potential, have all origin in the denominated "energy cultures":

- Bio-diesel (methyl ether): obtained mainly from canola oils or sunflower, by a process called chemical transetherification;
- Ethanol: it is the most common of the alcohols and it is characterized by being an organic compound, colourless, volatile, inflammable, and soluble in water, with characteristic smell and flavour. Produced from the fermentation of carbon hydrates (sugar, starch, and cellulose), with origin in cultures as the sugarcane or by synthetic processes;
- Methanol: the most common production processes are the natural gas synthesis and gasification through the wood.

Biomass energy uses the traditional technology of steam turbines connected to synchronous generators. In many cases, the biomass is used in cogeneration for jointed production of steam and electrical energy. In this case, the energy production depends on the steam demand.

1.6 – Cooperative Control of Distributed Generation: An Overview

Distributed generation (DG) can be operated to control voltages and power flows within the distribution networks. Improvements in distribution networks reliability and overall power system efficiency can be achieved by the integration of DG's. For load growth with brief peaks that occur during extreme

weather, DG's may provide lower-cost solutions than other approaches to system capacity upgrades [Short, 2004; Grigsby, 2007].

DG may provide resources for increasing the capacity of existing distribution facilities. When considering the increase of distribution networks capacity, DG's can be an alternative to new substation addition and replacing existing equipment with larger ones. A DG installed at the distribution level releases capacity throughout the system, from transmission through distribution. Transmission system losses are therefore eliminated, and distribution networks losses are reduced [Grigsby, 2007].

DG's across many circuits in distribution areas can be controlled from a single control point. That is, such DG's can be aggregated into a block of generation and made available for transmission system use. Figure 1.1 shows a generic configuration for the aggregation of DG's.

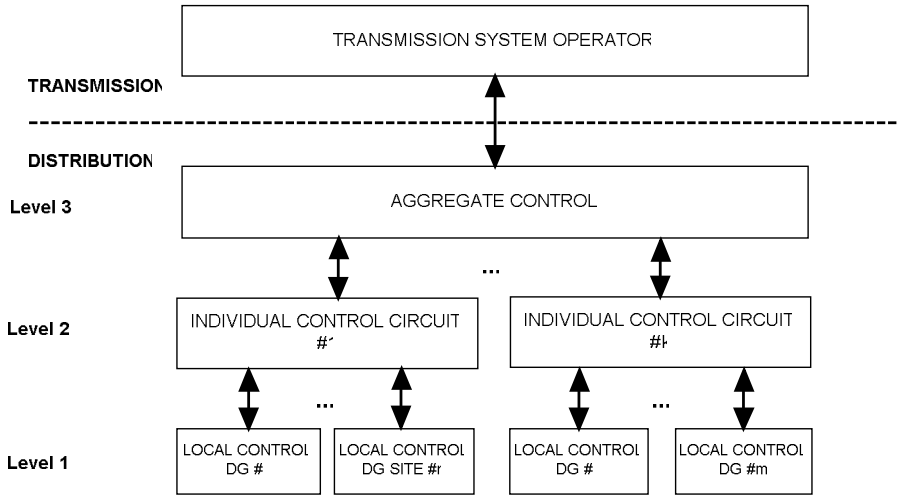

Figure 1.1 – Hierarchical View of the Control of Aggregated DG's [*idem*]

The aggregate control at level 3, shown in Figure 1.1, groups DG's together from many distribution circuits within a distribution service area. The aggregate control communicates to both a transmission system entity (the Transmission System Operator, in Figure 6.1) at a higher level and the circuit controls below at level 2. Each circuit at level 2 might have a number of DG sites from which the circuit can import power. Each DG site has a local controller (level 1) that can handle the local power/frequency balance processes. Essentially, the aggregate control, at level 3, evaluates the DG

power present at its lower levels and informs the Transmission System Operator about the DG power that can be made available for the transmission system use. After negotiations, the Transmission System Operator informs the aggregate control of the power they need. The aggregate control then communicates to the circuit controls, at level 2, in an attempt to provide the requested power in the best way possible.

In this work, namely in Chapter 6, only a conceptual part of the hierarchical control shown in Figure 1.1 will be developed and simulated. Actually, a cooperative control of DG's will be established with a two level hierarchy: the cooperative algorithm will be located at level 2 (at an individual control circuit) and the DG local site controls (of biomass and wind energy plants) will be at level 1.

1.7 – Combination of Renewable Energy Plants: Review

The massive integration of distributed generation without planning may be an issue in the near future for distribution system operators. This work has the main objective of proposing a contribution for the planning of the distributed generation integration, in terms of active power. This contribution will be done by means of the adaption and cooperation of the DG's involved: wind and biomass energy plants. Some contributions for combined systems of renewable energy plants over the last few years, in the specialized literature [Jurado & Saenz, 2002; Castronuovo & Peças Lopes, 2004; Billinton & Karki, 2001], are presented as follows.

Jurado and Saenz [2002] proposed the development of a controller for an autonomous combined production system of wind energy with thermal units (biomass energy plant). This controller was conceived using the recursive least square method and the algorithm of low variance control. The adaptive algorithm presented in this investigation allows the controller, according to the authors, to adjust automatically to alterations in the state variables and, consequently, to supply a uniform response of the combined system in a larger range of operation points.

The conception of systems combining wind energy production with conventional thermal production (known as Wind-Diesel Energy Systems, in the specialized literature) has been the base for several publications in the last years. Although those publications don't refer directly to the production of biomass energy, similarities exist among the conventional thermal production and the biomass energy production that make deserve its reference here. Therefore, some of those studies are described.

Uhlen and collaborators [1994] present a study where they implement multivariable techniques, in the frequency domain, for the conception and dynamic analysis of a controller for an autonomous system combining wind energy production and a thermal unit.

Bhatti and collaborators [1995] proposed a PI controller to be installed in a thermal unit for command signals generation that increase or decrease the gear ratio at the gearbox of the wind turbine, in response to frequency deviations in this last one. The results evidenced that, for an optimal transient response, the installed capacity of the wind energy plant should be similar to the one of the thermal unit.

Rajendiran and collaborators [2000] presented the analysis and simulation of a system combining wind energy production and a thermal unit, in steady-state, with several wind speeds. The wind energy production system is equipped, in this publication, with a doubly-fed induction aerogenerator.

Papathanassiou and Papadopoulos [2001] studied the dynamics of a small and autonomous system combining wind energy production and a thermal unit, using simplified models of the classic control theory. The authors' objective was to determinate the main factors which affect the combined system and to illustrate the roles of speed regulation in the thermal unit and pitch angle control in wind turbine on the system performance.

Kamwa [cf. in Chedid et al., 2002] presented the dynamic model and control of a system combining wind energy production and a thermal unit, through a PID controller-based programmable load leveller, installed in the thermal unit.

Chedid and collaborators [2002] proposed an adaptive controller based on fuzzy logic for a system combining wind energy production and a thermal unit. In this publication, the controller, which is present in the thermal unit, has

two meshes: the first one adjusts the fuel flow; the second adjusts the excitation voltage of the synchronous generator.

As well as in the case of combined systems of wind energy production with conventional thermal production, also exist several publications in the last years about combined systems of wind energy production with hydroelectric production (referred as Wind-Hydro Energy Systems, in the specialized literature). Afterwards, some of those publications are described.

Kaldellis and collaborators [2001] investigated the possibility of creating a combined system of wind energy production with hydroelectric production in an isolated island in the Aegean Sea, based on a technical-economical analysis. In this publication it is also shown a parametric analysis with the purpose of knowing the appropriate number of wind turbines and the optimal capacity of the reservoirs to implement.

Yanfang and collaborators [2001] also present the model, stability analysis and project of a combined system of wind energy production with hydroelectric production. In addiction, it is presented in this study an application to a particular case.

Castronuovo and Peças Lopes [2004] propose the use of water storage in hydroelectric reservoirs to improve the performance of wind farms and to smooth active power output fluctuations resultant from the wind intermittency. This paper presents an algorithm for optimizing, hourly, the strategy to be followed by the wind turbines and by the hydraulic pumping in order to reach an improvement of the active power profile to be delivered to the grid.

Hedman and Sheblé [2005] analysed, in a financial point of view, the hypothesis of using hydraulic pumping to smooth active power output of wind farms, decreasing, this way, the uncertainty associated to the wind power production.

Billinton and Karki [2001] evidenced an analysis of small isolated systems combining photovoltaic and wind technology, having in account considerations concerning its reliability.

Korpas and collaborators [2002] presented an algorithm based on dynamic programming for planning and operation of wind energy production systems, through the administration of energy storage. This energy storage can

be assured by several forms, from water storage in hydroelectric reservoirs to energy produced from fuel cells.

Jurado and Saenz [2003] presented an adaptive control between molten carbonate fuel cells and gas powered microturbines electrical energy production. They use this hybrid model with the objective of maximizing the efficiency of the gas powered microturbines, thus minimizing their greenhouse effect gases emissions, turning molten carbonate fuel cells more competitive.

Kinoshita and collaborators [2007] presented a cooperative control between a permanent magnet synchronous generator-based wind energy production plant and a hydrogen production plant, which is connected to wind energy power plant's terminals. The output power of the synchronous aerogenerator is smoothed by the AC-DC-AC cascade and delivered to the grid at the same time that a fraction of this power is used for the clean production of hydrogen, through an electrolyser, controlled by a DC-DC power electronic circuit.

1.8 – Summary

This chapter presented the motivation behind this work. Climate change brought up the importance of energy production forms less harmful for the global environment. In this extent, it is increasing the penetration of renewable energy plants in the distribution networks – the Distributed Generation. The problems behind the integration of Distributed Generation are a present concern, which will require the attention of distribution system operators in the years to come.

At the beginning of this chapter were introduced the main lines behind the denominated climate change. Afterwards, it was introduced the concept of Distributed Generation and how it has been evolving over the years. The following subsections presented a first and global look over the forms of renewable energy production used in this work: wind and biomass energy. Next, an overview of cooperative control of distributed generation was presented. At last, were shown some headlines about combined (adaptive and cooperative) control of renewable energy sources, with a closer focus on wind and biomass energy production plants.

Chapter 2 – Wind Energy Plants

List of Symbols and Suffices

Symbols		Suffices	
A	Area swept by the rotor	**a, b, c**	Rectangular coordinates
C_P	Power coefficient	**d**	Direct axis
D_a	Damping constant	**q**	Quadrature axis
GR	Gear ratio	**α**	Alfa axis
H	Inertia constant	**β**	Beta axis
i	Current	**el**	Electromagnetic
L	Inductance	**mec**	Mechanical
P	Active power / Power	**r**	Rotor
Q	Reactive power	**s**	Stator
R	Resistance	**m**	Magnetizing
T	Torque	**bl**	Blade
v	Voltage	**ref**	Reference
V	Wind speed		
β	Pitch angle		
λ	Tip speed ratio		
ρ	Air density		
ψ	Flux linkage		
ω	Angular frequency		
φ	Vector position		

2.1 – Introduction

In this chapter will be detailed the systems behind wind energy production: from a first approach, in which it will be presented the most important aerogenerator technologies and its generic constitution, to a more specific one where it will be explained the conventional induction generator and the doubly-fed induction generator. The reason behind this study is to obtain a wind energy plant equipped with conventional induction generator and other equipped with doubly-fed induction generator for simulation purposes in a test distribution network in Chapter 5 and Chapter 6, respectively.

In the first part of this chapter it will be shown the common constitution of the present time's wind energy production plants. Afterwards, it will be presented the nowadays' wind turbine model. After this, it will be specified the active power production control technologies associated to wind energy plants. Next, it will be shown the induction generator model, also known in this work as conventional induction generator, and the main aspects associated to the doubly-fed induction generator. At last, it will be detailed the control of a doubly-fed induction generator using the stator flux oriented vector control technique.

2.2 – How are Wind Energy Plants constituted?

The nowadays' wind energy conversion systems for electrical energy production purposes generally include the following essential components:

- Electric Generator;
- Wind turbine;
- Supervisory Control and Data Acquisition (SCADA) systems;
- Power transformer;
- Power converters, depending on the technology adopted;
- Communication facilities;

There are two main types of wind turbines, identified by its rotation axis orientation: horizontal axis turbines and vertical axis turbines. Horizontal axis turbines are the most used so they will be the adopted along this work for simulation purposes [Anderson & Bose, 1983]. The key elements behind a horizontal axis turbine-based wind energy conversion systems are [Vianna et al., 2000 a2]:

- Rotor (blades plus hub);
- Gear box;
- High-speed shaft;
- Low-speed shaft;
- Electric generator;
- Transmission system;
- Yaw drive and motor;
- Tower and nacelle;
- Sensors, control and communication facilities.

Currently, the wind energy conversion systems for electrical energy production purposes consist essentially of three main technologies [Almeida, 2006; Tande et al., 2004; Fox et al., 2007]:

a) Aerogenerator equipped with conventional Squirrel Cage Induction Generator;
b) Aerogenerator equipped with Permanent Magnet Synchronous Generator;
c) Aerogenerator equipped with Doubly Fed Induction Generator.

The aerogenerators equipped with conventional Squirrel Cage Induction Generators are simple and robust, representing a low investment cost, but they offer a reduced controllability. The aerogenerators of this type are constituted by an asynchronous generator directly coupled to the grid. Usually, the aerogenerator equipped with conventional Squirrel Cage Induction Generator operates in a narrow margin of angular speed (lightly above the synchronous angular speed $\omega_s = 2\pi.f_s$, where f_s is the synchronous system frequency), which is defined consonantly to the asynchronous generator's slip that, normally, varies between 1 and 2% in relation to the nominal operation slip (characteristic value supplied by the manufacturer of the generator). For this reason, they are denominated as fixed speed aerogenerators [Almeida, 2006]. Typically, these machines operate with an inductive power factor among 0.85 and 0.9. The individual power factor correction is usually accomplished through the use of capacitor banks with steps, being its service entrance / exit done in an automatic way. This individual compensation can be joined by some additional compensation per farm, in order to accomplish an overall capacitive power factor, as it happens at the moment in Portugal due to the present national tariff regulation. This national tariff regulation guarantees remuneration to reactive power supply by the wind farms in the peak load periods of the day [Castro, 2004]. In this work, the conventional Squirrel Cage Induction Generators will be used for simulations purposes in Chapter 5.

The aerogenerators equipped with Permanent Magnet Synchronous Generators are characterized by the synchronous generator's rotor excitation by permanent magnets, with operation in variable speed, in way to capture the maximum energy from the wind. The extracted maximum energy is then transferred to the electric power system through an AC-DC-AC cascade of electronic converters, which interconnect the aerogenerator's stator to the electric grid. The converter connected to the electric power system, besides regulating the electric system frequency at the output of the aerogenerator to the grid frequency, also allows the capacity of supplying reactive power [Almeida, 2006]. The aerogenerators equipped with Permanent Magnet Synchronous Generators will not be further detailed as they will not be used in this work.

In the case of the aerogenerators equipped with Doubly Fed Induction Generators, the electrical energy production control system imposes a mechanical torque control according to a predetermined curve of optimum torque. This control is not based on the grid frequency and the contribution of the machine for the inertia of the system is despised. In this technology, the AC-DC-AC cascade of converters is connected between the machine rotor and the grid. The converter connected to the grid operates at the grid frequency imposing, this way, the output frequency of the doubly-fed induction aerogenerator. In general, this converter is controlled to maintain the voltage of the DC bus constant. The control techniques associated to the doubly-fed induction generators conduct to an operation in a larger range of angular speed. Therefore, they are known as variable speed generators, allowing this way the extraction of more energy from the wind, besides offering the possibility of independent control of their active and reactive output powers [Almeida, 2006]. In this work, the doubly-fed induction generator will be used for simulations purposes in Chapter 6.

2.3 – Wind Turbine Modelling

The wind turbine is the component of the wind energy production system which allows the conversion of the kinetic energy of the wind in mechanical energy. This mechanical energy will become soon afterwards electrical energy, by the interaction with the generator that is coupled with the turbine. By other words, the wind turbine is the prime mover of the wind energy production system. Along this work, the horizontal axis wind turbine technology will be used.

The output mechanical power (P_{mec}) of a wind turbine is given by the Eq. (2.1):

$$P_{mec} = \frac{1}{2} \rho A C_P V^3 \text{ [W]} \qquad \text{Eq. (2.1)}$$

Where:

- ρ is the air density (kg/m^3);

- A is the area swept by the turbine rotor (m^2);
- C_P is the power coefficient;
- V is the wind speed (m/s).

The mechanical torque (T_{mec}) correspondent to the mechanical power given by the Eq. (2.1) is set by the Eq. (2.2):

$$T_{mec} = \frac{P_{mec}}{\omega_{mec}} \text{ [N.m]} \qquad \text{Eq. (2.2)}$$

Where:

- ω_{mec} is the angular mechanical speed of the induction generator (rad/s);

The air density is relatively low (800 times smaller than the water density, which serves as primary source to the hydroelectric production). Therefore, the wind turbine has to be a lot larger than a hydraulic turbine for the same power rating. Depending on the expected wind profile, a wind turbine of 1.5 MW should have a rotor diameter superior to 60 meters. Many of the modern wind turbines use the ascending force from its blades to guide the rotor. It is desirable a high blade angular speed, for reducing the gear ratio required by the wind turbine Eq. (2.3) [Burton et al., 2001].

$$\omega_{bl} = \frac{\omega_{mec}}{GR} \text{ [rad/s]} \qquad \text{Eq. (2.3)}$$

Where:

- ω_{bl} is the blade angular speed (rad/s);
- GR is the gear ratio required by the wind turbine.

The power coefficient C_P reflects the power fraction in the wind that can be truly converted by the turbine in mechanical power. It has a theoretical maximum value of 0.593 (Betz limit [Vianna et al., 2000 a2]) that probably will never be reached in practical terms Eq. (2.4) [Anderson & Bose, 1983].

$$C_P = \frac{1}{2} \times \left(\lambda - 0,022 \times \beta^2 - 5,6 \right) e^{-0,17 \times \lambda} \qquad \text{Eq. (2.4)}$$

Where:

- β is the pitch control angle, in degrees, which controls the output mechanical power of the turbine;
- λ is the tip speed ratio of the turbine.

It is common the aerogenerator's manufacturers characterize the performance of a certain wind turbine rotor by the $C_P \times \lambda$ curve, being λ given by Eq. (2.5):

$$\lambda = \frac{V}{\omega_{mec}} \text{ [m.s}^{-1}\text{/rad.s}^{-1}\text{]} \qquad \text{Eq. (2.5)}$$

Continuous improvements in the power coefficient are being sought in permanence by the industry, through small variations in the rotor format. Operating in variable speed mode, it is possible for the wind turbine rotor to maintain the maximum (optimal) power coefficient in an enlarged range of wind speeds. However, such improvements have a modest increment in the amount of delivered power. In order to obtain larger increments in the power produced, the increase of the area swept by the turbine blades (rotor diameter) and the location of wind turbines in places with larger wind speeds seem to be the right strategies. In the last 15 years, there has been a continuous growth of the rotor diameter dimensions, from 30 meters to more than 80 meters at the present time. This more than duplication of the rotor diameter led to the quadruplication of the output power of the turbines. The influence of the wind speed is more pronounced, given the cubic relationship between the wind speed and the produced mechanical power. In this way, wind speed duplication leads theoretically to eight times more mechanical output power produced by the wind turbine. This way, the widespread concern is to locate wind energy plants in areas of larger wind speeds and to dispose them optimally (due to subjects as the denominated stall effect [Burton et al., 2001]). In certain countries, there are being built very high towers (more than 80 meters) to take advantage of the wind speed growth with height.

Figure 2.1 shows the electric power in function of the angular speed of the aerogenerator for different wind speeds for a certain wind turbine. The

maximum point of the curves is the point from where it can be extracted the maximum power for a certain wind speed.

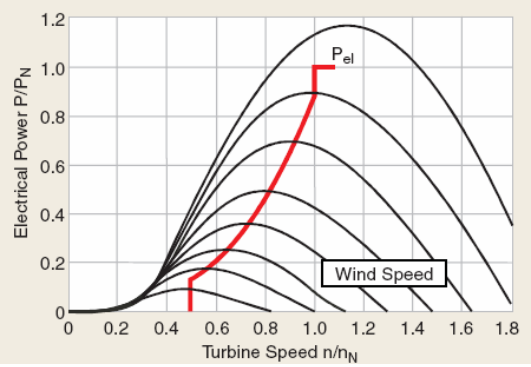

Figure 2.1 – Electric power in function of the angular speed of an aerogenerator; Different curves for different wind speeds [Muller, 2002]

If the machine is not working at the maximum point of the wind curve, it is assumed that is de-loaded.

Figure 2.2 presents the active power curve in function of wind speed, of the aerogenerator used along this work, Vestas V52 [Vestas, 2006].

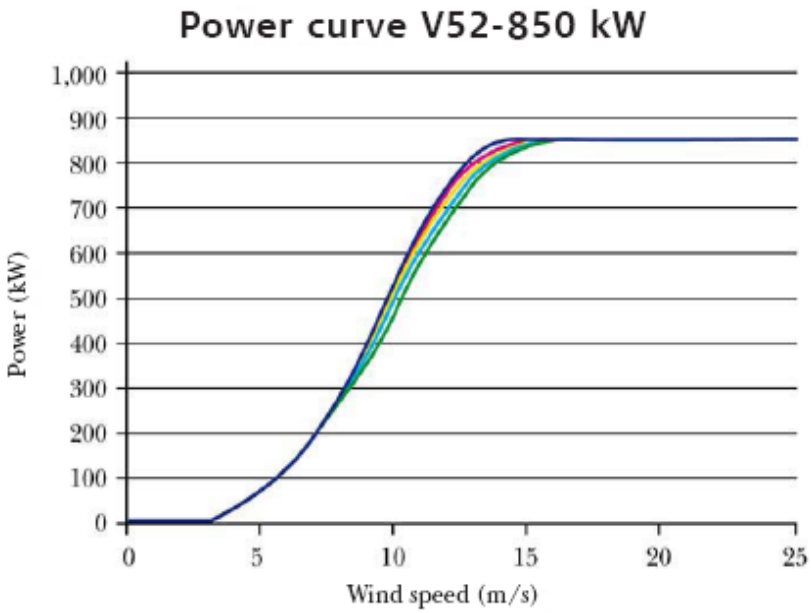

Figure 2.2 – Active power curve in function of wind speed of the aerogenerator Vestas V52 [Vestas, 2006]

2.4 – Power Production Control of Wind Energy Plants

Wind energy production systems have been, historically, based on the called fixed speed induction generators, with very little control on the dynamic performance (passive stall turbines). In the most recent years, significant progresses have been achieved on the development of active stall and pitch angle control technologies, not only for fixed speed but as well for variable speed wind turbines. This development is important not only in terms of turbine efficiency improvement, but as well as of control capabilities [DTI, 2004].

Summarizing, the production control strategies used by the wind energy production derive from aerodynamic strategies which explore [Anderson & Bose, 1983; Akhmatov, 2003]:

- The blade profiles of the wind turbines, through passive stall control, seek to protect the aerogenerator from extreme wind speeds. This control is typically applied to the conventional aerogenerators (squirrel cage) with installed power capacity inferior to 1MW;
- The orientation of turbine blades through active stall or pitch angle control to compensate speed variations of the rotor, as well as protecting the physical integrity of the wind energy production system during high wind speeds.

In this work, it will be used the pitch angle control shown in Figure 2.3 to limit wind energy production to the rated limits and, thus, protect the physical integrity of the wind energy production.

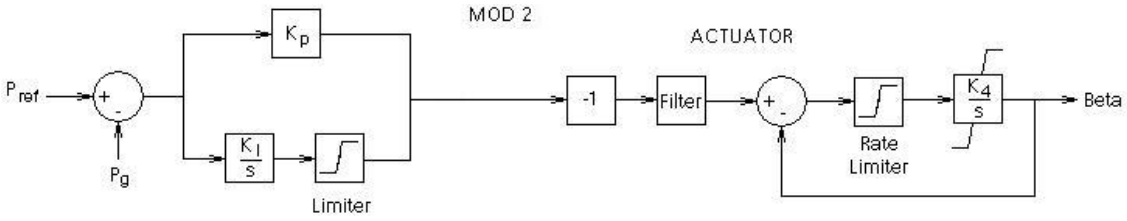

Figure 2.3 – Pitch angle control system [Anderson & Bose, 1983]

Based on the active power delivered (P_g) by the induction aerogenerator coupled to the wind turbine and on the reference active power (P_{ref}), the pitch angle control adjusts the angle β (Beta, in Figure 2.3) of the blades with the objective of maximizing the output mechanical power of the turbine. The control

quantities can be, instead of P_g and P_{ref} (electrical quantities), mechanical quantities (for instance, induction generator rotor angular speed) or a combination of electrical and mechanical values [Akhmatov, 2003].

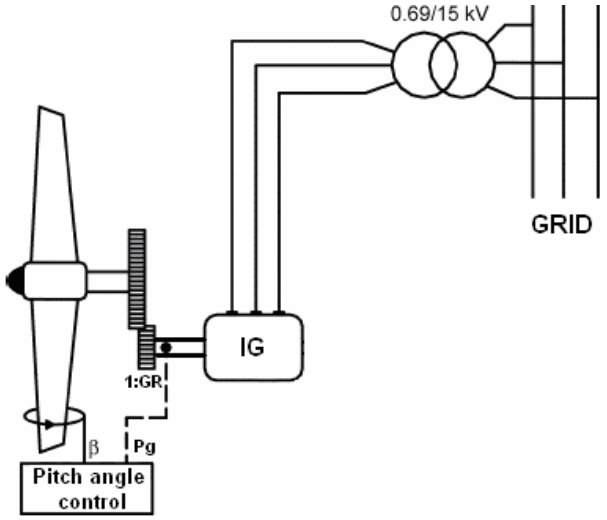

Figure 2.4 – General integration scheme of the pitch angle control in the wind energy production systems [adapted of Almeida, 2006]

In a global view, this control supplies proportional-integral (PI) control of the active power delivered by the electrical machine. The pitch angle control include, for this desiderate, a band-stop filter for reducing the oscillations of twice the rotational frequency, arising from wind shear phenomena, blade teetering and nacelle yaw [Anderson & Bose, 1983]. There is also a control mechanism which allows the activation/deactivation of the pitch angle control system for wind speeds out of the pre-established limits (lower and upper bound limits).

2.5 – Conventional Induction Generator Modelling

The induction machines, when working as generators, produce electric energy when its shaft rotates above the synchronous speed of the equivalent induction motor. This generators technology is mechanical and electrically simpler than any other existent type of generator. They are more rigid, not requiring brushes or switches. The induction generators in general are not

self-excited. Therefore, they need an external source to allow the establishment of their rotating magnetic field.

The induction generator rotor winding can be of squirrel cage type (squirrel cage induction generator) or wound type (wound rotor induction generator). The squirrel cage rotor winding is constituted by an aluminium cage, with the addiction of a small percentage of impurities, which is obtained by injection. The squirrel cage induction generator will be used in this work as the conventional induction generator. The electric circuit of a wound rotor induction generator contacts with the fixed part of the machine by a collecting ring system [Vaz Guedes, 1993].

Hence, the induction machine works as generator in the situations the angular speed of the rotor (ω_r) is superior to the angular speed of the rotating field (ω), in other words, for negative slips (s) (see the Eq. 2.6).

$$s = \frac{\omega - \omega_r}{\omega} \qquad \text{(Eq. 2.6)}$$

In generator operation, the machine works between the points corresponding to the null slip (approximately) and the point correspondent to the maximum admissible current value in the stator that, for the machine with the characteristic presented in Figure 2.5, is for a value of s approximately equal to -0.8 %.

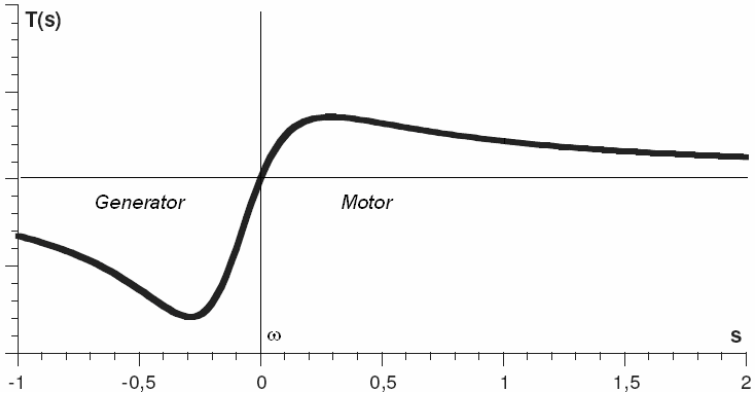

Figure 2.5 – Torque (T) – angular speed (ω) characteristic of the squirrel cage induction generator [Vaz Guedes, 1993]

This value of -0,8% is considerably inferior to that in which happens the maximum torque. Due to the very small variation allowed of the machine speed in relation to the synchronous speed, in practical terms, this machine behaves as a fixed speed machine [Jesus & Castro, 2004].

The 5th order induction machine model is here presented, based on the following conditions and assumptions:

- The stator current is assumed negative when flowing toward the network;
- The equations are derived in the synchronous reference frame using direct (*d*) and quadrature (*q*) axis representation;
- The *q*-axis is assumed to be 90º ahead of the *d*-axis in the direction of rotation;
- The DC component of the stator transient current is ignored, permitting representation of only fundamental frequency components.

Then, the per-unit 5th order induction machine model is presented as follows [Kundur, 1994; Ekanayake et al., 2003 a2; Nunes et al., 2004]:

$$\begin{cases} v_{ds} = -R_s i_{ds} - \omega_s \psi_{qs} + \dfrac{d\psi_{ds}}{dt} \\ v_{qs} = -R_s i_{qs} + \omega_s \psi_{ds} + \dfrac{d\psi_{qs}}{dt} \\ v_{dr} = 0 = R_r i_{dr} - (\omega_s - \omega_r)\psi_{qr} + \dfrac{d\psi_{dr}}{dt} \\ v_{qr} = 0 = R_r i_{qr} + (\omega_s - \omega_r)\psi_{dr} + \dfrac{d\psi_{qr}}{dt} \end{cases} \quad \text{[p.u.]} \qquad \text{Eq. (2.7)}$$

With

$$\begin{cases} \psi_{ds} = L_s i_{ds} + L_m i_{dr} \\ \psi_{qs} = L_s i_{qs} + L_m i_{qr} \\ \psi_{dr} = L_r i_{dr} + L_m i_{ds} \\ \psi_{qr} = L_r i_{qr} + L_m i_{qs} \end{cases} \quad \text{[p.u.]} \qquad \text{Eq. (2.8)}$$

Being *v* the terminal voltage of the machine, *R* is the resistance, *i* is the current, ω_s and ω_r are the stator (or supply's) and rotor electrical frequencies, ψ is the flux linkage, L_s, L_m and L_r correspond to stator, magnetizing and rotor

inductances. *ds*, *dr*, and *qs*, *qr* correspond to d-axis stator and rotor and q-axis stator and rotor indices, respectively.

The electromagnetic torque (T_{el}) equation associated is:

$$T_{el} = \psi_{qs} i_{ds} - \psi_{ds} i_{qs} \quad \text{[p.u.]} \qquad \text{Eq. (2.9)}$$

2.6 – Doubly-Fed Induction Generator

2.6.1 – A First Insight

Wind turbines equipped with doubly-fed induction generators (DFIG) use wound rotor induction generators. The associated control system enables the variable speed operation of the wind turbine, by decoupling the power system supply electrical frequency from the rotor mechanical frequency.

The doubly-fed induction machine allows power input/output into the rotor winding of a wound rotor induction machine and power output from the stator winding. Using such a machine as a generator, doubly-fed induction generator, it is possible to vary the machine power factor even when the machine speed is different from the synchronous speed [Almeida, 2006; Ramtharan et al., 2007]. DFIG machines can therefore operate without needing shunt compensation. Shunt compensation is commonly used in wind energy plants equipped with conventional induction generators for power factor correction purposes.

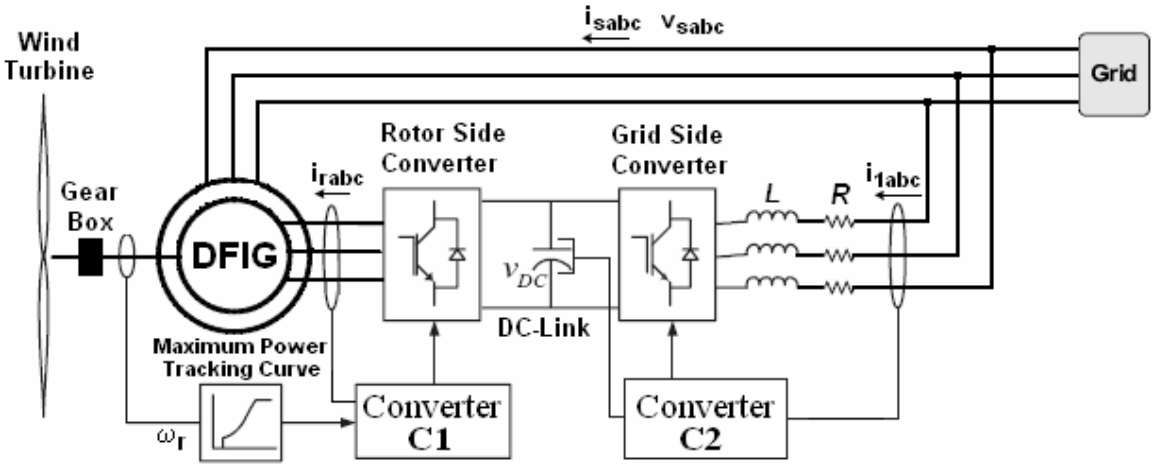

Figure 2.6 – Doubly-Fed Induction Generator Scheme

The stator of the wound rotor induction generator is directly connected to the grid while the rotor is fed through a variable frequency converter, as shown in Figure 2.6. In order to produce electrical power at constant voltage and frequency to the utility grid over a wide operation range from under to over the synchronous speed (i.e., 1 p.u.), the power flow between the rotor circuit and the grid must be controlled both in magnitude and direction [Akhmatov et al., 2000].

Therefore, the variable frequency converter consists of two four-quadrant IGBT (Insulated-Gate Bipolar Transistor) PWM (Pulse Width Modulation) converters connected back-to-back by a DC-link capacitor.

A crowbar can be used to short-circuit the rotor side converter in order to protect from overcurrents in the rotor circuit during grid faults. Here, the DFIG modelling will not consider the crowbar, as energy protection systems will not be considered.

The control of the variable frequency converter includes the rotor side converter controller – Converter C1 – and the grid side converter controller – Converter C2. The objective of the rotor side converter is to manage independently both the stator-side active and reactive powers [Tang & Xu, 1992; Pena et al., 1996]. The objective of the grid side converter is to keep the DC-link voltage constant regardless of the magnitude and direction of the rotor power [Svensson, 1998].

2.6.2 – Doubly-Fed Induction Generator Modelling

In this subsection, it will be developed the modelling of a DFIG. The DFIG model introduced in this subsection is a 5^{th} order model, as well it was established for the conventional induction generator model of subsection “Conventional Induction Generator Modelling”.

Then, the per-unit 5^{th} order machine model is presented as follows [Kundur, 1994; Ekanayake et al., 2003 a2; Nunes et al., 2004].

$$\begin{cases} v_{ds} = -R_s i_{ds} - \omega_s \psi_{qs} + \dfrac{d\psi_{ds}}{dt} \\ v_{qs} = -R_s i_{qs} + \omega_s \psi_{ds} + \dfrac{d\psi_{qs}}{dt} \\ v_{dr} = R_r i_{dr} - (\omega_s - \omega_r)\psi_{qr} + \dfrac{d\psi_{dr}}{dt} \\ v_{qr} = R_r i_{qr} + (\omega_s - \omega_r)\psi_{dr} + \dfrac{d\psi_{qr}}{dt} \end{cases} \quad \text{[p.u.]} \qquad \text{Eq. (2.10)}$$

With

$$\begin{cases} \psi_{ds} = L_s i_{ds} + L_m i_{dr} \\ \psi_{qs} = L_s i_{qs} + L_m i_{qr} \\ \psi_{dr} = L_r i_{dr} + L_m i_{ds} \\ \psi_{qr} = L_r i_{qr} + L_m i_{qs} \end{cases} \quad \text{[p.u.]} \qquad \text{Eq. (2.11)}$$

Being v the terminal voltage of the machine, R is the resistance, i is the current, ω_s and ω_r are the stator (or supply's) and rotor electrical frequencies, ψ is the flux linkage, L_s, L_m and L_r correspond to stator, magnetizing and rotor inductances. *ds*, *dr*, and *qs*, *qr* correspond to d-axis stator and rotor and q-axis stator and rotor indices, respectively.

It can be noticed the similarities between the Eq (2.10) and Eq (2.7). In fact, the only difference is the rotor is not short-circuited in the wound rotor induction generator [Eq. (2.10)], contrarily to the case of the squirrel cage induction generator (Eq. (2.7)). Thus, v_{dr} and v_{qr} are different of zero.

The described wound rotor induction generator is here controlled using a stator flux oriented vector-control scheme which assumes the rotor side converter is able to control the rotor currents (i_{ra}, i_{rb}, i_{rc}) to follow its reference values ($i_{ra,ref}$, $i_{rb,ref}$, $i_{rc,ref}$) at all times. Thus, it is assumed that $i_{dr} = i_{dr,ref}$ and $i_{qr} = i_{qr,ref}$. To be able to decouple the control of active and reactive power in the rotor, the DFIG is controlled in a synchronously rotating *d-q* axis frame, with the *d*-axis oriented along the stator flux vector position (φ_s). This means that the flux linkage with the stator in the q-axis corresponds to [Nunes et al., 2004]:

$$\psi_{qs} = L_s i_{qs} + L_m i_{qr} = 0 \qquad \text{[p.u.]} \qquad \text{Eq. (2.12)}$$

When the *d*-axis stator flux linkage is found, the *q*-axis stator current can be calculated as:

$$i_{qs} = -\frac{L_m}{L_s} i_{qr} \quad \text{[p.u.]} \qquad \text{Eq. (2.13)}$$

Then, to achieve decoupled active and reactive power control, are established two independent control loops in the rotor side converter: one for active power (by means of the machine rotor angular speed) and the other for reactive power.

Based on Eq. (2.10), considering the flux linkages with the stator and rotor given in Eq. (2.11), maintaining the previous reference frame and additionally taking into account the influence of the stator resistance (R_s) is small, the per-unit electromagnetic torque (T_{el}) can be expressed in decoupled form as a function of the q-rotor current component (i_{qr}) and terminal voltage (v) as:

$$T_{el} = -\frac{L_m v}{L_s + L_m} i_{qr} \qquad \text{[p.u.]} \qquad \text{Eq. (2.14)}$$

The electromagnetic torque control consists of the machine rotor speed control loop. The aim of the loop is to modify the electromagnetic torque of the machine according to speed variations. By acting upon Converter C1, see Figure 2.6, the speed control loop's purpose is to drive the system to the required operating point reference, set by the adopted control strategy. Here, the adopted control strategy to obtain the operating point reference is by setting a speed reference, based on the machine's maximum power tracking curve, which the system must follow. An example of such a maximum power tracking curve is illustrated in the Figure 2.7, by the ABCD curve superimposed to the mechanical power characteristics of a specific wind turbine, obtained at different wind speeds.

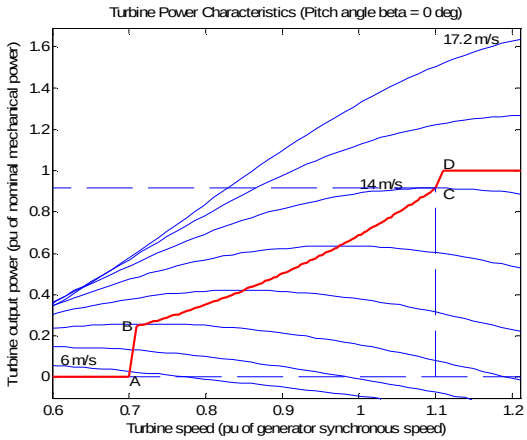

Figure 2.7 – Example of a Maximum Power Tracking Curve (ABCD) [based on Akhmatov, 2000]

The actual speed of the turbine (ω_r) is measured and the corresponding mechanical power of the maximum power tracking curve is used as the reference power for the power control loop. The maximum power tracking curve is defined by four points: A, B, C and D. From zero speed to speed of point A, the reference power is zero. Between point A and point B the maximum power tracking curve is a straight line, the speed of point B must be greater than the speed of point A. Between point B and point C the maximum power tracking curve is the locus of the maximum power of the turbine (maxima of the turbine power vs. turbine speed curves). The maximum power tracking curve is a straight line from point C and point D. The power at point D is one per unit (1 p.u.) and the speed of the point D must be greater than the speed of point C. Beyond point D, the reference power is a constant equal to 1 p.u. [Pena et al., 1996; Akhmatov et al., 2000].

The speed error, generated by the difference between the measured speed and the reference speed, then determines the q-reference rotor current ($i_{qr,ref}$) by means of a PI (Proportional-Integral) controller. The change in the rotor speed that results from the difference between electrical and mechanical torque can be calculated using the generator equation of motion, see the Eq. (2.15).

$$\frac{d\omega_r}{dt} = \frac{1}{2H}\left(T_{mec} - T_{el} - D_a\omega_r\right) \qquad \text{[p.u.]} \qquad \text{Eq. (2.15)}$$

Where H is the inertia constant of the machine in seconds, T_{mec} is the mechanical torque and D_a is the damping constant.

Considering the grid side converter operating at unity power factor, the reactive power at the stator of the DFIG (Q_s) varies with the stator currents as [Nunes et al., 2004]:

$$Q_s = v_{qs} i_{ds} - v_{ds} i_{qs} \qquad \text{[p.u.]} \qquad \text{Eq. (2.16)}$$

From Eq. (2.16) and considering the flux linkage with the stator d-axis ψ_{ds}, the following expression is obtained for the total grid side reactive power as a function of the d-axis rotor current (i_{dr}) and terminal voltage (v):

$$Q_s = -v\left(\frac{v + \omega_s L_m i_{dr}}{\omega_s (L_m + L_s)}\right) \qquad \text{[p.u.]} \qquad \text{Eq. (2.17)}$$

The reactive power control loop then compares the reactive power at the stator with a reference value (Q_{ref}), sending afterwards the deviation signal to a PI controller. The output signal of the PI controller is the d-axis reference rotor current ($i_{dr,ref}$).

The d-axis rotor current (i_{dr}) controls the reactive power. The stator magnetizing current and the flux linkage (ψ_{ds}) can be considered constant when the stator is connected to the grid and the influence of the stator resistance is small. When a change occurs in the d-axis rotor current (i_{dr}), the current at the stator d-axis (i_{ds}) will change. Because the flux linkage (ψ_{ds}) can be considered constant, the d-axis stator current (i_{ds}) is dependent on the rotor currents and the stator and magnetizing inductances L_s and L_m, as follows:

$$i_{ds} = \frac{\psi_{ds} - L_m i_{dr}}{L_s} \qquad \text{[p.u.]} \qquad \text{Eq. (2.18)}$$

The d- and q-axis rotor currents are finally transformed into three-phase reference currents ($i_{ra,ref}$, $i_{rb,ref}$, $i_{rc,ref}$) before being applied to the rotor side converter.

2.6.3 – Doubly-Fed Induction Generator Vector-Control Design

The vector-control approach, as used in this work, for a wind turbine equipped with a DFIG is explained as follows. The explanation is divided in two parts: “Rotor Side Converter and Controls” and “Grid Side Converter and Controls” [Tang & Xu, 1992; Pena et al., 1996; Svensson, 1998; Qiao et al., 2006].

2.6.3.1 – Rotor Side Converter and Controls

The wound rotor induction machine is controlled in a synchronously rotating *d-q* axis frame, with the *d*-axis oriented along the stator-flux vector position. In this way, a decoupled control between the electromagnetic torque and the rotor excitation current is obtained. The rotor-side current reference PWM converter provides the actuation driven by the control which requires the measurement of the stator and rotor currents, stator voltage and the rotor position. Subsequently, the stator active power (P_s) (and thus the machine rotor speed ω_r) and reactive power (Q_s) can be represented as functions of individual current components. Therefore, the reference values of the rotor d- and q- axis currents (i_{dr} and i_{qr}) can be determined directly from the stator reactive power (Q_s) and machine rotor speed (ω_r) commands. Since the stator is connected to the grid, and the influence of the stator resistance is small, the stator magnetising current can be considered constant [Pena et al., 1996].

The rotor currents *(*i_{ra}, $i_{rb,}$ i_{rc}) of the machine can be resolved into the direct and quadrature components i_{rd} and i_{rq}, respectively [Kundur, 1993]. The component i_{rd} produces a flux in the air gap which is aligned with the rotating flux vector linking the stator; the component i_{rq} produces flux at right angles to this vector. The torque in the machine is the vector cross product of these two vectors, and hence only the component i_{rq} contributes to the machine torque and, thus, to the delivered power. The component i_{rd} then controls the reactive power entering the machine. If i_{rd} and i_{rq} can be controlled precisely, then so can the stator side real and reactive powers.

The procedure used for ensuring that the correct values of i_{rd} and i_{rq} flow in the rotor is achieved by generating the corresponding phase currents references ($i_{ra,ref}$, $i_{rb,ref}$ and $i_{rc,ref}$), and then using a suitable voltage sourced converter based current source to force these currents into the rotor. The crucial step is to obtain the instantaneous position of the rotating flux vector in space in order to obtain the rotating reference frame. By the Lenz's law of electromagnetism, the stator voltage (after subtracting the rotor resistive drop) is simply the derivative of the stator flux linkage ψ_{sa}, as in the Eq. (2.19) which is written for phase the *a*.

$$v_{sa} - R_s i_{sa} = \frac{d\psi_{sa}}{dt} \quad [V] \qquad \text{Eq. (2.19)}$$

Where v_{sa}, i_{sa} and R_s are, respectively, the stator voltage (in V) and current (in A) on phase *a* and the stator resistance of the machine (in Ω).

The control structure shown in Figure 2.8 can, thus, be used to determine the present location of the rotating stator flux vector (φ_s).

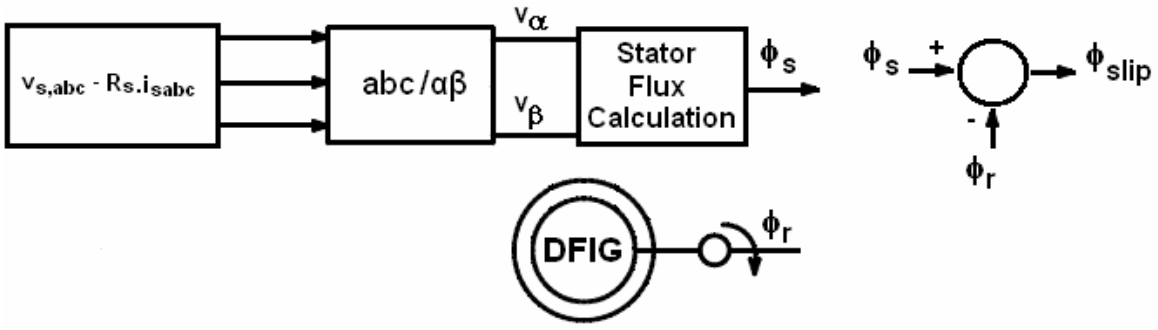

Figure 2.8 – Determination of Rotating Stator Flux Vector Location

In Figure 2.8, the three phase stator voltages (after removal of resistive voltage drop) are converted into the Clarke (α and β) components v_α and v_β, which are orthogonal in the balanced steady state [Pena et al., 1996]. This transformation is given by the Eq. (2.20):

$$\begin{bmatrix} v_\alpha \\ v_\beta \end{bmatrix} = \frac{2}{3} \cdot \begin{bmatrix} 1 & -1/2 & -1/2 \\ 0 & \sqrt{3}/2 & -\sqrt{3}/2 \end{bmatrix} \begin{bmatrix} v_a \\ v_b \\ v_c \end{bmatrix} \quad [V] \qquad \text{Eq. (2.20)}$$

Further information on these transforms can be obtained in Appendix D. Integrating v_α and v_β, we obtain $\psi_{s\alpha}$ and $\psi_{s\beta}$, the Clarke components of stator flux. This process is illustrated in Figure 2.8 in block "Stator Flux Calculation". Converting to polar form:

$$|\psi| = \sqrt{\psi_{s\alpha}^2 + \psi_{s\beta}^2}\ [Wb.turns], \qquad \phi_s = a\tan\left(\frac{\psi_{s\beta}}{\psi_{s\alpha}}\right)[rad] \qquad \text{Eq. (2.21)}$$

The angle φ_s gives the instantaneous location of the stator rotating magnetic field. In practical control circuits, as in Figure 2.8, filtering is required in order to rid the quantities $\psi_{s\alpha}$ and $\psi_{s\beta}$ of any residual DC component introduced in the integration process.

The machine rotor itself is rotating and is instantaneously located at the angle φ_r, the rotor angle, as shown on Figure 2.8 [Anaya-Lara et al., 2006]. Thus, with a reference frame attached to the rotor, the stator's magnetic field vector is at the instantaneous location (φ_s-φ_r), which we will refer from now on as slip angle, φ_{slip}.

With φ_{slip}, the instantaneous values for the desired rotor currents can then be calculated using the inverse *d-q* transformation, as shown in Figure 2.9.

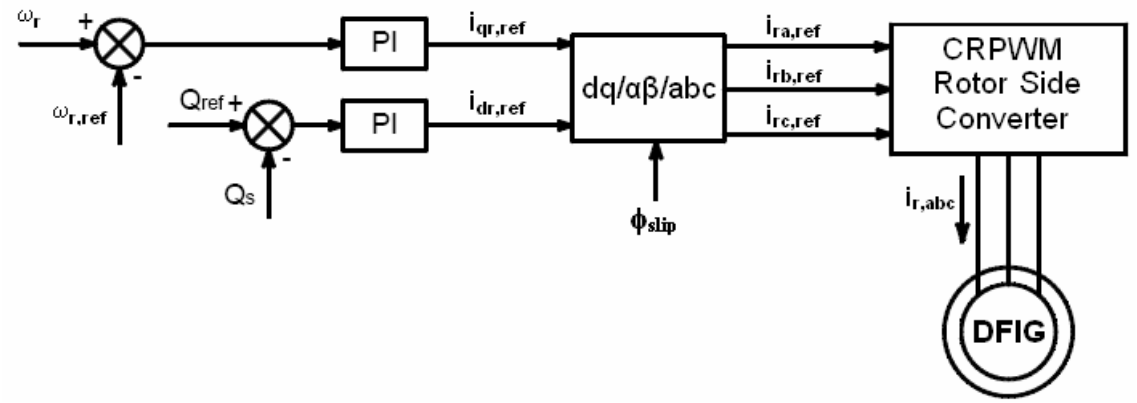

Figure 2.9 – Generation of Rotor Phase Reference Currents $i_{ra,ref}$, $i_{rb,ref}$, $i_{rc,ref}$

Once the reference currents ($i_{ra,ref}$, $i_{rb,ref}$, $i_{rc,ref}$) are determined, they can be generated using a voltage sourced converter operated with a current reference pulse width modulation (CRPWM) converter. The CRPWM converter allows for

the generation of any arbitrary current waveform in an R-L load. An upper and lower tolerance band is placed around the desired reference waveform for the actual current. The difference between the desired and actual currents is kept to within the tolerance band. By making the threshold smaller, the desired current can be approximated to any degree necessary. However, there is a limit to which this can be done, because the smaller the threshold, the smaller the switching periods, i.e., the higher the switching frequency and losses. So, this approach suffers from the drawback that the switching frequency is not predictable and can be very high, making the circuit less attractive for large ratings [Mohan et al., 2002].

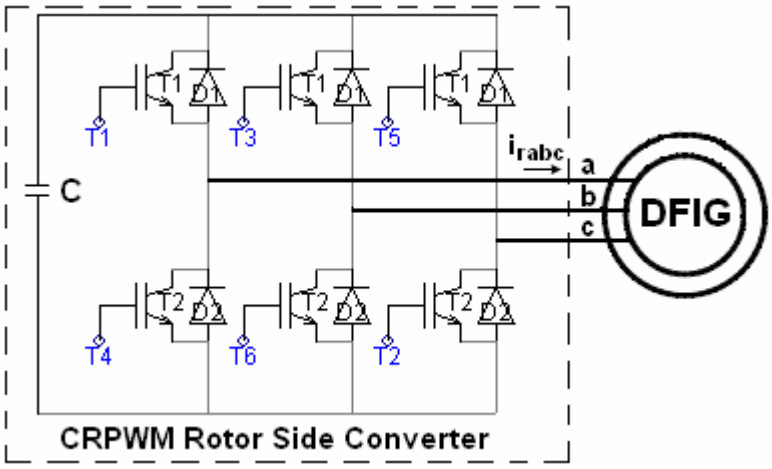

Figure 2.10 – CRPWM Rotor Side Converter

2.6.3.2 – Grid Side Converter and Controls

The objective of the grid side converter is to keep the DC-link voltage constant, regardless of the magnitude and direction of the rotor power. A vector-control approach is used in this work, with a reference frame oriented along the stator voltage vector position, enabling independent control of the active and reactive power flowing between the grid and the grid side converter. [Svensson et al., 1998, Qiao et al., 2006]

The grid side converter is operated so as to keep the DC voltage on the capacitor at a constant value. In effect, this means that the grid side converter is supplying the active power demands of the rotor side converter. The DC-link voltage is usually generated using another voltage sourced converter connected

to the AC grid at the generator stator terminals. A DC capacitor is used in order to remove ripple and keep the DC bus voltage smooth, see Figure 2.10.

The grid side controller is a feedback controller in which the error between the desired and measured currents is passed through a PI controller, which controls the output voltage of a conventional Sinusoidal PWM Controller (SPWM). The advantage of the SPWM controller versus the CRPWM controller is that the number of switchings in a cycle is fixed, so losses can be easily estimated.

On the grid side controller, the d-axis stator current is controlled by the d-component of the SPWM output waveform and the q-axis stator current via the q-component. However, this leads to a poor control system response, because attempting to change the *d*-axis stator current (i_{sd}) also causes the *q*-axis stator current (i_{sq}) to change transiently. Hence, modifications are made to the basic PI controller structure so that a decoupled response is possible, and a request to change i_{sd} changes i_{sd} and not i_{sq} and vice-versa. In a voltage sourced converter with constant DC bus voltage, connected to an AC grid through a coupling inductance *L* and resistance *R*, it can be shown that [Pena et al., 1996]:

$$\frac{d}{dt}\begin{bmatrix} i_{sd} \\ i_{sq} \end{bmatrix} = \begin{bmatrix} -\frac{R}{L} & \omega_s \\ -\omega_s & -\frac{R}{L} \end{bmatrix}\begin{bmatrix} i_{sd} \\ i_{sq} \end{bmatrix} + \frac{1}{L}\begin{bmatrix} v_{sd} - v_{sdref} \\ -v_{sqref} \end{bmatrix} = \begin{bmatrix} -\frac{R}{L} & 0 \\ 0 & -\frac{R}{L} \end{bmatrix}\begin{bmatrix} \frac{v_{sd} - v_{sdref}}{L} + \omega_s i_d \\ -\frac{v_{sqref}}{L} - \omega_s i_q \end{bmatrix} \quad \text{Eq. (2.22)}$$

Where v_{sd} is the d-axis stator voltage (in V), derived from V_{sa}, V_{sb} and V_{sc}. v_{sdref} and v_{sqref} are the d-axis and q-axis components of the reference voltages for the SPWM controller (in V), respectively. ω_s is the supply's angular frequency (in rad/s).

Assuming v_{sd} as the stator voltage (and thus, of the AC grid), the q-axis component of the stator voltage, v_{sq}, is by definition zero. The reference frame is rotating at ω_s, which is the supply's angular frequency. Then, resulting from the decoupled equations, the active and reactive power will be proportional to i_{sd} and i_{sq}, respectively.

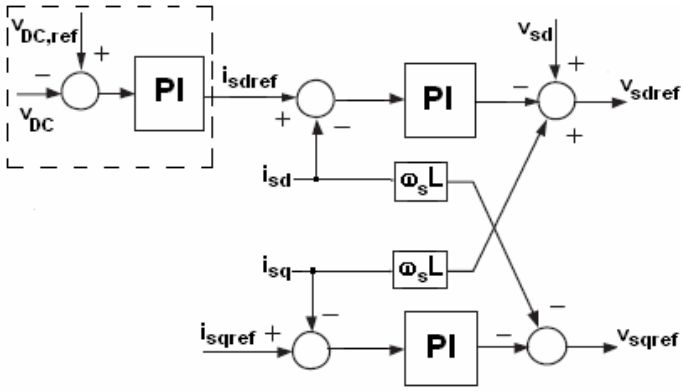

Figure 2.11 – Decoupled Grid Side Converter Controller

The selection of the d-axis stator current reference (i_{sdref}) for the grid side converter is through the dashed control circuit shown in Figure 2.11, which attempts to keep the capacitor voltage at its rated value by adjusting the amount of real power that flows through the DC-link.

The detection of the AC grid voltage reference angle ($\varphi_{s'}$) is shown on Figure 2.12.

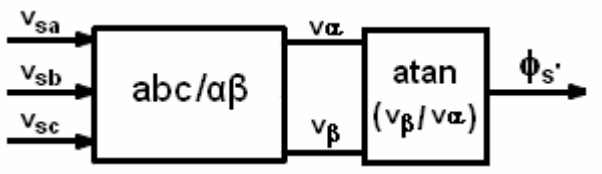

Figure 2.12 – Detection of the AC grid voltage reference angle $\varphi_{s'}$

The generation of the actual d-axis stator current (i_{sd}) and the q-axis stator current (i_{sq}), as required in Figure 2.11, is done using a *d-q* transformation, as show in Figure 2.13.

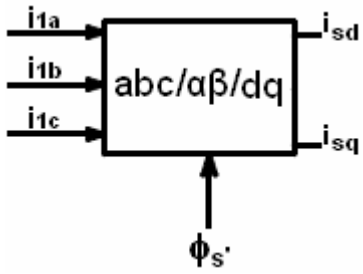

Figure 2.13 – Generation of i_{sd} and i_{sq} currents

Being these reference voltages v_{sdref} and v_{sqref} applied at the grid side converter, the desired stator currents i_{sdref} and i_{sqref} will flow in the circuit. The control block shown in Figure 2.14 converts the above references v_{sdref} and v_{sqref} to the reference three phase voltages v_{aref}, v_{bref} and v_{cref}, generated by an inverse Clarke transformation. The remaining parts of the controls are standard PWM controls, in which each of the phase voltages v_{aref}, v_{bref} and v_{cref} is compared with a high frequency triangle wave to determine the firing pulse patterns [Mohan et al., 2002].

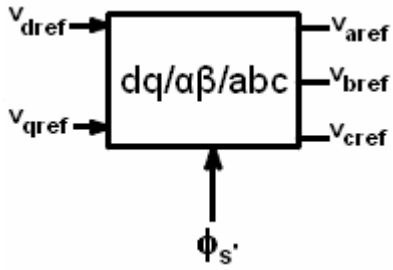

Figure 2.14 – Phase Reference Voltages Generation Block

2.7 – Summary

In this chapter were presented the key aspects of wind energy production systems. From a global overview of wind energy production systems to more specific approaches, specifically in terms of conventional and doubly-fed induction aerogenerators, were detailed the main characteristics of wind energy production systems. The wind energy plants equipped with conventional induction generators and with doubly-fed induction generators were specifically detailed as they will be used for simulation purposes on a test distribution network in Chapter 5 and Chapter 6, respectively.

At first, it was presented the common constitution of the present time's wind energy production plants. Afterwards, the wind turbine model and its power production control technologies were detailed. Next, it was shown the induction generator 5^{th} order model, also known in this work as conventional induction generator. Subsequently, it were referred the main aspects associated to the doubly-fed induction generator. After that, it was presented the 5^{th} order model of the doubly-fed induction generator and, at last, it was detailed the control of a doubly-fed induction generator using the stator flux oriented vector control technique.

Chapter 3 – Biomass Energy Plants

List of Symbols and Suffices

Symbols		Suffices	
D_a	Damping constant	‘	Transient
H	Inertia constant	‘’	Subtransient
i	Current	0	Open-circuit
K	Gain	a, b, c	Rectangular coordinates
L	Inductance	aux	Auxiliary
m	Steam mass flowrate	d	Direct axis
P	Power	el	Electromagnetic
R	Resistance, feedback gain	ex	Exciter
S	Saturation	exf	Exciter field
T	Torque, time constant	f	field
t	Time constant	g	Generator
V	Volume	m	Magnetizing
v, E	Voltage	max	Maximum
X	Reactance	mec	Mechanical
Z	Impedance	q	Quadrature axis
θ	Angular position	r	Rotor
ρ	Speed-droop coefficient	ref, R	Reference
ω	Angular frequency	s	Stator

3.1 – Introduction

In this chapter, it will be detailed the technology behind biomass energy production. As the biomass energy production that will be used in this work is based on the steam turbine-based synchronous generation technology, it will be here described the key aspects of this technology. From a first approach, where an overview of synchronous generation systems will be presented, to a more specific one, where it will be explained individually the core components of these systems, it will be portrayed the most important matters about steam turbine-based synchronous generation technology. So, the reason behind this study is to obtain a biomass energy plant for simulation purposes in a test distribution network in Chapter 5 and Chapter 6

At first, it will be shown a first global view of the steam turbine-based synchronous generation plants, in which are based biomass energy plants. Next, it will be presented the 5^{th} order model of the synchronous generator. Subsequently, it will be detailed the steam turbine technology. At last, are presented the speed and voltage regulation systems of the steam turbine-based synchronous generation plants.

3.2 – How are Biomass Energy Plants constituted?

A simplified typical synchronous generation system is shown on Figure 3.1. Electrical energy is produced by a synchronous generator driven by a prime mover, in this case a steam turbine. The steam turbine is equipped with a governor which either controls the speed and, consequently, the power output according to a preset power-frequency characteristic. The generator power is fed into the network via a step-up transformer. The DC excitation (or field) current, required to produce the magnetic field inside the generator, is provided by the exciter. The excitation current, and consequently the generator's terminal voltage is controlled by an Automatic Voltage Regulator (AVR) [Saccomanno, 2003].

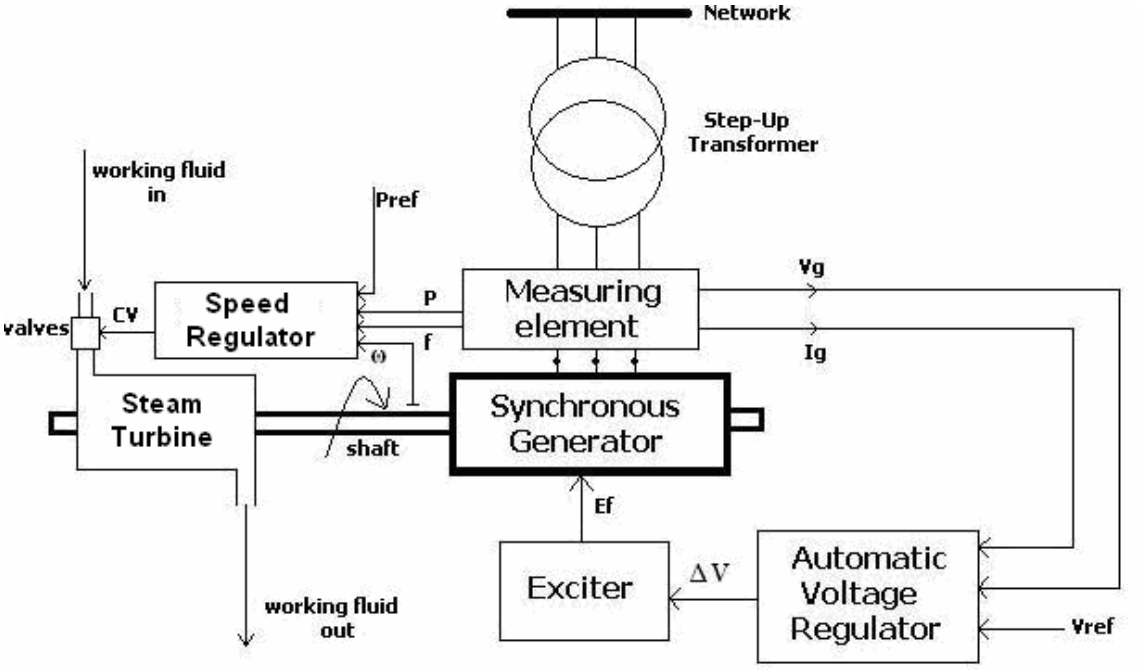

Figure 3.1 – Block diagram of a synchronous generation system (adapted from [Saccomanno, 2003])

The main components of the block diagram shown on Figure 3.1, that is, Synchronous Generator, Exciter, AVR, Steam Turbine and Speed Regulator, will be described as it follows.

3.3 – Synchronous Generator Modelling

The synchronous generator is a rotating electrical machine which promotes a high-efficiency transform of mechanical energy into electrical energy. These machines are very large, in general, with high nominal electrical power and inertia constants. The performance of synchronous machines is crucial in how the whole power system reacts when a disturbance occurs [Vaz Guedes, 1996; Laughton & Warne, 2002].

In Figure 3.2, it is shown the schematic representation of a two-pole synchronous generator, both in phase coordinates – *a, b, c, f* – and in Park coordinates – *d-q* [Kundur, 1994]. After the application of the Park's transformation, the electrical phase quantities are modelled on a two-phase rotating referential, synchronized with the rotor. This referential contains a pole-aligned axis – the direct-axis *d* – and an orthogonal axis in reference to the direct-axis – the quadrature-axis *q*.

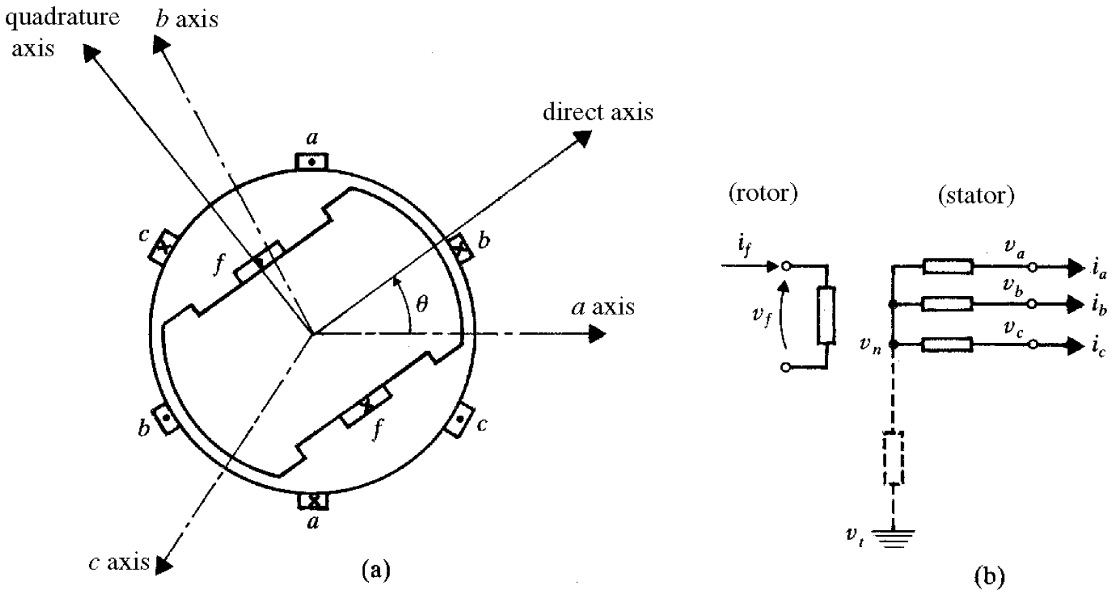

Figure 3.2 – Schematic representation of a bipolar synchronous generator with three-phase stator circuits (indices a, b, c) and one field rotor circuit (index f) [Saccomanno, 2003]

The following per unit (p.u.) 5th order mathematical model of the synchronous machine for transient stability studies is presented with the following basic assumptions [Elgerd, 1982; Machowski, 1997]:

- The stator current is assumed negative when flowing toward the network;

- The equations are derived in the synchronous reference frame using direct (*d*) and quadrature (*q*) axis representation – Park transformation [Kundur, 1994];
- The q-axis is assumed to be 90º ahead of the d-axis in the direction of rotation;
- There are no rotor circuits other than the field circuit (i.e., additional rotor circuits are not considered);
- There is no magnetic saturation;
- Stator transients are neglected due to being much faster than the rotor ones;
- The shaft is a rigid connection, without any torsional phenomena.

Other simplifying assumptions, considered of minor significance, may relate to, for example, the conductor distribution and the rotor profile – salient pole/wound rotor, as well as effects relatively negligible, such as the effects of the slots, winding radial sizes, magnetic hysteresis, and so on.

Then, the 5th order synchronous generator model is presented as follows [*idem*]:

$$\begin{cases} v_{ds} = -E_d^{''} - R_s i_{ds} + X_q^{''} i_{qs} \\ v_{qs} = -E_q^{''} - R_s i_{qs} + X_d^{''} i_{ds} \end{cases} \quad \text{[p.u.]} \qquad \text{Eq. (3.1)}$$

Being *v* the terminal voltage of the machine, *R* the resistance, *i* is the current, *E''* the subtransient voltage-behind-reactance and *X''* the subtransient reactance. *d* and *q* correspond to d-axis and q-axis indices, *ds* and *qs* are d-axis and q-axis stator indices, respectively, and *s* corresponds to stator.

Transient and subtransient phenomena in the rotor are represented by the following differential equations:

$$\begin{cases} \dfrac{dE_d^{''}}{dt} = -\dfrac{1}{t_{q0}^{''}}\left[E_d^{''} + i_{qs}(X_q^{'} - X_q^{''})\right] \\ \dfrac{dE_q^{''}}{dt} = -\dfrac{1}{t_{d0}^{''}}\left[E_q^{''} - E_q^{'} - i_{ds}(X_d^{'} - X_d^{''})\right] \\ \dfrac{dE_q^{'}}{dt} = -\dfrac{1}{t_{d0}^{'}}\left[E_q^{'} - E_f - i_{ds}(X_d - X_d^{'})\right] \end{cases} \quad \text{[p.u./s]} \qquad \text{Eq. (3.2)}$$

Where *E'* is the transient voltage-behind-reactance, *t''* and *t'* are the subtransient and transient time constants, respectively, *X'* is the transient reactance and E_f is the field voltage. The subscripts *d0* and *q0* refers to open-circuit in *d*- and *q*-axis circuits.

The synchronous generator equation of motion is given by the Eq. (3.3):

$$\frac{d\omega_r}{dt} = \frac{1}{2H}(T_{mec} - T_{el} - D_a\Delta_\omega) \qquad \text{[p.u./s]} \qquad \text{Eq. (3.3)}$$

Where ω is the angular speed of the generator, *H* is the inertia constant, *T* is the torque, D_a is the damping constant. *el* refers to electromagnetic, *mec* to mechanical and *r* to rotor.

The angular position of the rotor is given by the Eq. (3.4):

$$\frac{d\theta_r}{dt} = \omega_r - \omega_0 \qquad \text{[rad]} \qquad \text{Eq. (3.4)}$$

Where θ is the rotor angular position and ω_0 is the synchronous angular speed (1 p.u.).

The electromagnetic torque, T_{el}, is given by the Eq. (3.5):

$$T_{el} = E_q^{''} i_{qs} + E_d^{''} i_{ds} + (X_d^{''} - X_q^{''}) i_{ds} i_{qs} \quad \text{[p.u.]} \qquad \text{Eq. (3.5)}$$

3.4 – Steam Turbine Modelling

In power systems, synchronous generators are normally driven by steam, gas or hydraulic turbines. Each turbine is equipped with a governing system to

provide means by which the turbine can be started, run-up to operating speed and operated on load with the required power output [Machowski et al., 1997; Prime Mover, 1991; Laughton & Warne, 2002].

In coal-burn, oil-burn and nuclear power plants, the energy contained in the fuel is used to produce high pressure, high temperature steam in a boiler. The energy in steam is then converted to mechanical energy in axial flow steam turbines. Each turbine consists of a number of stationary and rotating blades concentrated into groups, or stages. Typically, a complete steam turbine is divided into three or more stages, with each turbine stage being connected on a common shaft. Dividing the turbine into stages allows the steam to be reheated between stages to increase its enthalpy and consequentially increase the overall efficiency of the steam cycle. Modern coal-fired steam turbines have thermal efficiency reaching 45% [Machowski et al., 1997].

Steam turbines can be classified as either non-reheat, single reheat or double reheat systems. In the case of the non-reheat turbines, the container introduces a time delay into the system as changes in the steam flow at the input take a finite time to appear in the output. This time delay can be quantified by considering a steam container of volume *V* as shown on Figure 3.3.

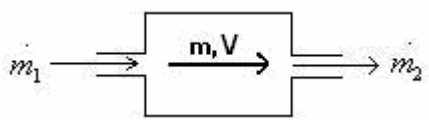

Figure 3.3 – Model of the steam flow through a steam container of capacity V [Machowski et al., 1997]

The non-reheat steam turbine model given by Figure 3.3 can be also represented by the following first-order transfer function:

$$\frac{\dot{m}_2}{\dot{m}_1} = \frac{1}{(1+T_{ACT}s)} \qquad \text{Eq. (3.6)}$$

Where $\dot{m}_1$ and $\dot{m}_2$ are the steam mass flowrates at the input and the output of the turbine, respectively, and T_{ACT} is the time constant of the turbine (typically between 0.2 to 0.5 s).

A comparison of the time response of a turbine with and without reheat to an incremental step increase in the opening of the governor valve is shown on Figure 3.4.

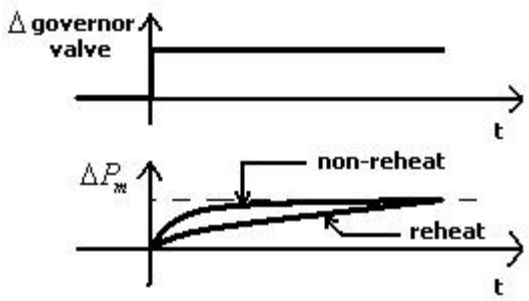

Figure 3.4 – Response of the linear turbine model to a step change in valve position [Machowski et al., 1997]

The most common turbine configuration used for large steam turbines is the single reheat arrangement. In this arrangement, the turbine has three sections: the High-Pressure (HP), Intermediate Pressure (IP), and the Low-Pressure (LP) stages.

The steam flow in the turbine is controlled by the regulating system. When the generator is synchronized, the emergency stop valves are kept fully open and the turbine speed and power regulated by controlling the position of the governor control valves and the intercept control valves. The speed signal to the governor is provided by the speed measuring device [Machowski et al., 1997].

3.5 – Speed Regulation System

The steam turbine speed regulation system (or governing system) has the purpose of controlling the speed and, consequently, the power output of the turbine according to a preset power-frequency characteristic. In fact, the steam turbine speed regulation system is responsible in the synchronous generation

system by the means by which the steam turbine is started, run-up to operating speed and operated on load with the required power output.

In general, turbine control is accomplished by regulating the position of the regulator valves whilst the emergency stop valves are kept fully open, which are only used in an emergency to stop the turbine. For many years, the turbine speed regulating systems were a mechanical-hydraulic type and used the Watt centrifugal mechanism as the speed regulator [Prime Mover, 1991; Machowski et al., 1997].

The original Watt mechanism used two flyballs as the speed responsive device. On new machines the Watt regulator has been replaced by an electro-hydraulic one. In these systems, the turbine rotor speed is measured electronically, with high accuracy, using a toothed wheel and a probe. The resulting electrical signal is amplified and acts on the pilot valve via an electro-hydraulic converter. The schematic diagram of the electro-hydraulic system in Figure 3.5 shows that its operation does not differ much from that of the mechanical-hydraulic system shown in Figure 3.5a, but the flexibility of electronic regulators enables additional control loops to be introduced linking the boiler and the turbine control systems [idem].

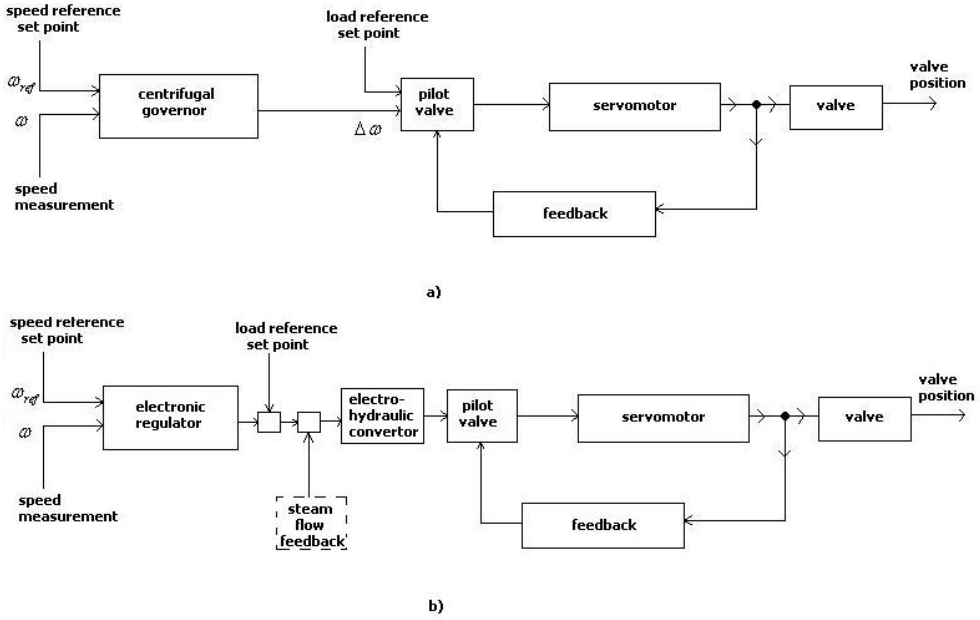

Figure 3.5 – Schematic diagram of the regulating system: a) mechanical-hydraulic; b) electro-hydraulic [Machowski et al., 1997]

The steam flow feedback function is to prevent from valves being opened by the speed regulator when the steam inlet pressure is too low. The reference speed is set electronically in the speed reference set point. It is also possible to change the turbine power using an additional signal that is added to the control circuit at the load reference set point.

The way power output of a turbine varies with speed is the key to its characterization. For stable operation, a turbine must have a power-speed characteristic such as the speed increases as much as the mechanical input reduces. This will restore the balance between the electrical output power and the mechanical input power. Similarly a decrease in speed should result in an increase in the mechanical power [*idem*]. If the steam flow feedback in the electro-hydraulic regulating system is neglected and the regulator response assumed to be dominated by the servomotor time constant, both the mechanical-hydraulic and the electro-hydraulic governors shown in Figure 3.5 may be represented by the simplified block diagram shown in Figure 3.6.

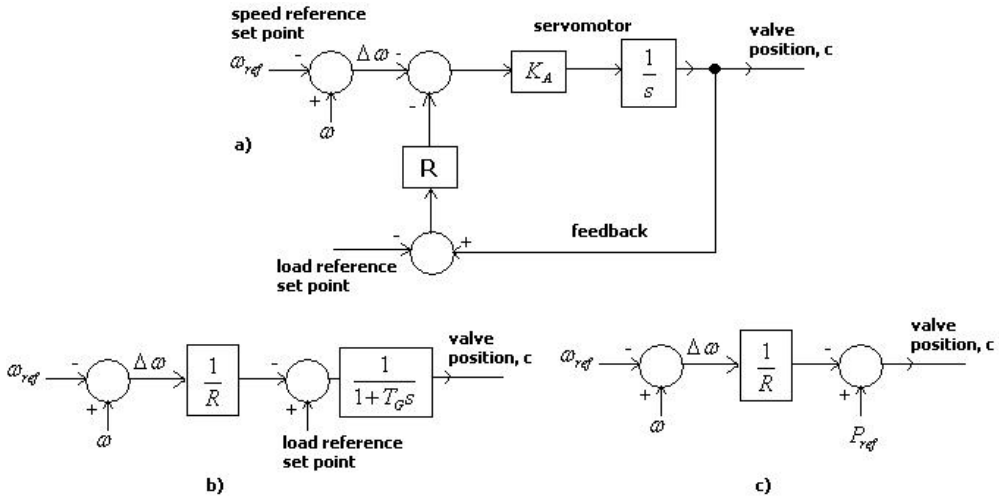

Figure 3.6 – Simplified model of the steam turbine governing system: a) block diagram with negative feedback; b) equivalent block diagram; c) equivalent block diagram for the steady-state [Machowski et al., 1997]

The coefficient K_A in Figure 3.6a corresponds to the amplification gain of the servomotor, while coefficient R corresponds to the gain of the feedback loop. Transformation of the block diagram allows R to be eliminated from the feedback loop by moving it into the main loop to obtain the block diagram

shown in Figure 3.6b where T_G=1/($K_A R$), which is the effective regulator time constant.

A good control system should ensure that any load fluctuation ΔP_m (mechanical power) would only produce a small speed change $\Delta\omega$. This is achieved by making the droop ρ (ρ= R/ω) small. However it should be noticed that the droop cannot be zero or negative. When droop is positive (ρ>0), the turbine power increases when its rotational speed decreases. In this case, a small disturbance in frequency (turbine speed) causes the system to return automatically to the equilibrium point. For example, if there is a momentary increase in frequency, then the disturbed load power is greater than the disturbed turbine power. When the droop is negative (ρ<0), any increase in frequency will cause the turbine power to be greater than the load power. This would result in an increase in turbine speed and a further increase in the power imbalance. Similarly, a decrease in frequency would result in the turbine power being less than the load power with further movement away from the equilibrium point. Such a droop characteristic is not resistant to disturbances and the system is unstable. The case when ρ=0 is the marginal stability case and corresponds to the absence of the negative feedback loop on valve position. Without this negative feedback, the regulating system would be of constant speed type. Such a regulator can not be used if two or more generators are electrically connected to the same set point or else they would “fight” each other, each trying to pull the system frequency to its own setting. Typical values of the speed-droop coefficient (in per unit) are between 0.04 and 0.09 with the lower value corresponding to turbogenerators and the higher to hydrogenerators [Machowski et al., 1997].

A further advance in steam regulators is the digital-hydraulic regulator, where the control functions are implemented in software thus providing even greater flexibility. The regulator model with the speed relay replaced by the general transfer function (1+$T_3 s$)/(1+$T_2 s$), to provide any phase compensation, forms a good basis for modelling an electric-hydraulic regulator.

When analyzing electromechanical dynamics in a time interval of around 10 seconds, the boiler pressure can be assumed to be constant and can be equated to the initial power P_o. With this assumption, the regulator block

diagram can be simplified to the one shown in Figure 3.7, by multiplying the limits and initial conditions, in the servomotor model, by P_o [Prime Mover, 1991].

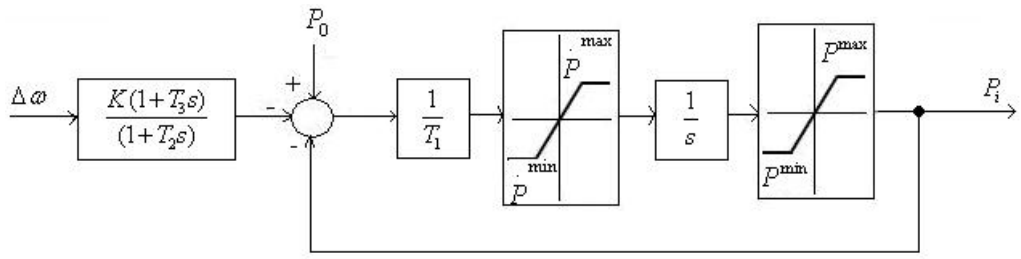

Figure 3.7 – Simplified electro-hydraulic regulator model [Prime Mover, 1991]

In this model, the regulator and the speed relay transfer functions have been replaced by a general control block *K*(1+*T3s*)/(1+*T2s*) to enable this model to be used for both mechanical-hydraulic and electro-hydraulic regulators. The additional time constant now allows both types of governors to be modelled by the correct choice of values. Intercept valve control is not shown on this diagram as it is assumed they are kept fully open at all times.

3.6 – Voltage Regulation System

The voltage regulation system consists of an exciter and an automatic voltage regulator (AVR), and is necessary to supply the synchronous generator with DC field current for its excitation. In some cases, a backup AVR is also provided. The interface between the exciter and the AVR with the generator is through the variable E_f, which represents the generator main field voltage, v_f, referred to the generator armature winding (v_f is also the exciter output voltage v_{ex}). The voltage rating of the exciter does not normally exceed 1000 V as any higher voltage would require additional insulation of the field winding [Machowski et al., 1997; Laughton & Warne, 2002].

3.6.1 – Exciter

In general, exciters can be classified by either rotating or static. In the rotating exciters, the excitation current is supplied either by a DC generator or by an AC generator with rectifiers. Modern excitation systems usually employ either a brushless AC exciter or a static exciter with either an analogue or digital AVR, although digital AVR's are becoming more common. However, many older generators are fitted with DC excitation systems and consequently these models are still typical of the voltage regulation systems in use today. Thus, here it will be detailed the main characteristics of DC exciters [Machowski et al., 1997].

To be used as DC exciters, DC generators are usually cascaded to obtain the necessary output, as they have relatively low power ratings. Due to commutation problems with DC generators, this type of exciter cannot be used for large generators which require large excitation currents. However, they are a very suitable option in small generation systems [IEEE, 2006].

Two different models of DC exciters are shown in Figure 3.8: the first is a separately-excited model and the second, a self-excited one.

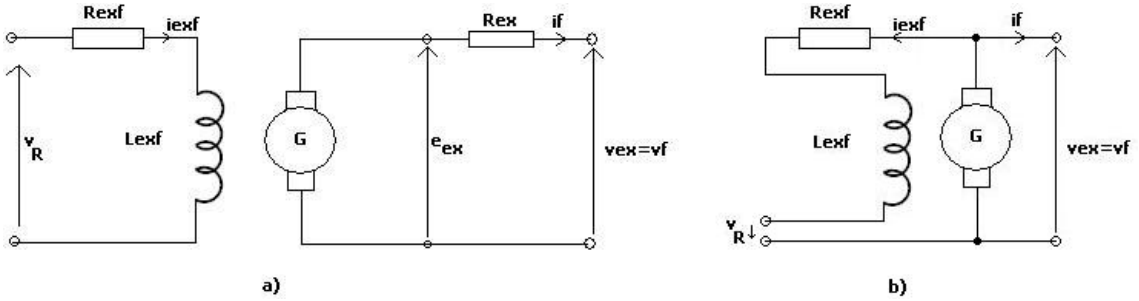

Figure 3.8 – Equivalent circuit diagrams of DC exciters: a) separately excited; b) self-excited [Machowski et al., 1997]

In order to develop a mathematical model of these two exciters, it should be considered first the separately-excited case in Figure 3.8a. A change in the exciter field current, i_{exf}, can be described by the Eq. (3.7):

$$v_R = R_{exf} i_{exf} + L_{exf} \frac{di_{exf}}{dt} \qquad \text{Eq. (3.7)}$$

Where L_{exf} depends on saturation and is an incremental inductance. The relationship between the exciter field current, i_{exf}, and the electromotive force, e_{ex}, induced in the exciter armature is non-linear because of magnetic saturation in the exciter core, whilst the exciter output voltage v_{ex} depends on both the saturation characteristic and the armature loading. Both of these effects are included in the modelling process by using the constant resistance load saturation curve (Figure 3.9).

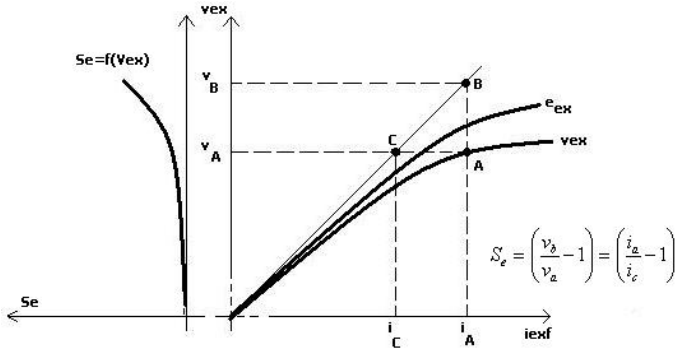

Figure 3.9 – Illustration to define the saturation coefficient: e_{ex} is the no-load curve, v_{ex} is the constant resistance load saturation curve. The saturation characteristic is shown only around saturation knee and has been exaggerated for clarity [Machowski et al., 1997]

The slope of the air-gap line is tangential to the linear part of the no-load saturation curve and can be represented by a resistance with the value $R=v_A/i_C$. The exciter field current that corresponds to the non-linear part of the constant resistance load characteristic can then be expressed by:

$$i_A = i_C \frac{v_B}{v_A} = i_C (1+S_e) = \frac{v_A}{R}(1+S_e) \qquad \text{Eq. (3.8)}$$

Where S_e is a saturation coefficient with reference to the constant reference load saturation curve. This means that any point on the constant resistance load saturation is defined by:

$$i_{exf} = \frac{v_{ex}}{R}(1+S_e) \qquad \text{Eq. (3.9)}$$

To easily interface the exciter with the generator model, the exciter base quantities are defined with the base exciter voltage, e_{exb}, being that voltage which gives rated open-circuit generator voltage, v_0, on the generator air-gap line.

Noting that $E_f=v_{ex}$ and writing $\frac{L_{exf}}{R}\left[\frac{di_{exf}}{dv_{ex}}\right]_{Vex0} = T_E$, then

$$v_R = (K_E + S_E)E_f + T_E \frac{dE_f}{dt} \qquad \text{Eq. (3.10)}$$

Where $K_E=R_{exf}/R$ and $S_E=(R_{exf}/R)S_e$. This Eq. (3.10), shown in block diagram form in Figure 3.10, comprises an integrating element, with integration time T_E, and two negative feedback loops with gains K_E and S_E, respectively.

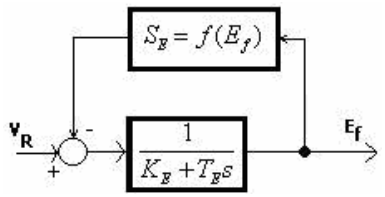

Figure 3.10 – Block diagram of the regulated DC exciter [Machowski et al., 1997]

The negative feedback loop with gain S_E models the saturation in the exciter iron. As the saturation increases, so does the value of S_E, the magnitude of the negative feedback signal increases, and the influence of the regulator on the exciter voltage E_f is reduced.

A DC exciter that is separately excited usually operates with $R_{exf}<R$, so that K_E typically varies from 0.8 to 0.95. Often approximated values of K_E equal to 1 and S_E equal to S_e are assumed in the exciter model. The constant T_E is under one second and is often taken to be approximately 0.5 s.

If the exciter is self-excited, then the voltage v_R is the difference between the exciter internal electromotive force and the excitation voltage v_{ex}. Including this in the Eq. (3.10) would give a differential equation that is identical to the Eq. (3.10), except that $K_E= (R_{exf}/R-1)$. Consequently, the exciter block diagram in Figure 3.10 is also valid for self-excited exciters. Typically, R_{exf} is slightly less than R, so that K_E assumes a small negative value in the range -0.05 to -0.2.

The block diagram of the main part of the voltage regulation system can now be formulated by combining the block diagram of the exciter with the block diagram of the regulator and the stabilizing feedback signal as shown in Figure 3.11.

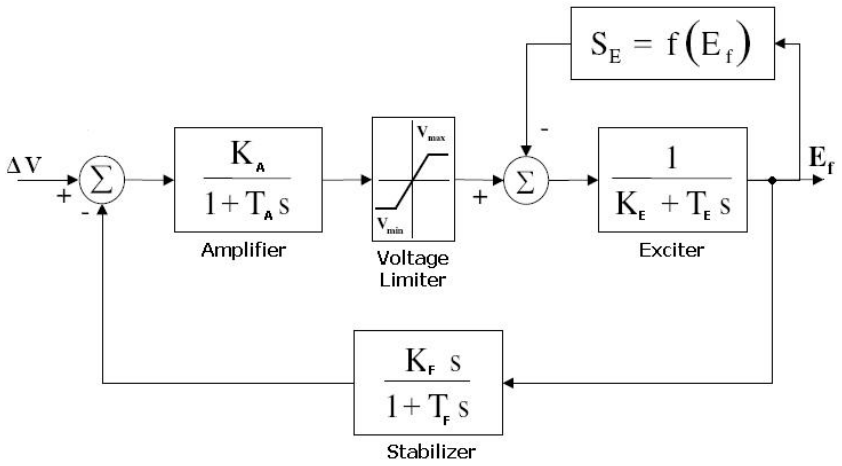

Figure 3.11 – Block diagram of a voltage regulation system with a DC exciter – IEEE type I (adapted from [IEEE, 2006])

The regulator is represented by a first-order transfer function with a time constant T_A and gain K_A. Typical values of these parameters are: T_A from 0.05 to 0.2 s and K_A from 20 to 400. The high regulator gain is necessary to ensure small voltage regulation of the order 0.5 %. Although this high gain ensures low steady-state error, when coupled with the length of the time constants the transient performance of the exciter is less satisfactory. To achieve acceptable transient performance the system must be stabilized in some way that reduces the transient (high frequency) gain. This is achieved by a feedback stabilization signal represented by the first-order differentiating element with gain K_F and time constant T_F. Typical values of the parameters in this element are: T_F from 0.35 to 1 s and K_F from 0.01 to 0.1 s [IEEE, 2006].

Despite the saturation function S_E=f(E_f) can be approximated by any non-linear function, an exponential function of the form $S_E=A_{ex}\ e^{BexEf}$ is commonly used. As this function models the saturation characteristic over a wide range of exciter operating conditions, the parameters A_{ex} and B_{ex} of the exponential function are determined by considering the heavily saturated region of the

characteristic corresponding to high excitation voltage and higher exciter field current.

It is important to note that the limits on E_f are linked to the regulator limit and the saturation function such that the maximum value, E_{f_Max}, is obtained from:

$$V_{\max} - (K_E E_{f\_Max} + S_{E\_Max}) = 0 \qquad \text{Eq. (3.11)}$$

Nowadays, DC generators have been almost entirely replaced by alternators which are simpler and more reliable. This change to alternators has been possible because of the advances in power electronics which are allowing cheap, high-power rectifiers to be used in conjunction with the AC exciter. As the cost of high-power rectifiers decrease and reliability increases, static exciters are becoming the main source of excitation for high-power generators [Machowski et al., 1997; IEEE, 2006].

3.6.2 – Automatic Voltage Regulator

The Automatic Voltage Regulator (AVR) regulates the generator terminal voltage by controlling the amount of current supplied to the generator field winding by the exciter.

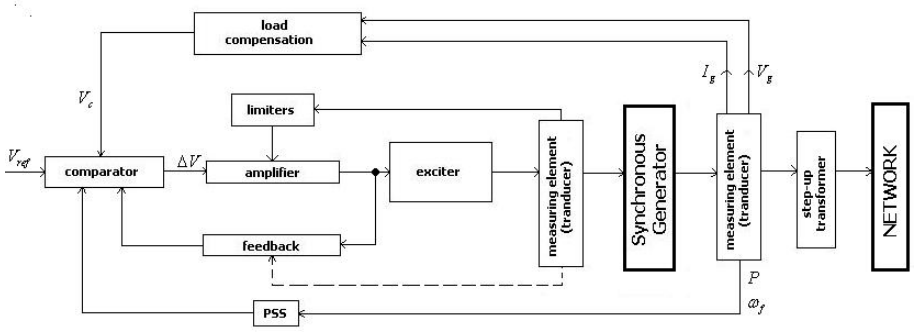

Figure 3.12 – Block diagram of the excitation and AVR system [Machowski et al., 1997]

The measuring element senses the current, power, terminal voltage and frequency of the generator. The measured generator terminal voltage V_g is compensated for the load current I_g and compared with the desired voltage V_{ref}

to produce the voltage error ΔV. This error is then amplified and used to alter the exciter output, and consequently the generator field current, so that the voltage error is eliminated. The regulation process is stabilized using a negative feedback-loop taken directly from either the amplifier or the exciter.

Figure 3.13 shows the block diagram of the measuring element and comparator together with the load compensation element, which corrects the generator terminal voltage according to the value of the compensation impedance. The second block represents the delay introduced by the signal measuring elements. Normally, the equivalent time constant is small so this block is often neglected. The third element represents the comparator at which the corrected voltage is added algebraically to the reference voltage V_{ref}.

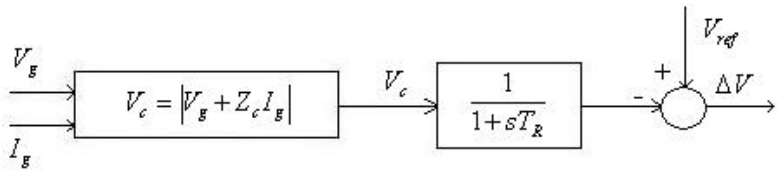

Figure 3.13 – Block diagram of the measuring element (transducer) and comparator [Machowski et al., 1997]

In conclusion, the voltage drop across the compensation impedance, Z_c, due to generator current, I_g, is added to the generator voltage, V_g, to produce the compensated voltage, V_c, according to the Eq. (3.12):

$$V_c = \left|\bar{V} + (R_c + jX_c)\bar{I}_g\right| \qquad \text{Eq. (3.12)}$$

Where $\bar{Z}_c = R_c + jX_c$ is the compensation impedance. If load compensation is not employed $\bar{Z}_c = \bar{0}$, $V_c = V_g$, and AVR subsystem maintains constant generator terminal voltage.

The AVR subsystem also includes a number of limiters whose function is to protect the AVR, exciter and generator from excessive voltages and currents. They do this by maintaining the AVR signals between preset limits. Thus, the amplifier is protected against excessively high input signals; the exciter and the

generator against too high a field current; and the generator against too high an armature current and to high a power angle. The three last limiters have in-built time delays to reflect the thermal time constant associated with the temperature rise in the winding.

3.6.3 – Power System Stabilizer (PSS)

A power system stabilizer (PSS) is sometimes added to the AVR subsystem to help damping power swings in the system. PSS is typically a differentiating element with phase shifting corrective elements. Its input signals may be proportional to rotor speed, generator output frequency or the electrical real power output of the generator [Machowski et al., 1997].

PSS can help to damp generator rotor oscillations by providing an additional input signal that produces a torque component in phase with the rotor speed deviation. The general structure of a PSS consists on the following main elements (Figure 3.14): the signal sensor, a low-pass filter, a high-pass filter, (at least one) lead compensation element, an amplifier and a limiter.

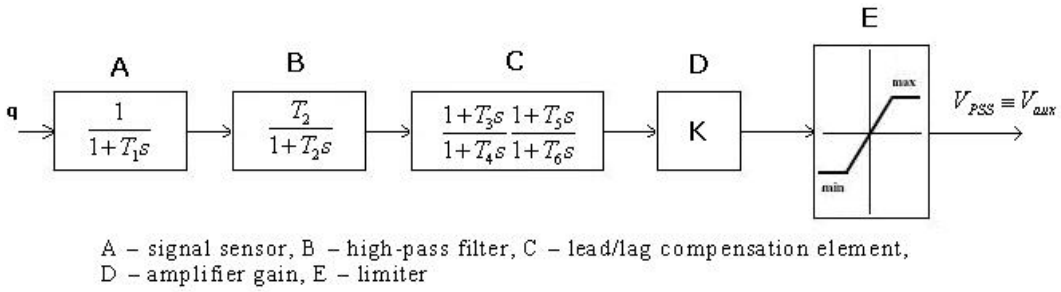

Figure 3.14 – Block diagram of the power system stabilizer (PSS) [Machowski et al., 1997]

The input signal q can be rotor speed, real power, frequency, or some other signal. The output signal, shown in Figure 3.14 as V_{PSS}, is passed to the AVR as the auxiliary signal V_{aux}. The parameters within the PSS are carefully selected for each PSS, depending on its input signals and location on the system.

3.7 – Summary

This chapter presented the technology behind biomass energy production, more precisely, behind steam turbine-based synchronous generation technology. From a first approach, where an overview of synchronous generation systems was made, to a more specific one, where it was explained individually the core components of these systems, it were shown the most important aspects about steam turbine-based synchronous generation technology. This study had the purpose of obtaining a biomass energy plant for simulation purposes in a test distribution network in Chapter 5 and Chapter 6.

At first, it was presented a first overview of the steam turbine-based synchronous generation plants, in which are based biomass energy plants. It followed the 5^{th} order model of the synchronous generator. Afterwards, it was detailed the steam turbine technology. At last, were explained the speed and voltage regulation systems of the steam turbine-based synchronous generation plants.

Chapter 4 – Doubly-Fed Induction Generator: The Proportional-Integral Controller Tuning

4.1 – Introduction

In this chapter, it will be shown the tuning process of the PI (Proportional-Integral) controller gains of the rotor side converter of the doubly-fed induction generator (DFIG), presented in Chapter 2, for the optimization of its performance. The PI controllers of the rotor side converter of the DFIG are very important for the optimization its active and reactive powers delivered. The PI controllers referred eliminate the real-time errors between the active and reactive power reference values and the actual ones, when a change in the reference values occurs. As the PI controller gain tuning process using the classic control theory techniques may be complex in this case, these won't be used. The tuning process will, instead, consist in the use of meta-heuristics applied to power systems, namely Particle Swarm Optimization (PSO) and Evolutionary Particle Swarm Optimization (EPSO). Appendix E details the PSO and EPSO algorithms.

At first, it will be given a first approach on the motivation and general aspects of the optimal PI controller gain determination. Secondly, it will follow the detail of PSO and EPSO approaches of the PI controller gain tuning. At last, it will be shown, using the software package *Matlab*®, the results obtained by each meta-heuristic and discussed its comparative performance.

4.2 – DFIG PI Controller Tuning: Motivation

The optimal performance of the doubly-fed induction generator (DFIG) is assured by its ability of optimizing the delivered active and reactive powers. The rotor side converter's PI (Proportional-Integral) controllers are essential for this achievement, as they allow a quick convergence between the reference and actual values of the active and reactive powers delivered, when a change in the reference values occurs.

In this work, the determination of the optimal values for the PI controller gains (K_{p1}, K_{i1}, K_{p2}, K_{i2}) has the goal of obtaining equally optimal steady-state step responses of the controlled system when step changes in the reference values occur [Qiao et al.,2006; Vieira et al., 2007; Tapia & Otaegui, 2005]. Therefore, the optimal set of PI controller tunings (K_{p1}, K_{p2}, K_{i1}, K_{i2}) will be the one that, ideally, inducing no overshoot at the response to a step input, reduces to the minimum the transient time of the response, i.e., its settling time. Hence, this optimal set of PI controller tunings will lead the controlled system to a quick and stable convergence to the expected steady-state final values.

PI controller tuning can be done by several ways, from the classic control theory techniques, such as Ziegler-Nichols method, to other methods as trial and error [Martins de Carvalho, 1993]. The classic control techniques offer, in general, solid results but as the controlled system complexity increases, the tuning process also increases its complexity. In the case of the rotor side converter's PI controller tuning, it may be difficult and, furthermore, problematical to achieve proper tuning due to the nonlinearity and the high complexity of the system, using the classic control techniques. Thus, in this work, for the tuning of the rotor side converter's PI controller gains it will be used meta-heuristics instead of the classic control techniques. Meta-heuristics offer the possibility of obtaining good results avoiding most of the complexity of the controlled system.

Over the years, meta-heuristic algorithms such as evolutionary algorithms, taboo search and simulated annealing, among others, have been used for nonlinear optimization, due to its high efficiency in searching global optimal solutions in the search space. However, when the parameters to be

optimized are highly correlated, the performance of these meta-heuristic algorithms seems to degrade [Gaing, 2004; Qiao et al., 2006]. The appearance of a new technique based on swarm intelligence called Particle Swarm Optimization (PSO) has been found to be robust in solving continuous nonlinear optimization problems [*idem*]. Thus, the meta-heuristics used in this work will be Particle Swarm Optimization (PSO) and Evolutionary Particle Swarm Optimization (EPSO), which combines PSO with evolutionary algorithms. Further information on these meta-heuristics is available in Appendix E [Shi & Eberhart, 1999; Miranda et al., 2007].

4.3 – DFIG PI Controller Tuning: Meta-Heuristic Approaches

Proportional-integral (PI) controller tuning can be done by several ways, from the classic control theory techniques, such as Ziegler-Nichols method, to other methods as trial and error. In this work, meta-heuristics will be used for the tuning of the rotor side converter's PI controller gains (K_{p1}, K_{i1}, K_{p2}, K_{i2}).

Recalling, the generic PI controller transfer function, $TF_{PI}(s)$, is given by the Eq (4.1):

$$TF_{PI}(s) = K_p + \frac{K_i}{s} \qquad \text{Eq. (4.1)}$$

Where K_p and K_i are the proportional and integral gains, respectively.

In Figure 4.1, it is presented the controlled system with the two PI controllers to be tuned in this work, in order to achieve the steady-state response capabilities required. That is, the response to step inputs in active and reactive power control loops must induce no overshoot, reducing to the minimum the transient time of the response.

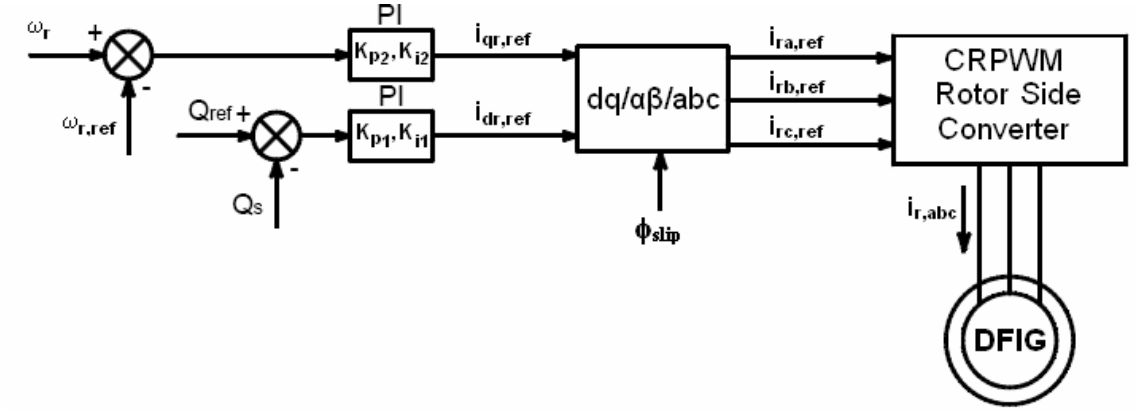

Figure 4.1 – Rotor side converter controllers, in which K_{p1}, K_{i1}, K_{p2} and K_{i2} are the gains to tune

In Figure 4.1, PI controller gains K_{p1} and K_{i1} refer to the reactive power control loop, while K_{p2} and K_{i2} refer to the angular speed control loop, which are responsible for the active power control.

In this work, each set of possible PI controller gain tunings will be from now on called particle. Thus, each particle *i* position in the search space will refer to a set of possible PI controller gain tunings, that is, X_i= [K_{p1}, K_{p2}, K_{i1}, K_{i2}]. Hence, the population dimension is $N \times 4$, being *N* the number of particles of the population and 4 the number of elements in each particle.

Follows the detailed explanation of PSO and EPSO-based algorithms to tune the PI controllers of the DFIG rotor side converter.

4.3.1 – Particle Swarm Optimization (PSO): DFIG PI Controller Tuning

The PSO-based algorithm to generate the optimal gains of the rotor side converter's PI controllers is detailed as it follows, from **Step 1)** to **Step 9).**

Step 1) Specification of the PSO parameters;

- **o** Number of maximum iterations (*itmax*) = 50
- **o** Number of particles (*N*) = 15
- **o** Maximum inertia – strategic parameter (W_{max}) = 0.9
- **o** Minimum inertia – strategic parameter (W_{min}) = 0.4

- **o** Acceleration parameters c_1 and c_2 – corresponding, respectively, to strategic parameters memory and cooperation = 2
- **o** Upper bound position of the particles (X_{max}) = [10; 10; 10; 10]
- **o** Lower bound position of the particles (X_{min}) = [0.01; 0.01; 0.01; 0.01]
- **o** Upper bound velocity of the particles (V_{max}) = $X_{max} \times 0.1$
- **o** Lower bound velocity of the particles (V_{min}) = $-X_{max} \times 0.1$

Step 2) Random initialization of the particle positions (X_i) and its velocities (V_i); setting of the initial personal ($p_{best,i}$) and global best positions (g_{best});

Step 3) For each particle *i*, test of the closed-loop system stability and calculation of the values of the four performance criteria in the time domain, namely [Gaing, 2004]: M_p (overshoot – maximum output of the step response in percentage of the steady-state final value); T_r (rise time – time required for the step response to change from a lower to an upper band value, in this case, from 10% to 90% of the steady-state final value, in seconds); T_s (settling time – time until the step response reaches a specified 2% error band around the steady-state final value, in seconds); E_{ss} (steady-state error – difference between the expected steady-state final value and the occurred steady-state final value, in percentage) [Martins de Carvalho, 1993].

The evaluation of these four performance criteria is done by, at a steady-state time instant t_o (in seconds), making the following step changes:

$$Q_{ref} = -0.1 MVar \xrightarrow{t=t_o} Q_{ref} = -0.2 MVar$$

$$\omega_{ref} = 1.12 p.u. \xrightarrow{t=t_o} \omega_{ref} = 1.2 p.u.$$

The change in ω_{ref} corresponds to a step from 13 m/s to 14 m/s in the wind speed (at the instant t_o).

Step 4) Calculation of the evaluation value of each particle *i* in the population, using the fitness function *F* given by [Gaing, 2004], which the objective is to minimize, by the evaluation of the four PI performance parameters in the time domain: overshoot (M_p), rise time (T_r), settling time (T_s) and steady-state error (E_{ss}).

$$Faux_i(K_{p1}, K_{i1}) = (1 - e^{-\beta}).(G.M_p + E_{ss}) + e^{-\beta}.(T_s - T_r)$$
$$Faux_i^{'}(K_{p2}, K_{i2}) = (1 - e^{-\beta}).(G.M_p^{'} + E_{ss}^{'}) + e^{-\beta}.(T_s^{'} - T_r^{'}) \quad \text{Eq. (4.2)}$$

$$F_i = Faux_i + Faux_i^{'} \quad \text{Eq. (4.3)}$$

Where β is a weighting factor of the performance parameters, which is set to β equal to one (1). *G* is a very large positive constant (one hundred) used to penalize high values of overshoot (M_p). Thus, the evaluation value of each particle *i*, given by fitness function *F*, is as "fit" as it is lower. In other words, the purpose of each particle *i* is to decrease its evaluation value F_i.

Step 5) Comparison of each particle's present position X_i with its personal best ($p_{best,i}$) based on the fitness evaluation. If the current position X_i is better than $p_{best,i}$, then $p_{best,i} = X_i$. If $p_{best,i}$ is updated, then compare each particle's $p_{best,i}$ with the population global best position g_{best} based on the fitness evaluation. If $p_{best,i}$ is better than g_{best}, then $g_{best} = p_{best,i}$.

Step 6) At iteration *it*, a new velocity for each particle *i* is updated by the Eq. (4.4):

$$V_i(it+1) = W.V_i(it) + c_1\varphi_1\left[b_i(it) - X_i(it)\right] + c_2\varphi_2\left[b_g(it) - X_i(it)\right] \quad \text{Eq. (4.4)}$$

Where φ_1 and φ_2 are uniformly distributed random numbers in [0,1]. The velocity parameter of each particle V_i is then evaluated if it violates the limits [V_{min}, V_{max}]. If this happens, it is set to the relevant upper or lower bound value (V_{min} or V_{max}).

Step 7) Based on the updated velocity, each particle *i* then changes its position according to the Eq. (4.5).

$$X_i(it+1) = X_i(it) + V_i(it+1) \qquad \text{Eq. (4.5)}$$

The position of each particle X_i is then evaluated if it violates the limits [X_{min}, X_{max}]. If this happens, it is set to the relevant upper or lower bound value (X_{min} or X_{max}).

Step 8) If the number of iterations (*it*) reaches the maximum (*itmax*), continuous onto Step 9). Otherwise, go back to Step 3).

Step 9) The particle that generates the latest global best (g_{best}) is the optimal solution of the problem, in this case, the optimum set of PI controller gains.

4.3.2 – Evolutionary Particle Swarm Optimization (EPSO): DFIG PI Controller Tuning

The EPSO-based algorithm to generate the optimal gains of the rotor side converter PI controllers is described as it follows, from **Step 1)** to **Step 12)**.

Step 1) Specification of the EPSO parameters;

- **o** Number of maximum iterations (*itmax*) = 50
- **o** Number of particles (*N*) = 15
- **o** Noise ratio to disturb $p_{best,i}$ and g_{best} = 0.001
- **o** Learning parameter – fixed (τ) = 0.1
- **o** Strategic parameters mutation ratio = 0.9
- **o** Communication factor (*P*) = 0.2
- **o** Upper bound position of the particles (X_{max}) = [10; 10; 10; 10]
- **o** Lower bound position of the particles (X_{min}) = [0.01; 0.01; 0.01; 0.01]
- **o** Upper bound velocity of the particles (V_{max}) = $X_{max} \times 0.1$

- **o** Lower bound velocity of the particles (V_{min}) = $-X_{max} \times 0.1$

Step 2) Random initialization of the particle positions (X_i) and its velocities (V_i), setting of the initial personal ($p_{best,i}$) and global best positions (g_{best}), initialization of the strategic parameters for each particle *i* [inertia (Wi_i), cooperation (Wc_i) and memory (Wm_i)];

Step 3) Replication of each particle *i*, creating X_m_i, the velocity V_m_i and the initial positions $p_{best,i\_}m$ and $g_{best\_}m$, where the subscript *m* refers to mutated;

Step 4) The strategic parameters for each particle *i* (inertia cooperation and memory) are mutated to give Wi_m_i, Wc_m_i and Wm_m_i, respectively.

Step 5) At iteration *it*, a new velocity for each particle *i* is updated by the Eq. (4.6):

$$V_i(it+1) = Wi^*_i \cdot V_i(it) + Wm^*_i \cdot \left[p_{best,i}(it) - X_i(it)\right] + Wc^*_i \cdot \left[g^*_{best}(it) - X_i(it)\right] \cdot P \quad \text{Eq. (4.6)}$$

Where the superscript * refers to parameters subject to mutation. The same process is done to obtain V_m_i (*it*+1), with the mutated values of the strategic and object parameters. The velocity parameter of each particle V_i (and V_m_i) is then evaluated if it violates the limits [V_{min}, V_{max}]. If this happens, it is set to the relevant upper or lower bound value (V_{min} or V_{max}).

Step 6) Based on the updated velocity, each particle *i* then changes its position according to the Eq. (4.7).

$$X_i(it+1) = X_i(it) + V_i(it+1) \quad \text{Eq. (4.7)}$$

The same process is done to obtain X_m_i (it+1). The position of each particle X_i (and X_m_i) is then evaluated if it violates the limits [X_{min}, X_{max}]. If this happens, it is set to the relevant upper or lower bound value (X_{min} or X_{max}).

Step 7) For each particle i, test of the closed-loop system stability and calculation of the values of the four performance criteria in the time domain, namely [Gaing, 2004]: M_p (overshoot – maximum output of the step response in percentage of the steady-state final value); T_r (rise time – time required for the step response to change from a lower to an upper band value, in this case, from 10% to 90% of the steady-state final value, in seconds); T_s (settling time – time until the step response reaches a specified 2% error band around the steady-state final value, in seconds); E_{ss} (steady-state error – difference between the expected steady-state final value and the occurred steady-state final value, in percentage) [Martins de Carvalho, 1993].

The evaluation of these four performance criteria is done by, at a steady-state time instant t_o (in seconds), making the following step changes:

$$Q_{ref} = -0.1 MVar \xrightarrow{t=t_o} Q_{ref} = -0.2 MVar$$

$$\omega_{ref} = 1.12 p.u. \xrightarrow{t=t_o} \omega_{ref} = 1.2 p.u.$$

The change in ω_{ref} corresponds to a step from 13 m/s to 14 m/s in the wind speed (at the instant t_o).

Step 8) Calculation of the evaluation value of each particle i (normal and mutated) in the population, using the fitness function F (and F_m) given by [Gaing, 2004], which the objective is to minimize, by the evaluation of the four PI performance parameters in the time domain: overshoot (M_p *and* M_p*'* for the case of the mutated function), rise time (T_r and T_r*'*), settling time (T_s and T_s*'*) and steady-state error (E_{ss} and E_{ss}*'*).

$$Faux_i(K_{p1}, K_{i1}) = (1 - e^{-\beta}).(G.M_p + E_{ss}) + e^{-\beta}.(T_s - T_r)$$
$$Faux_i^{'}(K_{p2}, K_{i2}) = (1 - e^{-\beta}).(G.M_p^{'} + E_{ss}^{'}) + e^{-\beta}.(T_s^{'} - T_r^{'}) \quad \text{Eq. (4.8)}$$

$$F_i = Faux_i + Faux_i^{'} \quad \text{Eq. (4.9)}$$

Where β is a weighting factor of the performance parameters, which is set to β equal to one (1). *G* is a very large positive constant (one hundred) used to penalize high values of overshoot (M_p). Thus, the evaluation value of each particle *i*, given by fitness function *F (and F_m)*, is as "fit" as it is lower. In other words, the purpose of each particle *i* is to decrease its evaluation value F_i (and F_m_i).

Step 9) Comparison of each particle *i* present position X_i with its personal best ($p_{best,i}$) based on the fitness evaluation. If the current position X_i is better than $p_{best,i}$, then $p_{best,i} = X_i$. If $p_{best,i}$ is updated, then compare each particle's $p_{best,i}$ with the population global best position g_{best} based on the fitness evaluation. If $p_{best,i}$ is better than g_{best}, then $g_{best} = p_{best,i}$. The same process is done to the mutated particles, using the present positions X_m_i, personal best positions $p_{best,i}\_m$ and global best g_{best}_m.

Step 10) Comparison if g_{best} is better than g_{best}_m, based on the fitness evaluation (F_i versus F_m_i). If g_{best}_m is better than g_{best}, $g_{best} = g_{best}\_m$. Otherwise, $g_{best} = g_{best}$. If g_{best} is updated, the mutated strategic parameters substitute the normal ones, i.e., $Wi_i = Wi\_m_i$, $Wc_i = Wc\_m_i$ and $Wm_i = Wm\_m_i$.

Step 11) If the number of iterations (*it*) reaches the maximum (*itmax*), then continuous onto Step 12). Otherwise, go back to Step 4).

Step 12) The particle that generates the latest global best (g_{best}) is the optimal solution of the problem, in this case, the optimum set of PI controller gains.

4.4 – PSO and EPSO: Comparative Results on the PI Controller Tuning

PSO and EPSO are compared on the approaches of the PI controller gains tuning by the results obtained from simulations with the software package *Matlab*®.

Table 4.1 shows the optimal PI controller gain values obtained by PSO and its associated performance criteria in the time domain.

TABLE 4.1
OPTIMAL PI CONTROLLER GAIN VALUES AND PERFORMANCE CRITERIA USING PSO

PI CONTROLLER GAIN VALUES			
K_{p1}	K_{i1}	K_{p2}	K_{i2}
1.423	4.9806	0.6783	5.1505

PERFORMANCE CRITERIA IN THE TIME DOMAIN							
Mp (%)	*Tr (s)*	*Ts (s)*	*Ess (%)*	*M'p (%)*	*T'r (s)*	*T's (s)*	*E'ss (%)*
0.207	0.886	2.131	0.01	0.017	7.845	12.588	0.01

Figures 4.2 and 4.3 show, respectively, the step responses correspondent to the data given in Table 4.1. Figure 4.2 corresponds to gains K_{p1} and K_{i1} (reactive power control loop) and Figure 4.3 corresponds to gains K_{p2} and K_{i2} (angular speed control loop).

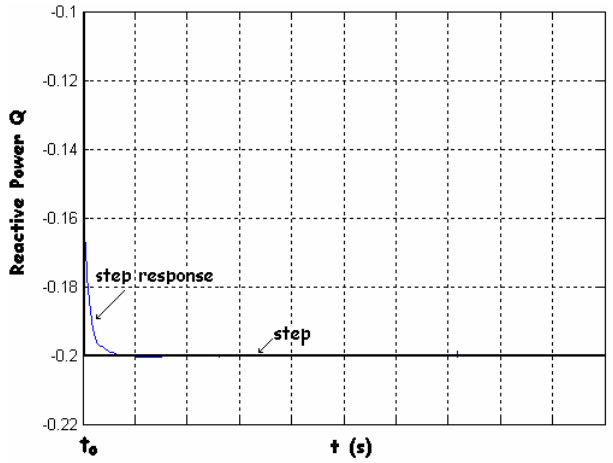

Figure 4.2 – Step response of the reactive power control loop, using the gains obtained from PSO

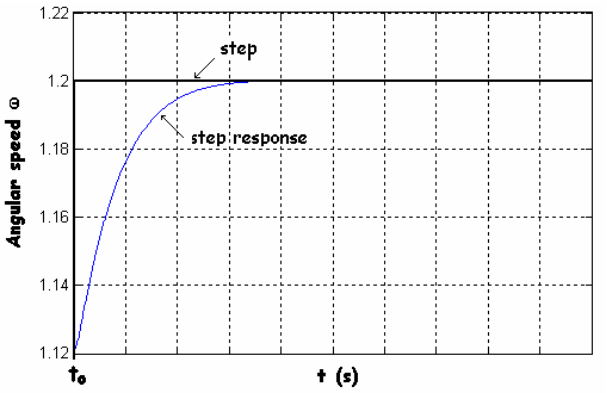

Figure 4.3 – Step response of the angular speed control loop, using the gains obtained from PSO

Table 4.2 shows the optimal PI controller gain values obtained by EPSO and its associated performance criteria in the time domain.

TABLE 4.2
OPTIMAL PI CONTROLLER GAIN VALUES AND PERFORMANCE CRITERIA USING EPSO

PI CONTROLLER GAIN VALUES							
K_{p1}		K_{i1}		K_{p2}		K_{i2}	
1.3126		4.9954		0.6279		3.3773	
PERFORMANCE CRITERIA IN THE TIME DOMAIN							
Mp (%)	*Tr (s)*	*Ts (s)*	*Ess (%)*	*M'p (%)*	*T'r (s)*	*T's (s)*	*E'ss (%)*
0.200	0.873	2.087	0.01	0.00037	7.599	12.33	0.01

Figures 4.4 and 4.5 show, respectively, the step responses correspondent to the data given in Table 4.2. Figure 4.4 corresponds to gains K_{p1} and K_{i1} (reactive power control loop) and Figure 4.5 corresponds to gains K_{p2} and K_{i2} (angular speed control loop).

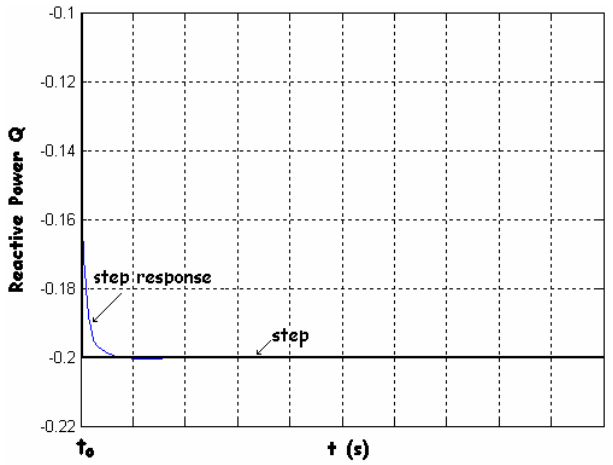

Figure 4.4 – Step response of the reactive power control loop, using the gains obtained from EPSO

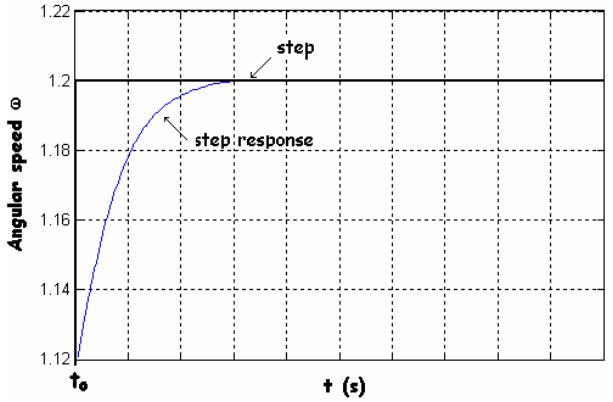

Figure 4.5 – Step response of the angular speed control loop, using the gains obtained from EPSO

In Table 4.3 are presented the optimal fitness evaluation *F* values for PSO and EPSO, obtained from the data given in Tables 4.1 and 4.2, as described in the Steps 4) and 8) of PSO-based and EPSO-based algorithms, respectively. It must be recalled the fitness function *F* is a function to minimize.

TABLE 4.3
OPTIMAL FITNESS EVALUATION VALUES FOR PSO AND EPSO

OPTIMAL FITNESS (F) – PSO	OPTIMAL FITNESS (F) – EPSO
31.0892	30.7633

Figure 4.6 shows the comparative performance of the fitness functions during the iterative processes of PSO and EPSO (number of iterations is equal to 50).

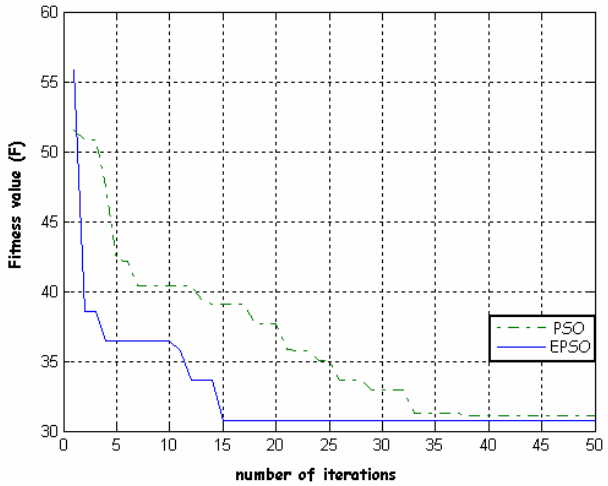

Figure 4.6 – Comparative performance of the fitness functions in PSO and EPSO

From Table 4.3 and Figure 4.6, it can be denoted that EPSO seems to have more ability to converge to a more "fit" solution than PSO, in this case. Not only EPSO converges to a "fitter" solution, but as well arrives to a better evaluation value in a much less number of iterations than PSO. This better performance may derive from the self-adaptive nature of the strategic parameters in EPSO, which seems to conduct the population to the optimal location in a more effective way than PSO, where the strategic parameters are defined *a priori*.

Therefore, in simulations of Chapter 6, the doubly-fed induction generator rotor side converter's PI controller gains used will be the ones obtained by EPSO, i.e., the values of Table 4.2.

4.5 – Summary

This chapter shown the tuning process of the doubly-fed induction generator rotor side converter's PI controller gains, presented in the Chapter 2, for its performance optimization. The tuning process consisted in the use of meta-heuristics, as they offer the possibility of obtaining good results avoiding most of the complexity of the controlled system. The meta-heuristics used were Particle Swarm Optimization (PSO) and Evolutionary Particle Swarm Optimization (EPSO). An overview of these two meta-heuristics is available in Appendix E. EPSO seemed to achieve superior convergence for the optimum than PSO, in this case. Not only EPSO converged to a "fitter" solution, but as well arrived to a better evaluation value in a much less number of iterations than PSO.

Firstly, was given a first approach on the specific motivation and general aspects of the determination of the rotor side converter's PI controller gains. After the detail of PSO and EPSO approaches for the PI controller tuning, were, at last, shown the results obtained by each meta-heuristic and discussed its comparative performance.

Chapter 5 – Adaptive Control to Provide Predictable Active Power Output

5.1 – Introduction

This chapter will present an adaptive control of Distributed Generation (DG) to provide predictable active power output at the primary distribution substation. It will be detailed an algorithm which aims to predict the active power output from the aggregation of wind and biomass energy at the primary distribution substation of a typical distribution network, knowing that biomass primary energy can be stored transported whenever and where it is needed. This algorithm uses the steam turbine synchronous generation technology of the biomass energy plant to cover the unpredictable energy that comes from the wind energy plant. It is assumed wind and biomass energy plants are onto the same distribution network but not necessarily onto the same feeder.

Firstly, a brief overview of the aim of this study is presented. Secondly, it is detailed the modelling of the referred algorithm. Next, in order to evaluate the performance of the algorithm, a typical 60/15 kV radial distribution network with the integration of distributed generators will be simulated with the electromagnetic transient package PSCAD/EMTDC®. The technical performance of the algorithm on the simulated test network will be then presented. Finally, it will be analyzed and discussed the impact of the proposed algorithm in the simulated test network.

5.2 – Predictable Active Power Output: A Present Concern

Concern over the global climate change led the EU and the Portuguese Government to set targets to the share of electricity produced from renewable sources in 22.1% and 39% in the EU and Portugal respectively by 2010 [European Parliament, 2001]. In order to meet those targets, higher penetrations of Distributed Generation (DG) are expected to be connected to the distribution network.

Often, distribution networks accommodate renewable energy from different energy sources and thus using different energy conversion sources. As the amount of generation that comes from intermittent renewable sources (e.g. wind energy) increases, network operators start to concern with the uncertainty of generation.

Biomass energy is a renewable energy with the advantage of having a secure contribution to the network, assuring predictable active power output, as it uses the well-established steam turbine synchronous generation technology.

However, there are other forms of renewable energy (e.g. wind energy), produced from existing wind farms which have no facility in providing fully predictable active power output, mainly due to its character of intermittency. The increase of intermittent energy concerns the network operators because of the decrease of security and consequently leading to the increase of network operational costs.

The combining of biomass with wind energy plants may lead to a larger amount of secure renewable energy penetration on the distribution networks. Thus, it may have the advantage of increasing the availability and reliability of renewable sources and consequently the operation costs of the network can be lowered [Djapic et al., 2007]. On other point of view, this larger amount of secure renewable energy penetration in the distribution networks may lead the DG owners to go in market.

With the aggregation of biomass and wind energy, the errors associated with the wind power forecast and consequent energy production can be attenuated. Thus, power systems can potentially accommodate increased levels

of intermittent wind energy as the imbalances between generation and demand do not increase.

From the point of view of Distribution Network Operators (DNOs), they have then the possibility of avoiding the reinforcement of their networks and make a reconfiguration of the network as the DG will have an adaptive control. DNOs though have a localized network support as they can control DG active power output.

5.3 – Adaptive DG Active Power Prediction Algorithm

5.3.1 – How the Algorithm was modelled?

The Adaptive DG Active Power Prediction Algorithm aims to predict the active power output at the primary distribution substation. The algorithm also tries to minimize the fluctuations in the active power output of the primary distribution substation. The algorithm controls the non-intermittent energy plant and, thus, predicts the active power output from both intermittent and non-intermittent energy plants. The intermittent energy plant considered in this work is a conventional wind energy plant (i.e. equipped with a conventional induction generator), which is described in Chapter 2. The non intermittent energy plant considered in this work is a typical biomass energy plant (i.e. equipped with steam turbine synchronous generation technology), which is described in Chapter 3.

The Adaptive DG Active Power Prediction Algorithm changes the biomass energy plant's load reference to follow the variations of the wind energy plant's active power output and, thus, minimize the fluctuations of the primary distribution substation's active power output. The Adaptive DG Active Power Prediction Algorithm changes the biomass energy plant's load reference as shown in Figure 5.1 b).

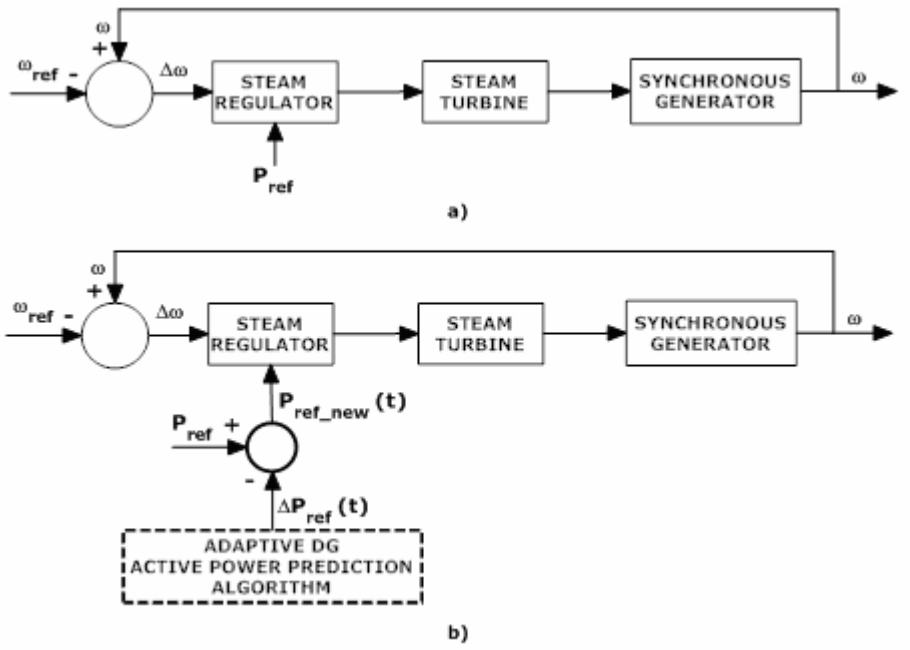

Figure 5.1 – a) Load Frequency Control Block Diagram of the Biomass Energy Plant; b) Load Frequency Control Block Diagram of the Biomass Energy Plant with the Adaptive DG Active Power Prediction Algorithm

As wind speed variations produce active power fluctuations at the output of the wind energy plant and, consequently, at the output of the primary substation, the Adaptive DG Active Power Prediction sets the biomass energy plant's load reference to change the biomass energy plant's active power output accordingly. Figure 5.2 shows the flow chart of the Adaptive DG Active Power Prediction Algorithm.

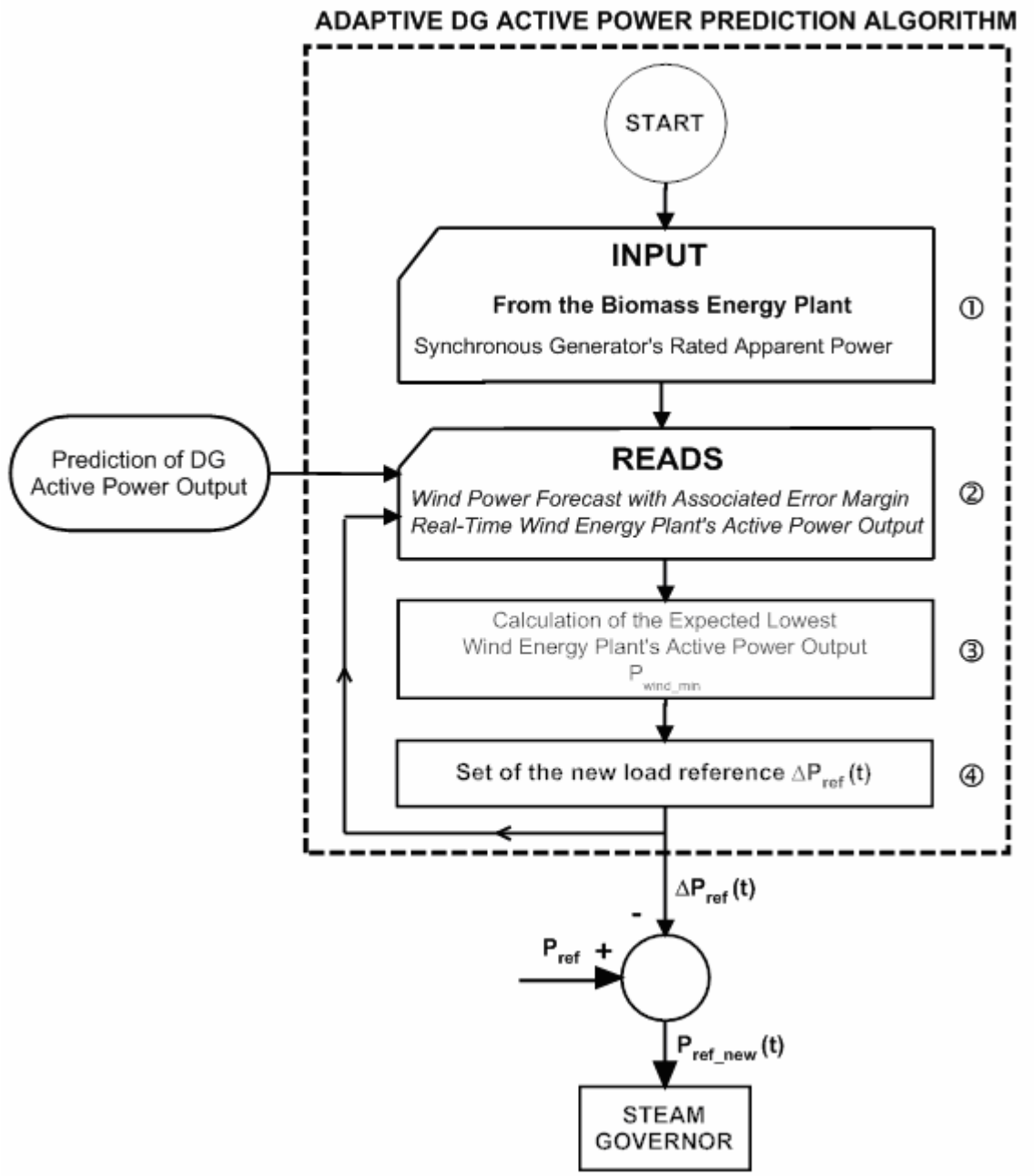

Figure 5.2 – Flowchart of the Adaptive DG Active Power Prediction Algorithm

It follows the detailed explanation of the Adaptive DG Active Power Prediction Algorithm. Firstly, it is necessary to input the synchronous generator's rated apparent power to enable the running of the Adaptive DG Active Power Prediction Algorithm at the specific biomass energy plant. Secondly, it starts the real-time closed loop of the Adaptive DG Active Power Prediction Algorithm. Every loop cycle, the Adaptive DG Active Power Prediction Algorithm reads the wind power forecast given by the wind power

forecast centre for the wind energy plant considered. This wind power forecast is given with an associated error margin based on the wind energy plant installed capacity, dependant on the desired look-ahead time for prediction. The Adaptive DG Active Power Prediction Algorithm also reads, every loop cycle, the real time wind energy plant's active power output, see ②.

Next, for the desired time in which DG's active power output is predicted, it is calculated the predicted lowest wind energy plant's active power output, see ③. The predicted lowest wind energy plant's active power output is obtained from the lowest wind power given by the wind power forecast, for the desired time.

Finally, the Adaptive DG Active Power Prediction Algorithm sets the biomass energy plant's load reference. The setting of the biomass energy plant's load reference consists in the subtraction from the old load reference, P_{ref}, of a real time quantity ΔP_{ref} (t+Δt). In ④, it is indicated the setting of ΔP_{ref} (t+Δt), which is given by the Eq. (5.1).

$$\Delta P_{ref}(t+\Delta t) = \frac{P_{wind\_actual}(t) - P_{wind\_min}}{S_{biomass}} \quad \text{[p.u.]} \qquad \text{Eq. (5.1)}$$

Where P_{wind_actual} (t) is the measured real-time active power output from the wind energy plant in W, P_{wind_min} is the predicted lowest active power output from the wind energy plant in W, $S_{biomass}$ is the rated apparent power of the biomass energy plant in VA.

5.3.2 – Comments on the Implementation of the Algorithm

The Adaptive DG Active Power Prediction Algorithm is a feedback control which, for a good performance, requires fast response capabilities of the biomass energy plant. In conventional wind energy plants, i.e. equipped with conventional induction generators, severe wind speed fluctuations conduct to equally severe fluctuations in the wind active power delivered to the network. These severe wind active power fluctuations conduct, with the use of the Adaptive DG Active Power Prediction Algorithm, to deviations from the nominal

angular speed of the biomass energy plant's synchronous generator, as shown in the Eq. (5.2).

$$\Delta\omega = \omega - \omega_{ref} = -\Delta P_{ref} \frac{1}{R^{-1} + D} \quad \text{[p.u.]} \qquad \text{Eq. (5.2)}$$

Where $\Delta\omega$ is the angular speed deviation from the reference angular speed ω_{ref} of the synchronous generator, ω is the real-time angular speed of the synchronous generator, R is the steam regulator's droop constant and D is the synchronous generator's damping constant.

The deviations from the nominal angular speed of the biomass energy plant and the consequent active power deviations should follow the wind active power fluctuations, in order to smooth the aggregated active power output. This objective is as well accomplished as faster the biomass energy plant responds to deviations from its nominal angular speed. However, it is not expected the biomass energy plant can fully respond to all the wind active power fluctuations, mainly due to the inertia constant of the synchronous generator.

5.4 – Adaptive DG Active Power Prediction Algorithm: Simulation Test

5.4.1 – Distribution Network Modelling

Figure 5.3 shows the distribution network considered in this work to simulate and validate the Adaptive DG Active Power Prediction Algorithm.

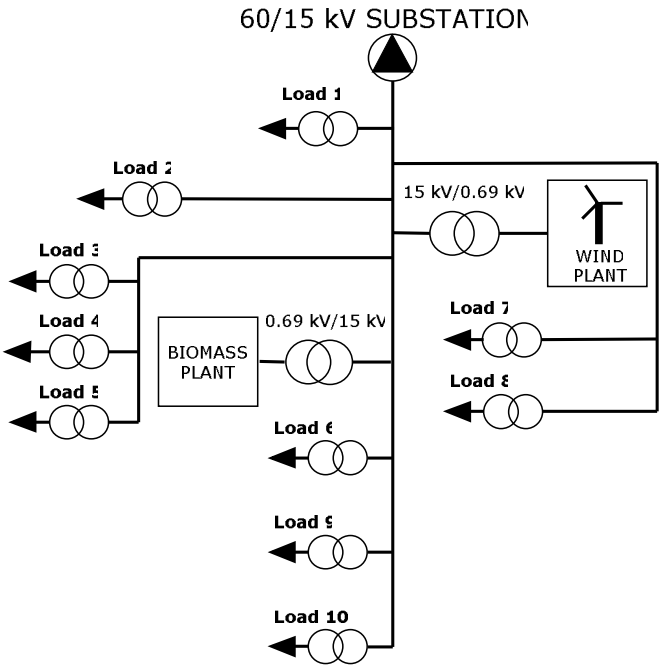

Figure 5.3 – Typical distribution network

The load active power demand, P_{load}, is 1.83 MW and the load reactive power demand, Q_{load}, is 0.37 MVAr, at the nominal voltage of 15 kV. Details are available in Appendix C.

The biomass energy plant considered in this work consists on a two pole synchronous generator [Kundur, 1994; Machowski et al., 1997], with an IEEE Type I DC exciter [IEEE, 2006]. The primary energy source for the biomass energy plant is the residual forest biomass. The steam regulating system is of digital electro-hydraulic technology, by Westinghouse [Prime Mover, 1991]. The prime mover is a non-reheat steam turbine, which can be described by a first order model. Further details are available in Appendix F.

The wind energy plant considered in this work consists on a fixed-speed pitch controlled wind turbine, connected to a conventional induction generator [Anderson & Bose, 1983; Burton et al., 2001; Fox et al., 2007]. The wind power models considered in this work, for simulation purposes, are based on a generic model for stability studies on wind turbine systems, which is fully described in [Anderson & Bose, 1983]. A capacitor bank, for power factor correction purposes, is included on the plant. Details are also available in Appendix F.

5.4.2 – Simulation with no-action of the Adaptive DG Active Power Prediction Algorithm

The following simulations refer to an hour of a generic day, on the distribution network shown on Figure 5.3. It is assumed to be known the wind power forecast for the look-ahead time of one hour. This wind power forecast is assumed to be given with 10% error margin based on the wind energy plant's installed capacity. Thus, the predicted wind power profile for the next hour, P_{wind} (t), is shown on Figure 5.4.

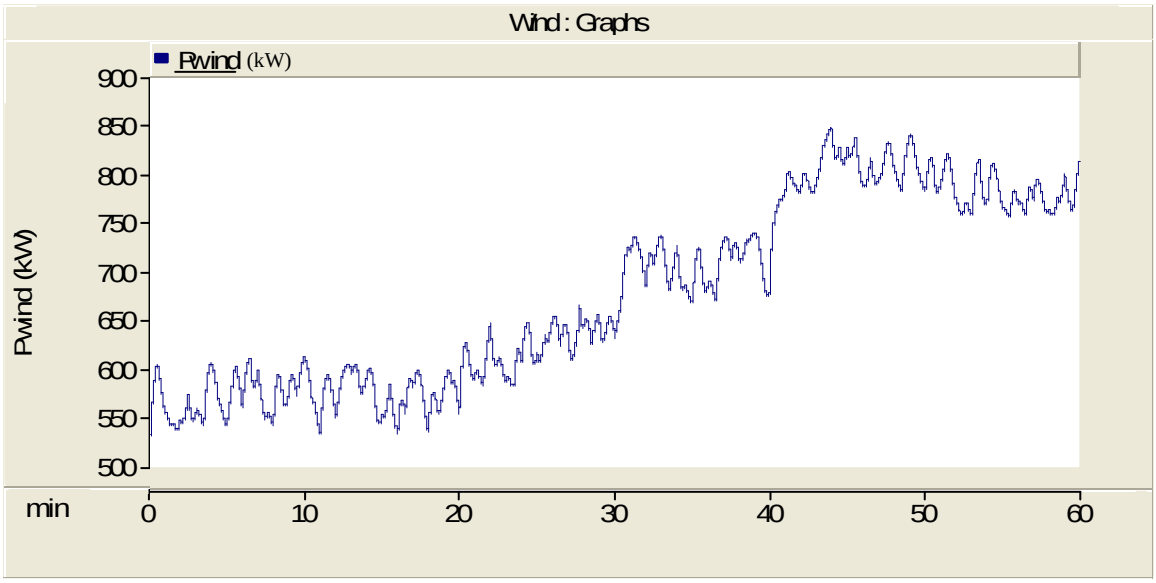

Figure 5.4 – Predicted wind power profile for the next hour P_{wind} (t)

Figures 5.5 and 5.6 show, in the hour considered, the active power required to the primary distribution substation, $P_{substation}$ (t), shown on Figure 5.3 ("60/15 kV Substation"). In both Figures 5.5 and 5.6, the biomass energy plant is set to produce at full-load and the wind energy plant is set to track the maximum wind active power utilization. However, Figure 5.5 shows $P_{substation}$ (t) being the wind power profile in the hour 5% higher than the wind power forecast P_{wind} (t), i.e., $1.05P_{wind}$ (t). Figure 5.6 shows $P_{substation}$ (t) being the wind power profile in the hour 5% lower than the wind power forecast P_{wind} (t), i.e., $0.95P_{wind}$ (t). $P_{substation}$ (t) is given in kW.

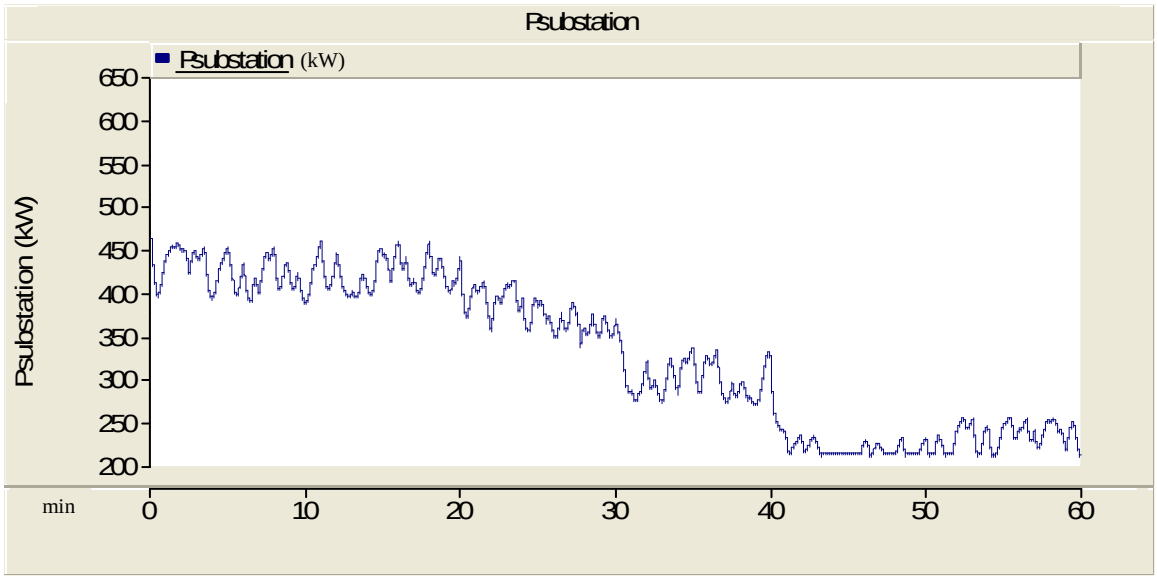

Figure 5.5 – $P_{substation}$ (t) in the hour considered, with 1.05P_{wind} (t)

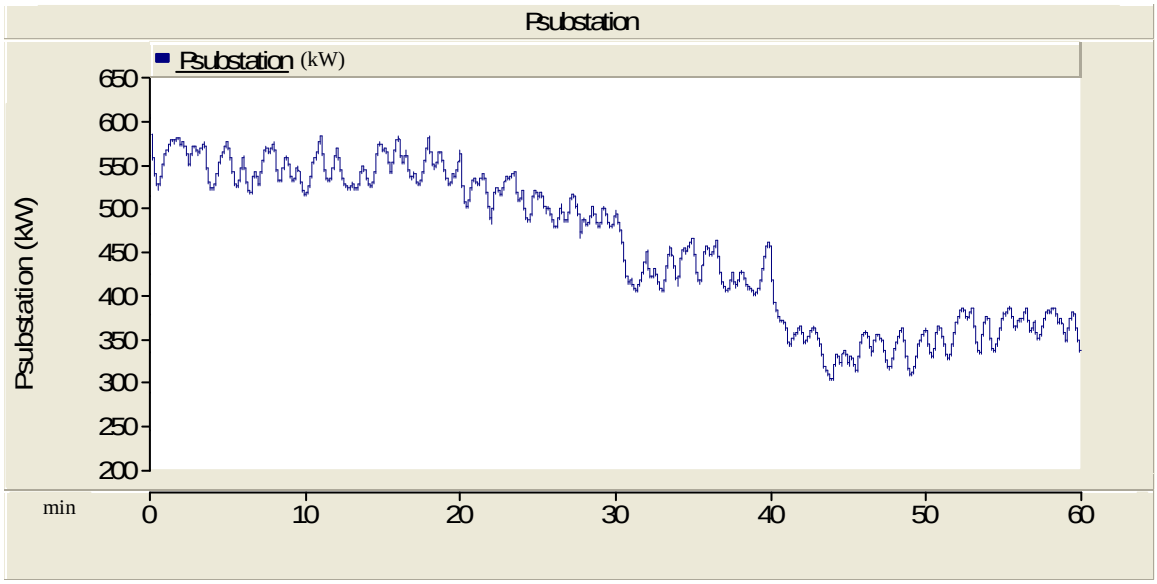

Figure 5.6 – $P_{substation}$ (t) in the hour considered, with 0.95P_{wind} (t)

Table 5.1 presents statistical information on the energy delivered in the hour considered by the DG's, at the conditions described for Figures 5.5 and 5.6.

TABLE 5.1

$P_{biomass}(t) + P_{wind\_actual}(t)$ IN THE HOUR CONSIDERED

$P_{biomass}(t)+ P_{wind\_actual}(t)$ With $1.05P_{wind}(t)$		$P_{biomass}(t)+ P_{wind\_actual}(t)$ With $0.95P_{wind}(t)$	
Mean Value for the Hour (kWh)		*Mean Value for the Hour (kWh)*	
1584,1671		1445,9323	
Average Absolute Deviation From the Mean Value for the Hour		*Average Absolute Deviation From the Mean Value for the Hour*	
(kWh)	(%)	(kWh)	(%)
85,9764	5,9465	85,7545	5,4132
Maximum Deviation from the Mean Value for the Hour		*Maximum Deviation from the Mean Value for the Hour*	
(kWh)	(%)	(kWh)	(%)
168,8696	11,6789	142,6379	9,0039

The mean value for the hour is given by the Eq. (5.3), where $x = (P_{biomass} + P_{wind\_actual})$ and the superscript _ refers to a mean value.

$$\bar{x} = \int_{t=0}^{t=1hour} f(x)dx \qquad \text{Eq. (5.3)}$$

The average absolute deviation from the mean value for the hour, *AAD*, is given by the Eq. (5.4).

$$AAD = \int_{t=0}^{t=1hour} \left| f(x - \bar{x}) \right| dx \qquad \text{Eq. (5.4)}$$

The maximum deviation from the mean value for the hour, *MD*, is given by the Eq. (5.5).

$$MD = \max_{t=0}^{t=1hour} \left[f(x - \bar{x}) \right] \qquad \text{Eq. (5.5)}$$

5.4.3 – Adaptive DG Active Power Prediction Algorithm Performance

The following simulations also refer to an hour of a generic day, on the distribution network shown on Figure 5.3. It is assumed the predicted wind power profile for the next hour is P_{wind} (t), which is given in Figure 5.4.

With the predicted wind power profile shown on Figure 5.4, it is calculated the predicted lowest wind energy plant's active power output, P_{wind_min}, for the next hour.

Figures 5.7 and 5.8 show $P_{substation}$ (t) with the use of the Adaptive DG Active Power Prediction Algorithm, in the hour considered. Figure 5.7 shows $P_{substation}$ (t), being the wind power profile in the hour 5% higher than the wind power forecast P_{wind} (t), i.e., 1.05P_{wind} (t). Figure 5.8 shows $P_{substation}$ (t), being the wind power profile in the hour 5% lower than the wind power forecast P_{wind} (t), i.e., 0.95P_{wind} (t). $P_{substation}$ (t) is given in kW.

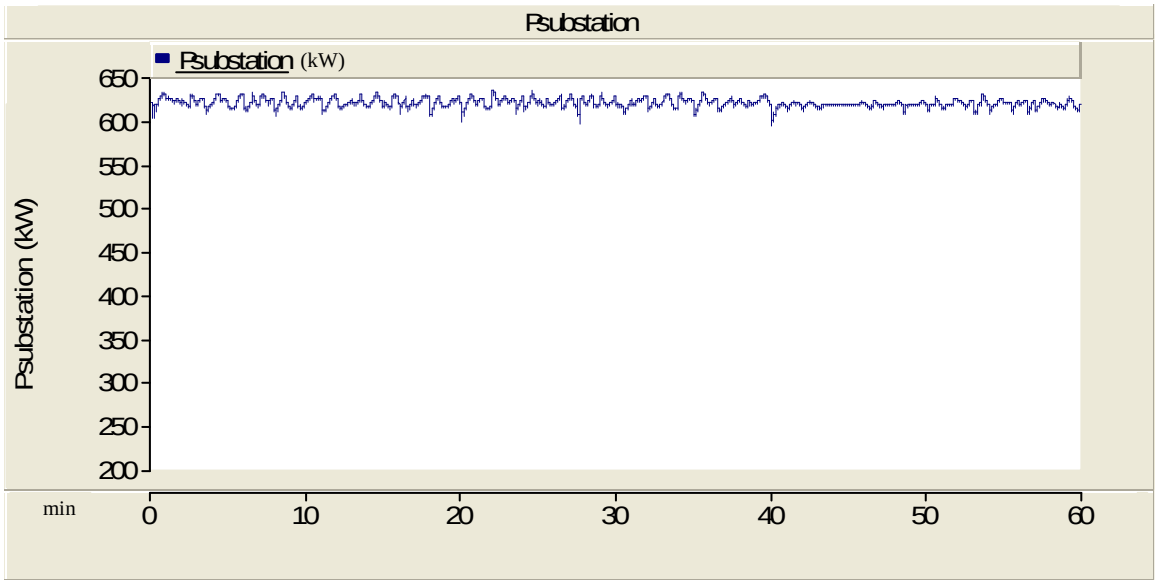

Figure 5.7 – $P_{substation}$ (t) with the Adaptive DG Active Power Prediction Algorithm in the hour considered, with 1.05P_{wind} (t)

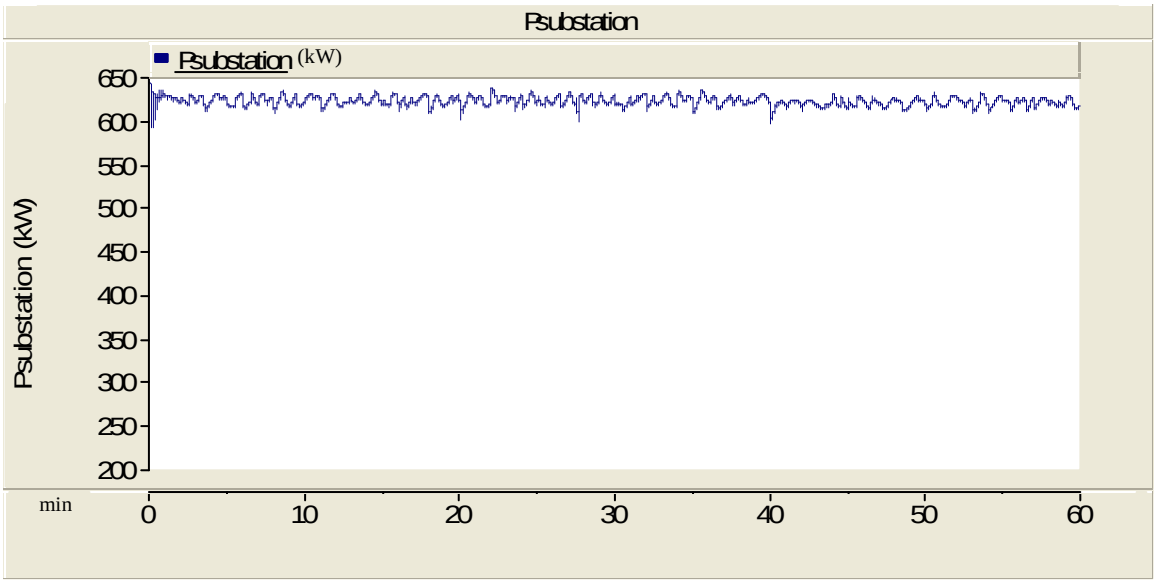

Figure 5.8 – $P_{substation}$ (t) with the Adaptive DG Active Power Prediction Algorithm in the hour considered, with 0.95P_{wind} (t)

Table 5.2 presents statistical information on the energy delivered in the hour considered by the DG's, at the conditions described for Figures 5.7 and 5.8, i.e., using the Adaptive DG Active Power Prediction Algorithm.

TABLE 5.2

$P_{biomass}$ (t) + P_{wind_actual} (t) IN THE HOUR CONSIDERED, WITH THE ADAPTIVE DG ACTIVE POWER PREDICTION ALGORITHM

$P_{biomass}$ (t)+ P_{wind_actual} (t) With 1.05P_{wind} (t)		$P_{biomass}$ (t)+ P_{wind_actual} (t) With 0.95P_{wind} (t)	
Mean Value for the Hour (kWh)		*Mean Value for the Hour (kWh)*	
1306,4581		1307,8956	
Average Absolute Deviation From the Mean Value for the Hour		*Average Absolute Deviation From the Mean Value for the Hour*	
(kWh)	(%)	(kWh)	(%)
4,1301	0,3161	3,6622	0,2800
Maximum Deviation from the Mean Value for the Hour		*Maximum Deviation from the Mean Value for the Hour*	
(kWh)	(%)	(kWh)	(%)
23,5052	1,7972	22,5143	1,7233

5.5 – Discussion on the Adaptive DG Active Power Prediction Algorithm

The aggregation of biomass and wind energy, done by the Adaptive DG Active Power Prediction Algorithm, can lead to an increase of secure renewable energy penetration on the distribution networks. The biomass energy's ability of storing and using the feedstocks whenever and wherever needed may represent an extra profit with the use of the Adaptive DG Active Power Prediction Algorithm, as the biomass primary energy can be saved in opposition to wind energy.

The use of the Adaptive DG Active Power Prediction Algorithm in the distribution network shown in Figure 5.3, in the hour considered, led to an increased amount of non delivered energy by the DG's comparatively with the case where the Adaptive DG Active Power Prediction Algorithm is not enabled. This increased non delivered energy varied, in average values, from 138 kWh to 277 kWh whether the wind power profile equalled $0.95P_{wind}$ (t) or $1.05P_{wind}$ (t) (extreme conditions) respectively, where P_{wind} (t) is the predicted wind power profile for the next hour. However, the Adaptive DG Active Power Prediction Algorithm increased the predictability of the delivered energy by the DG's, as it reduced significantly the average absolute deviation from the mean value of the delivered energy by the DG's.

The Adaptive DG Active Power Prediction Algorithm requires communication facilities for the provision of the wind power forecast and the real-time wind energy plant's active power output.

With the increase of secure renewable energy penetration on the distribution networks, the availability and reliability of the renewable sources will be improved. In consequence, network operation and expansion costs can be lowered and, in addiction, the increase of secure renewable energy penetration on distribution networks may lead the DG owners to go on the market. Thus, power systems can potentially accommodate increased levels of intermittent DG as the imbalances between generation and demand will not increase.

5.6 – Summary

This chapter presented an adaptive control of Distributed Generation to provide predictable active power output at the primary distribution substation.

The use of the Adaptive DG Active Power Prediction Algorithm led, in the validation of the algorithm, to an increased amount of non delivered energy by the DG's comparatively with the case where the Adaptive DG Active Power Prediction Algorithm is not enabled. Though, the Adaptive DG Active Power Prediction Algorithm provided a greater amount of predictable delivered energy by the aggregation of DG's, as it reduced significantly its average absolute deviation from the mean value. Hence, the aggregation of biomass and wind energy, done by the Adaptive DG Active Power Prediction Algorithm, can lead to an increased amount of secure renewable energy penetration on the distribution networks.

After an overview of the objectives of this study, it was detailed the modelling of the referred algorithm. In order to evaluate the performance of the algorithm, a typical 60/15 kV radial distribution network with the integration of distributed generators was simulated with the electromagnetic transient package PSCAD/EMTDC®. The technical performance of the algorithm on the simulated test network was shown. At last, it was analyzed and discussed the impact of the proposed algorithm in the simulated test network.

Chapter 6 – Cooperative Control to Provide Predictable Active Power Output

6.1 – Introduction

This chapter will present a cooperative control of Distributed Generation (DG) to provide predictable active power output at the primary distribution substation. An algorithm in which both wind and biomass energy plants cooperate to provide a smooth active power output profile at the primary distribution substation will be presented. The cooperative control aims to anticipate the active power output from the aggregation of wind and biomass energy at the primary distribution substation of a typical distribution network, knowing that biomass primary energy can be stored and transported whenever and where it is needed. It is assumed wind and biomass energy plants are onto the same distribution network but not necessarily onto the same feeder.

Firstly, it is detailed the modelling of the cooperative control algorithm. Then, in order to evaluate the performance of the algorithm, a typical 60/15 kV radial distribution network with the integration of distributed generators will be simulated with the electromagnetic transient package PSCAD/EMTDC®. The technical performance of the algorithm at the simulated test network will be exposed afterwards. Finally, it will be analyzed and discussed the impact of the proposed algorithm in the simulated test network.

6.2 – Cooperative DG Active Power Prediction Algorithm

6.2.1 – How the Algorithm was modelled?

The Cooperative DG Active Power Prediction Algorithm intends to predict the active power output at the primary distribution substation. The importance of achieving a predictable active power output is detailed in Section 5.2 of Chapter 5. The algorithm also tries to minimize the fluctuations in the active power output of the primary distribution substation. Located at the primary distribution substation, the algorithm controls hierarchically both non-intermittent and intermittent energy plants and, thus, predicts their active power output. The intermittent energy plant considered in this work is a doubly-fed induction generator, which is described in Chapter 2. The non-intermittent energy plant considered in this work is a typical biomass energy plant (i.e. equipped with steam turbine synchronous generation technology), which is described in Chapter 3.

The Cooperative DG Active Power Prediction Algorithm changes the biomass energy plant's load reference to follow the variations of the wind energy plant's active power output; the wind energy plant, by an inertia term defined by the Cooperative DG Active Power Prediction Algorithm, smoothes its own active power production – this is done in order to allow a more compatible response of the biomass energy plant to active power fluctuations from the wind energy plant. Thus, the cooperation of biomass and wind energy plants tends to minimize the fluctuations of the primary distribution substation's active power output.

Figure 6.1 shows the block diagram of the Cooperative DG Active Power Prediction Algorithm.

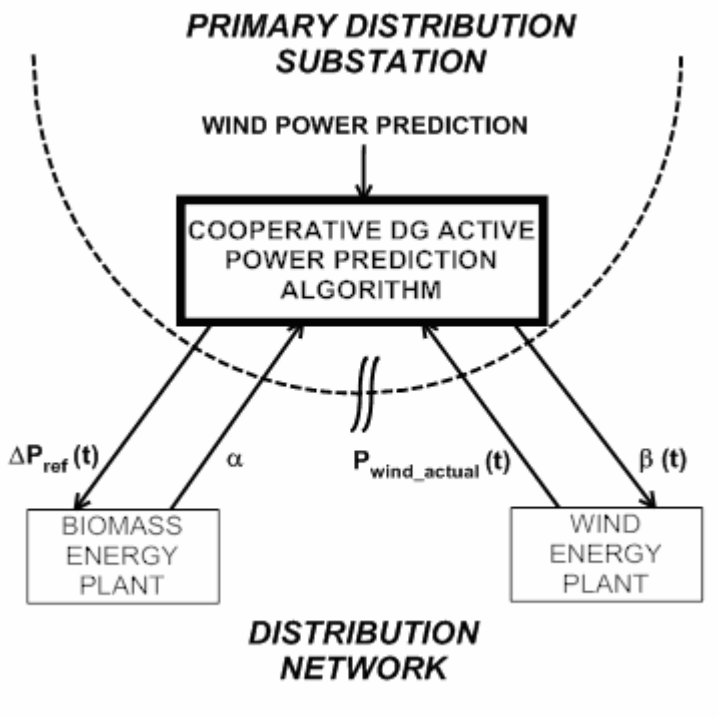

Figure 6.1 – Block Diagram of the Cooperative DG Active Power Prediction Algorithm

In Figure 6.1, *α* refers to the communication of the synchronous generator rated power, $S_{biomass}$, and the value of the total inertia of the biomass energy plant, $H_{total\_biomass}$; *β(t)* refers to the following expression: $H_{total\_biomass} \cdot \frac{dP_{wind\_actual}(t)}{dt}$.

The Cooperative DG Active Power Prediction Algorithm changes the biomass energy plant's load reference as shown in Figure 6.2 b).

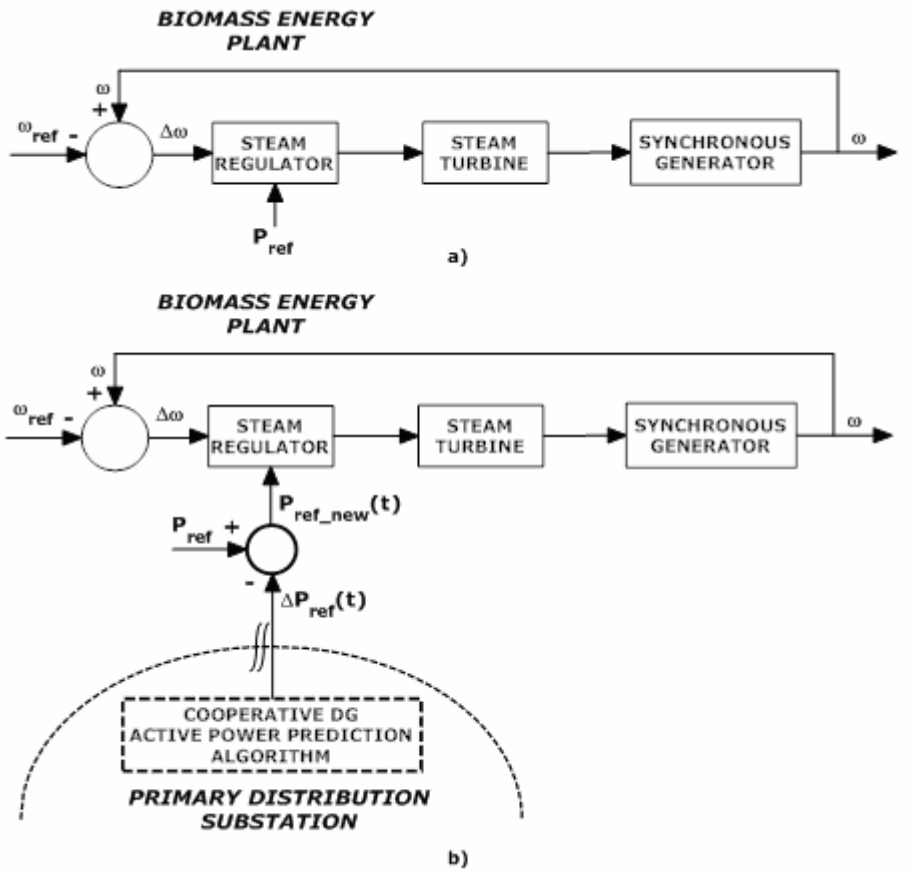

Figure 6.2 – a) Load Frequency Control Block Diagram of the Biomass Energy Plant; b) Load Frequency Control Block Diagram of the Biomass Energy Plant with the Cooperative DG Active Power Prediction Algorithm

The setting of the quantity ΔP_{ref} (t) is not done locally at the biomass energy plant, but in the primary distribution substation, at a hierarchically superior level, which is where the algorithm is located.

The Cooperative DG Active Power Prediction Algorithm changes the wind energy plant's active power production as shown in Figure 6.3 b), by acting at the angular speed control loop.

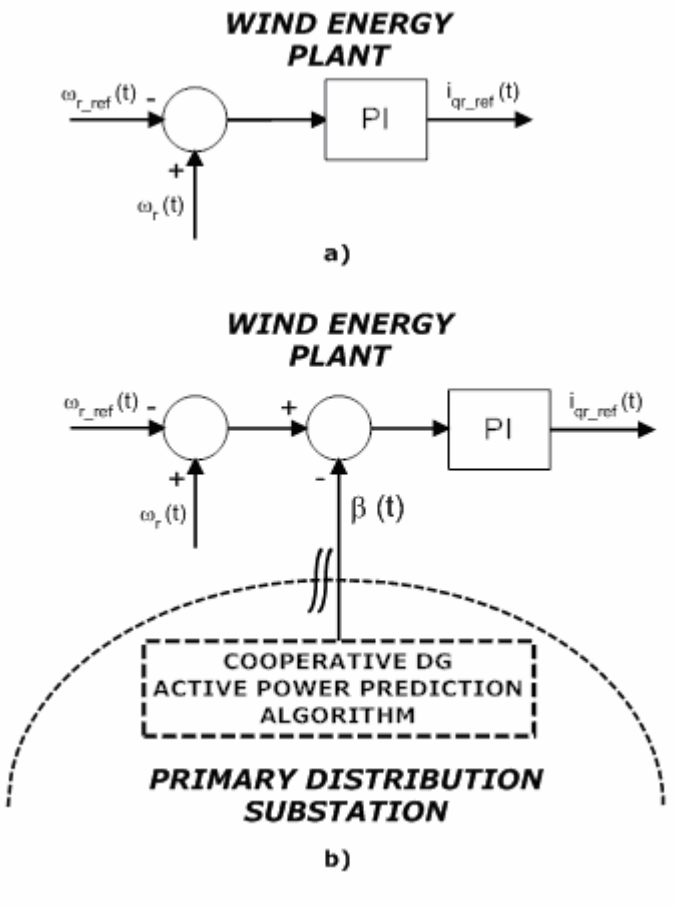

Figure 6.3 – a) Part of the Angular Speed Control Loop of the Wind Energy Plant; b) Part of the Angular Speed Control Loop of the Wind Energy Plant with the Cooperative DG Active Power Prediction Algorithm

Where ω_r is the rotor angular speed of the wind energy plant, ω_{r_ref} is the reference rotor angular speed and i_{qr_ref} is the reference quadrature rotor injected current.

As wind speed variations produce active power fluctuations at the output of the wind energy plant and, consequently, at the output of the primary substation, the Cooperative DG Active Power Prediction sets either biomass and wind energy plants to cooperate for a predictable active power output at the primary distribution substation. Figure 6.4 presents the flowchart associated to the Cooperative DG Active Power Prediction Algorithm.

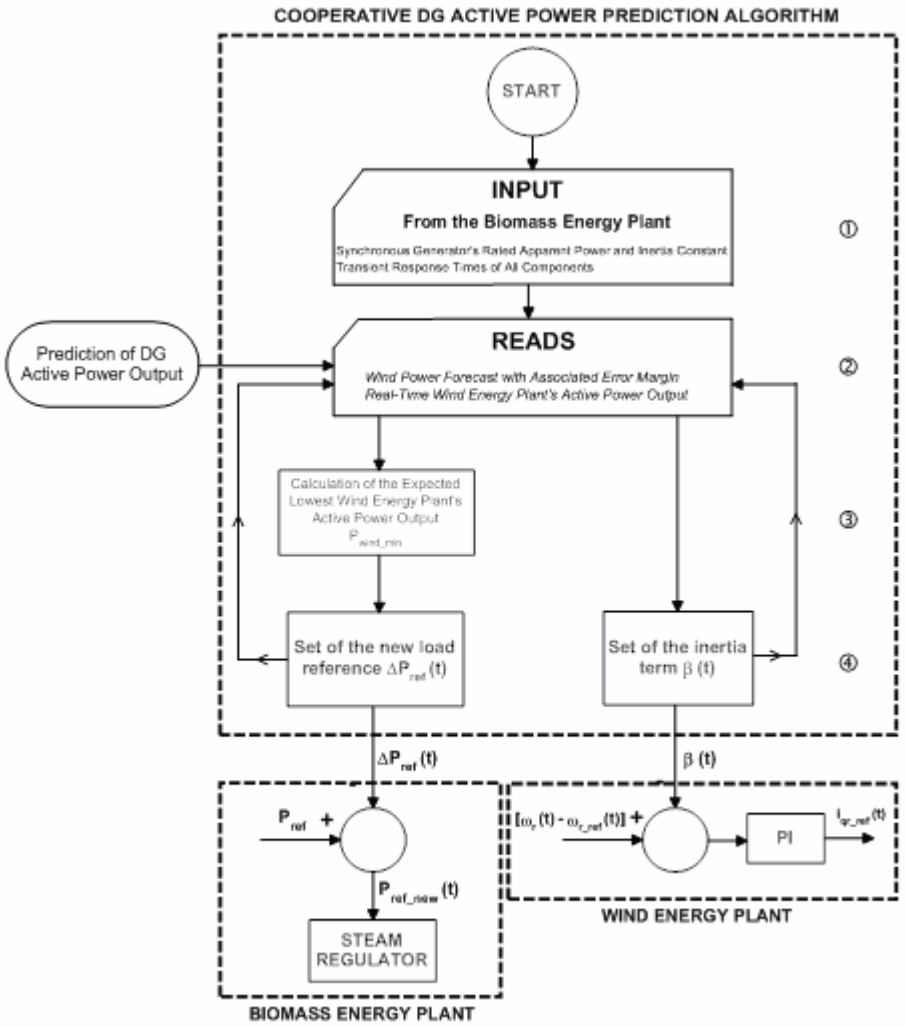

Figure 6.4 – Flowchart of the Cooperative DG Active Power Prediction Algorithm

It follows the detailed explanation of the Cooperative DG Active Power Prediction Algorithm. Firstly, from the biomass energy plant, it is necessary to input the rated apparent power of the synchronous generator, $S_{biomass}$, and the transient response times associated to the biomass energy plant, that is, the inertia constant of the synchronous generator, $H_{generator}$, and the transient response times of the other components, which will be correlated by the Eq. (6.1).

$$H_{total\_biomass} = H_{generator} + t_{turbine} + t_{regulator} \quad [s] \qquad \text{Eq. (6.1)}$$

Where $t_{turbine}$ and $t_{regulator}$ are the steam turbine and steam regulator transient response times (in seconds) to a load input, respectively. The input of

$S_{biomass}$ and $H_{total\_biomass}$ is fundamental to enable the running of the Cooperative DG Active Power Prediction Algorithm at the specific biomass energy plant.

Secondly, it starts the real-time closed loop of the Cooperative DG Active Power Prediction Algorithm. Every loop cycle, the Cooperative DG Active Power Prediction Algorithm reads the wind power forecast given by the wind power forecast centre for the wind energy plant considered. This wind power forecast is transmitted with an associated error margin based on the wind energy plant characteristics and installed capacity, dependant on the desired look-ahead time for prediction. The Cooperative DG Active Power Prediction Algorithm also reads, every loop cycle, the real-time wind energy plant's active power output, $P_{wind\_actual}(t)$, see ②.

Next, for the desired time in which DG's active power output is predicted, it is calculated the predicted lowest wind energy plant's active power output, P_{wind_min}, see ③. The predicted lowest wind energy plant's active power output is obtained from the lowest wind power given by the wind power forecast, for the desired time.

Finally, the Cooperative DG Active Power Prediction Algorithm sets the biomass energy plant's load reference and the wind energy plant's active power production reference. The setting of the biomass energy plant's load reference consists in the subtraction from the old load reference, P_{ref}, of a real time quantity $\Delta P_{ref}(t+\Delta t)$. In ④, it is indicated the setting of $\Delta P_{ref}(t+\Delta t)$, which is given by the Eq. (6.2).

$$\Delta P_{ref}(t+\Delta t) = \frac{P_{wind\_actual}(t) - P_{wind\_min}}{S_{biomass}} \quad \text{[p.u.]} \qquad \text{Eq. (6.2)}$$

Where P_{wind_actual} (t) is the measured real-time active power output from the wind energy plant in W, P_{wind_min} is the predicted lowest active power output from the wind energy plant in W, $S_{biomass}$ is the rated apparent power of the biomass energy plant in VA.

The setting of the wind energy plant's active power production reference set-point by the Cooperative DG Active Power Prediction Algorithm is done by

means of an alteration on the angular speed control loop (which controls active power output): the addiction of a supplementary control loop, see Figure 6.5.

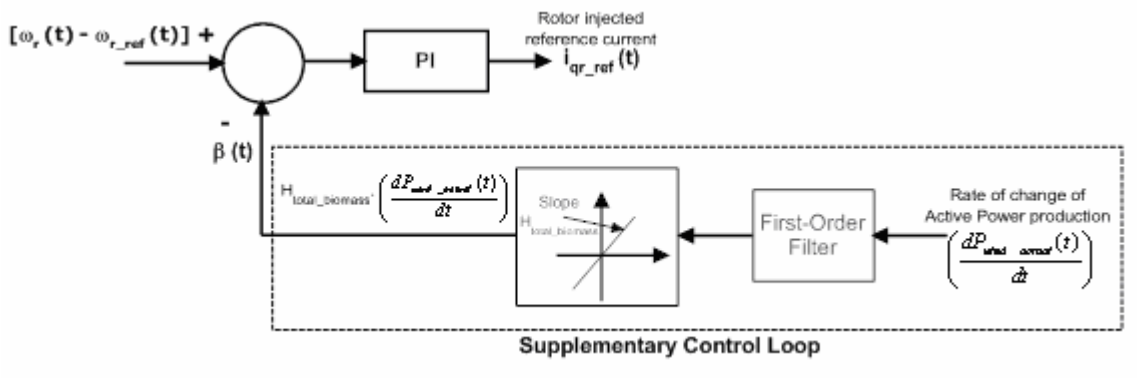

Figure 6.5 – Supplementary control loop for wind energy plant's active power production

This supplementary control loop introduces a change to the angular speed set-point such as to subtract, every loop cycle, the term $H_{total\_biomass} \cdot \frac{dP_{wind\_actual}(t)}{dt}$, creating a synthesised inertia effect. This synthesized inertia effect has the goal of allowing a better response of the biomass energy plant to the wind energy plant's active power fluctuations. The supplementary control loop smoothes the wind energy plant's active power production with an inertia equivalent to the total inertia of the biomass energy plant, $H_{total\_biomass}$. Therefore, the biomass energy plant's response to the active power fluctuations from the wind energy plant will be more efficient than in the other case – with no supplementary control loop. The first-order filter shown in Figure 6.5 has the purpose of not only reducing noise and the rate of increase of the angular speed $\omega_r(t)$, minimizing mechanical stresses, but also reducing the magnitude of the peak angular speed.

6.2.2 – Comments on the Implementation of the Algorithm

The Cooperative DG Active Power Prediction Algorithm is a feedback control which, for a good performance, requires fast response capabilities of the biomass energy plant. Wind energy plant's active power fluctuations conduct, with the use of the Cooperative DG Active Power Prediction Algorithm, to

deviations from the nominal angular speed of the biomass energy plant's synchronous generator, as shown in the Eq. (6.3).

$$\Delta\omega = \omega - \omega_{ref} = -\Delta P_{ref} \frac{1}{R^{-1} + D} \quad \text{[p.u.]} \qquad \text{Eq. (6.3)}$$

Where $\Delta\omega$ is the angular speed deviation from the reference angular speed ω_{ref} of the synchronous generator, ω is the real-time angular speed of the synchronous generator, R is the steam regulator's droop constant and D is the synchronous generator's damping constant.

The deviations from the nominal angular speed of the biomass energy plant and the consequent active power deviations should follow the wind active power fluctuations, in order to attenuate the aggregated active power output. This objective is as well accomplished as faster the biomass energy plant responds to deviations from its nominal angular speed.

In the wind energy plant, the Cooperative DG Active Power Prediction Algorithm uses the control of power converters (by means of angular speed/frequency control) instead of blade pitch angle control for the active power production control. Blade pitch angle control is likely to be preferred for occasional frequency response as it allows large, rapid changes in output active power. However, it implies de-loading of wind energy production, which is not attractive in continuous frequency response as no fuel savings result from this action, incurring in a waste of energy. The control of the power converters, despite being only possible over a narrow active power range, may be useful, as suggested in this work, to alter output active power for continuous frequency response. The addition of the supplementary control loop, shown in Figure 6.5, does not require the wind turbine to be de-loaded and the kinetic energy induced (with a magnitude equivalent to the global inertia of the biomass energy plant) seems to have a negligible impact on the rotational speed and hence performance of the aerodynamic wind turbine rotor. Finally, as no moving parts are involved in the control of the power converters, it may be advantageous in opposition to the blade pitch angle control, as relatively insignificant mechanical issues are expected from this strategy.

6.3 – Cooperative DG Active Power Prediction Algorithm: Simulation Test

6.3.1 – Distribution Network Modelling

The distribution network considered in this work to simulate and validate the Cooperative DG Active Power Prediction Algorithm is the one shown in Figure 5.3, i.e., is the same distribution network used in Chapter 5.

The biomass energy plant considered in this work consists on a two pole synchronous generator [Kundur, 1994; Machowski et al., 1997], with an IEEE Type I DC exciter [IEEE, 2006]. The primary energy source for the biomass energy plant is the residual forest biomass. The steam regulating system is of digital electro-hydraulic technology, by Westinghouse [Prime Mover, 1991]. The prime mover is a non-reheat steam turbine, which can be described by a first order model. Further details are available in Appendix G.

The wind energy plant considered in this work consists on a pitch controlled doubly-fed induction generator [Anderson & Bose, 1983; Pena et al., 1996; Nunes et al., 2004]. The wind power models considered in this work, for simulation purposes, are based on a generic model for stability studies on wind turbine systems, which is fully described by Anderson and Bose [1983]. Details are also available in Appendix G.

6.3.2 – Simulation with no-action of the Cooperative DG Active Power Prediction Algorithm

The following simulations refer to an hour of a generic day, on the distribution network shown on Figure 5.3. It is assumed to be known the wind power forecast for the look-ahead time of one hour. This wind power forecast is assumed to be given with 10% error margin based on the wind energy plant's characteristics and installed capacity. Thus, the predicted wind power profile for the next hour, P_{wind} (t), is shown on Figure 6.6.

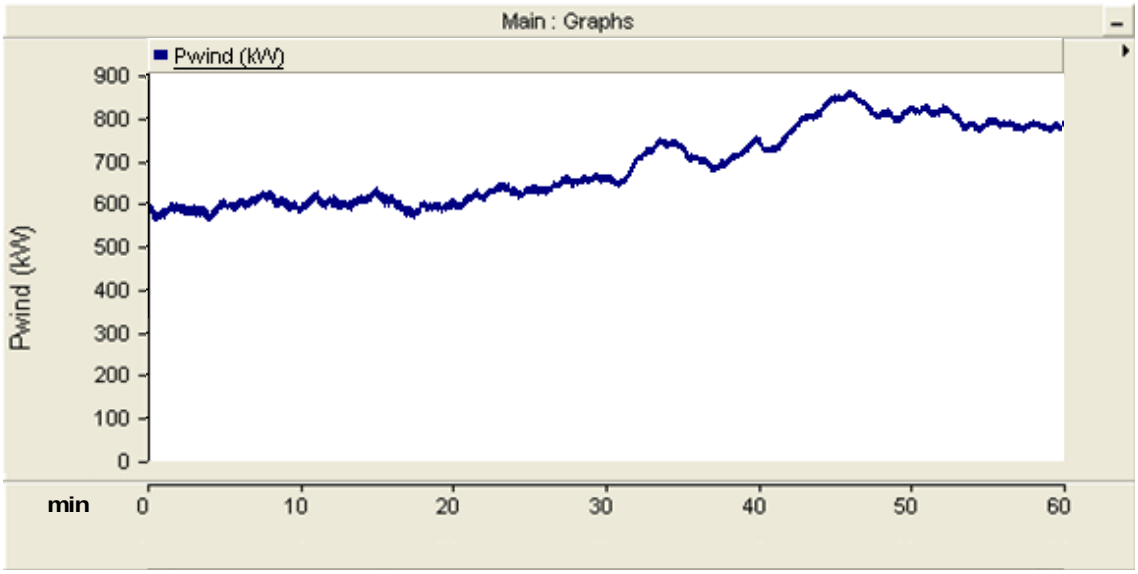

Figure 6.6 – Predicted wind power profile for the next hour P_{wind} (t)

Figures 6.7 and 6.8 show, in the hour considered, the active power required to the primary distribution substation, $P_{substation}$ (t), shown on Figure 5.3 ("60/15 kV Substation"). In both Figures 6.7 and 6.8, the biomass energy plant is set to produce at full-load and the wind energy plant is set to track the maximum wind active power utilization. However, Figure 6.7 shows $P_{substation}$ (t) being the wind power profile in the hour 5% higher than the wind power forecast P_{wind} (t), i.e., $1.05P_{wind}$ (t). Figure 6.9 shows $P_{substation}$ (t) being the wind power profile in the hour 5% lower than the wind power forecast P_{wind} (t), i.e., $0.95P_{wind}$ (t). $P_{substation}$ (t) is given in kW.

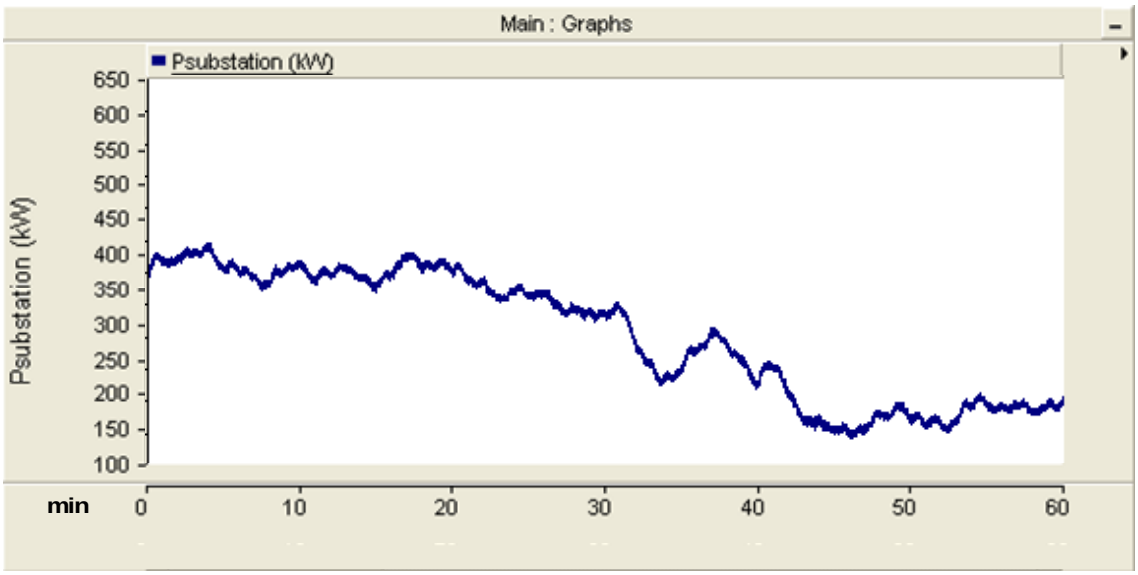

Figure 6.7 – $P_{substation}$ (t) in the hour considered, with $1.05P_{wind}$ (t)

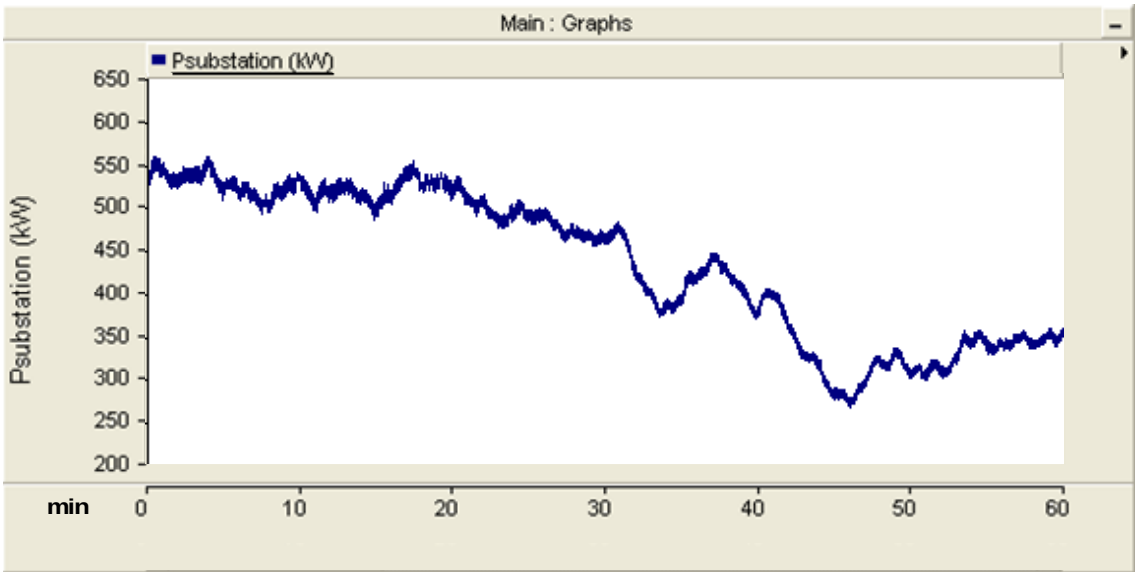

Figure 6.8 – $P_{substation}$ (t) in the hour considered, with 0.95P_{wind} (t)

Table 6.1 presents statistical information on the energy delivered in the hour considered by the DG's, at the conditions described for Figure 6.7 and Figure 6.8.

TABLE 6.1

$P_{biomass}$ (t) + P_{wind_actual} (t) IN THE HOUR CONSIDERED

$P_{biomass}$ (t)+ P_{wind_actual} (t) With 1.05P_{wind} (t)		$P_{biomass}$ (t)+ P_{wind_actual} (t) With 0.95P_{wind} (t)	
Mean Value for the Hour (kWh)		*Mean Value for the Hour (kWh)*	
1592,4752		1454,1433	
Average Absolute Deviation From the Mean Value for the Hour		*Average Absolute Deviation From the Mean Value for the Hour*	
(kWh)	(%)	(kWh)	(%)
93,4031	5,8653	80,5784	5,5413
Maximum Deviation from the Mean Value for the Hour		*Maximum Deviation from the Mean Value for the Hour*	
(kWh)	(%)	(kWh)	(%)
169,94	10,6715	174,6730	12,0121

The mean value for the hour is given by the Eq. (6.4), where $x = (P_{biomass} + P_{wind\_actual})$ and the superscript _ refers to a mean value.

$$\bar{x} = \int_{t=0}^{t=1hour} f(x)dx \qquad \text{Eq. (6.4)}$$

The average absolute deviation from the mean value for the hour, *AAD*, is given by the Eq. (6.5).

$$AAD = \int_{t=0}^{t=1hour} \left| f(x - \bar{x}) \right| dx \qquad \text{Eq. (6.5)}$$

The maximum deviation from the mean value for the hour, *MD*, is given by the Eq. (6.6).

$$MD = \max_{t=0}^{t=1hour} \left[f(x - \bar{x}) \right] \qquad \text{Eq. (6.6)}$$

6.3.3 – Cooperative DG Active Power Prediction Algorithm Performance

The following simulations also refer to an hour of a generic day, on the distribution network shown on Figure 5.3. It is assumed the predicted wind power profile for the next hour is $P_{wind}(t)$, which is given by the Figure 6.6.

With the predicted wind power profile shown on Figure 6.6, it is calculated the predicted lowest wind energy plant's active power output, P_{wind_min}, for the next hour. With the reading of the real-time wind energy plant's active power output, $P_{wind\_actual}(t)$, it can be set the inertia term $\beta(t)$.

Figures 6.9 and 6.10 show $P_{substation}(t)$ with the use of the Cooperative DG Active Power Prediction Algorithm, in the hour considered. Figure 6.9 shows $P_{substation}(t)$, being the wind power profile in the hour 5% higher than the wind power forecast $P_{wind}(t)$, i.e., $1.05P_{wind}(t)$. Figure 6.10 shows $P_{substation}(t)$, being the wind power profile in the hour 5% lower than the wind power forecast $P_{wind}(t)$, i.e., $0.95P_{wind}(t)$. $P_{substation}(t)$ is given in kW.

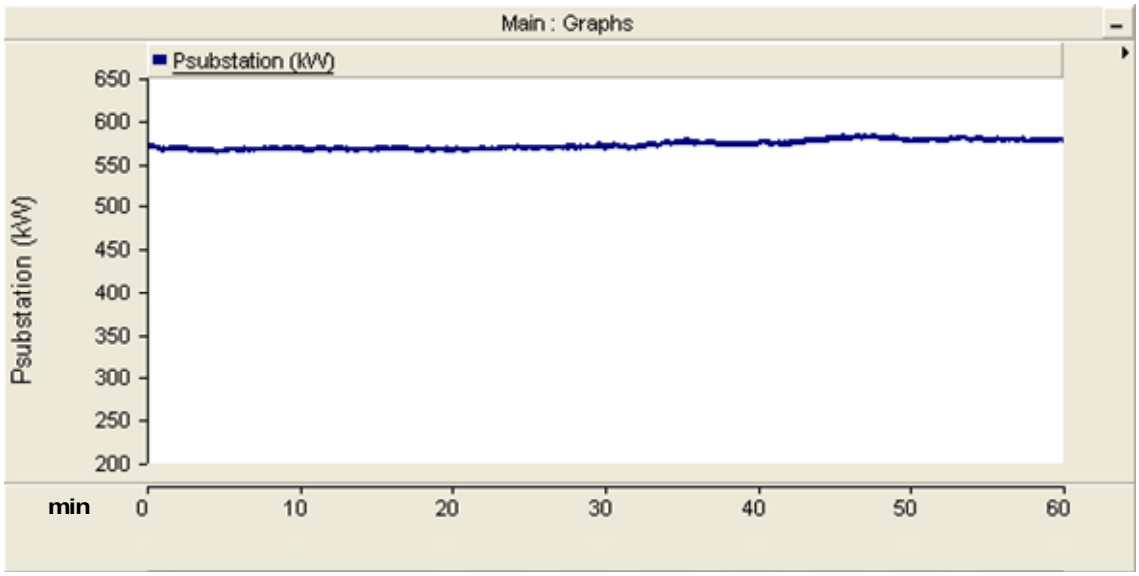

Figure 6.9 – $P_{substation}$ (t) with the Cooperative DG Active Power Prediction Algorithm in the hour considered, with 1.05P_{wind} (t)

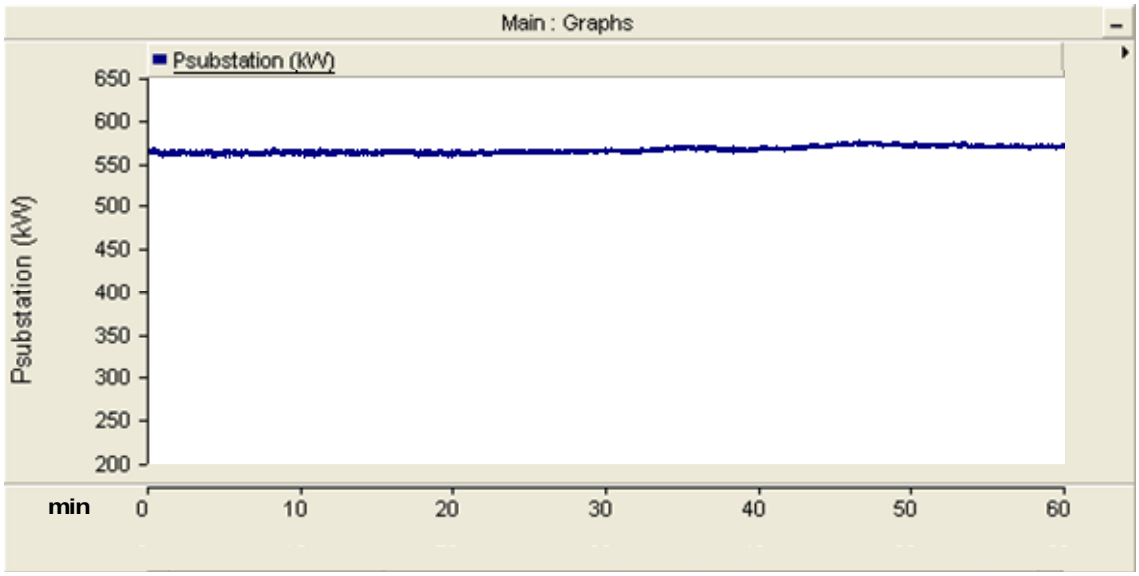

Figure 6.10 – $P_{substation}$ (t) with the Cooperative DG Active Power Prediction Algorithm in the hour considered, with 0.95P_{wind} (t)

Table 6.2 presents statistical information on the energy delivered in the hour considered by the DG's, at the conditions described for Figure 6.9 and Figure 6.10, i.e., using the Cooperative DG Active Power Prediction Algorithm.

TABLE 6.2

$P_{biomass}$ (t) + P_{wind_actual} (t) IN THE HOUR CONSIDERED, WITH THE COOPERATIVE DG ACTIVE POWER PREDICTION ALGORITHM

$P_{biomass}$ (t)+ $P_{wind\ actual}$ (t) With 1.05P_{wind} (t)		$P_{biomass}$ (t)+ $P_{wind\ actual}$ (t) With 0.95P_{wind} (t)	
Mean Value for the Hour (kWh)		*Mean Value for the Hour (kWh)*	
1322,3024		1324,2849	
Average Absolute Deviation From the Mean Value for the Hour		*Average Absolute Deviation From the Mean Value for the Hour*	
(kWh)	(%)	(kWh)	(%)
1,8108	0,1369	1,5499	0,1170
Maximum Deviation from the Mean Value for the Hour		*Maximum Deviation from the Mean Value for the Hour*	
(kWh)	(%)	(kWh)	(%)
7,9242	0,5993	7,6048	0,5743

6.4 – Discussion on the Cooperative DG Active Power Prediction Algorithm

The aggregation of biomass and wind energy, done by the Cooperative DG Active Power Prediction Algorithm, can lead to an increase of secure renewable energy penetration on the distribution networks. The biomass energy's ability of storing and using the feedstocks whenever and wherever needed may represent an extra profit with the use of the Cooperative DG Active Power Prediction Algorithm, as the biomass primary energy can be saved in opposition to wind energy.

The use of the Cooperative DG Active Power Prediction Algorithm in the distribution network shown in Figure 5.3, in the hour considered, led to an increased amount of non delivered energy by the DG's comparatively with the case where the Cooperative DG Active Power Prediction Algorithm is not enabled. This increased non delivered energy varied, in average values, from 130 kWh to 270 kWh whether the wind power profile equalled 0.95P_{wind} (t) or 1.05P_{wind} (t) (extreme conditions) respectively, where P_{wind} (t) is the predicted wind power profile for the next hour. However, the Cooperative DG Active Power Prediction Algorithm increased the predictability of the delivered energy by the DG's, as it reduced significantly the average absolute deviation from the mean value of the delivered energy by the DG's. Moreover, simulations seemed

to confirm that the introduction of the inertia effect did not have a significant impact on the aerodynamics of the wind turbine rotor.

The Cooperative DG Active Power Prediction Algorithm requires communication facilities between the DG's and the primary distribution substation, which is where the algorithm is located, and between the primary distribution substation and the wind power forecast centre, for the provision of the hour-ahead wind power forecast.

With the increase of secure renewable energy penetration on the distribution networks, the availability and reliability of the renewable sources will be improved. In consequence, network operation and expansion costs can be lowered and, in addiction, the increase of secure renewable energy penetration on distribution networks may lead the DG owners to go on the market. Thus, power systems can potentially accommodate increased levels of intermittent DG as the imbalances between generation and demand will not increase.

6.5 – Summary

This chapter presented a cooperative control of Distributed Generation to provide predictable active power output at the primary distribution substation. The use of the Cooperative DG Active Power Prediction Algorithm led, in the validation of the algorithm, to an increased amount of non delivered energy by the DG's comparatively with the case where the Cooperative DG Active Power Prediction Algorithm is not enabled. However, the Cooperative DG Active Power Prediction Algorithm increased the predictability of the delivered energy by the DG's, as it reduced significantly its average absolute deviation from the mean value. Comparing with the Adaptive DG Active Power Prediction Algorithm, detailed in Chapter 5, the average absolute deviation from the mean value as well as the maximum deviation from the mean value of the delivered energy by the DG's decreased, in percent values.

After a brief outline of cooperative control of distributed generation, it was detailed in this chapter the modelling of the referred algorithm. In order to evaluate the performance of the algorithm, a typical 60/15 kV radial distribution network with the integration of distributed generators was simulated with the electromagnetic transient package PSCAD/EMTDC®. The technical performance of the algorithm on the simulated test network was shown. Finally, it was analyzed and discussed the impact of the proposed algorithm in the simulated test network.

Chapter 7 – Conclusions and Future Work

7.1 – Final Remarks

With the work developed in this dissertation, it is possible to withdraw the following conclusions.

1. **The use of meta-heuristics in the tuning of the rotor side converter's PI controllers (detailed in Chapter 4):**

- The use of Particle Swarm Optimization (PSO) and Evolutionary Particle Swarm Optimization (EPSO) in the tuning of the rotor side converter's PI controllers conduced not only to feasible but also to very good solutions in both algorithms, in steady-state operation;
- The use of these meta-heuristics, hence, has avoided successfully the use of the classic control theory techniques, such as Ziegler-Nichols method, for example, which could have been difficult due to the nonlinearity and high complexity of the system;
- EPSO seemed to achieve fitter and quicker results than PSO, which may result from the self-adaptive character of the strategic parameters in EPSO, that increase the search space roaming. In PSO, the strategic parameters are more "case dependant" and, thus, difficult to adjust;
- Other reason why EPSO achieved better results than PSO seemed to be the increased capability of roaming the search space and, therefore, new possible solutions, by means of the communication factor that only communicates the best fitness so far to a part of the population, each iteration.

2. **The Adaptive DG Active Power Prediction Algorithm (detailed in Chapter 5):**

- The Adaptive DG Active Power Prediction Algorithm, located at the non-intermittent energy plant, i.e. the biomass energy plant, predicted

the active power output of the primary distribution substation in the hour considered, by only acting upon the biomass energy plant. From this action derives the name “Adaptive”, as no extra control with this purpose is required to the wind energy plant;

- The Adaptive DG Active Power Prediction Algorithm is a feedback control which, for a good performance, requires fast response capabilities of the non-intermittent energy plant, in this case, the biomass energy plant;
- The Adaptive DG Active Power Prediction Algorithm requires communication facilities between the DG’s, in this case, between the biomass and wind energy plants, and between the wind energy plant and the wind power forecast centre, for the provision of the hour-ahead wind power forecast;
- Mainly due to the lower inertia of the wind energy plant versus the inertia of the biomass energy plant, the Adaptive DG Active Power Prediction Algorithm, via the biomass energy plant, could not provide full response to all the wind active power fluctuations;
- The use of the Adaptive DG Active Power Prediction Algorithm in the distribution network implemented in Chapter 5, in the hour considered, led to an increased amount of non delivered energy by the DG’s comparatively with the case where the Adaptive DG Active Power Prediction Algorithm is not enabled. This increased non delivered energy varied, in average values, from 138 kWh to 277 kWh whether the wind power profile equalled $0.95P_{wind}$ (t) or $1.05P_{wind}$ (t) (extreme conditions) respectively, where P_{wind} (t) is the predicted wind power profile for the next hour;
- The use of the Adaptive DG Active Power Prediction Algorithm in the distribution network implemented in Chapter 5 in the hour considered, on the other hand, increased the predictability of the energy delivered by the aggregation of DG’s, which can be measured by the absolute average deviation and maximum deviation from the mean value indicators of Tables 5.1 and 5.2 of Chapter 5.

3. **The Cooperative DG Active Power Prediction Algorithm (detailed in Chapter 6):**

- The Cooperative DG Active Power Prediction Algorithm, located at the primary distribution substation and, thus, with a hierarchical control over the DG's local controls, provided predictable active power output at the primary distribution substation in the hour considered, in which both biomass and wind energy plants cooperated on this effort. From this cooperation is originated the name "Cooperative";
- The Cooperative DG Active Power Prediction Algorithm is a feedback control which, for a good performance, requires fast response capabilities of the non-intermittent energy plant, in this case, the biomass energy plant;
- The Cooperative DG Active Power Prediction Algorithm, to smooth the active power production of the wind energy plant, uses the control of the rotor side power converters, instead of the blade pitch angle control. This may be advantageous as no moving parts are involved and a negligible impact on the performance of the aerodynamic wind turbine rotor derived from the simulations, avoiding a de-load from the wind energy plant;
- The Cooperative DG Active Power Prediction Algorithm requires communication facilities between the DG's and the primary distribution substation, which is where the algorithm is located, and between the primary distribution substation and the wind power forecast centre, for the provision of the hour-ahead wind power forecast;
- The inertia effect introduced by the supplementary control loop shown in the Figure 6.5 of Chapter 6 conduced to an improved predictability of the active power output at the primary distribution substation, comparatively with the Adaptive DG Active Power Prediction Algorithm. This can be measured by the absolute average deviation and maximum deviation from the mean value indicators of Tables 5.1 and 5.2 of Chapter 5 and Tables 6.1 and 6.2 of Chapter 6. Although, it must be noted that the inclusion of this supplementary control loop is

not possible in the conditions of the Adaptive DG Active Power Prediction Algorithm, as a conventional generator is used instead of a doubly-fed generator;

- The use of the Cooperative DG Active Power Prediction Algorithm in the distribution network shown in Chapter 6, in the hour considered, led to an increased amount of non delivered energy by the DG's comparatively with the case where the Cooperative DG Active Power Prediction Algorithm is not enabled. This increased non delivered energy varied, in average values, from 130 kWh to 270 kWh whether the wind power profile equalled $0.95P_{wind}(t)$ or $1.05P_{wind}(t)$ (extreme conditions) respectively, where $P_{wind}(t)$ is the predicted wind power profile for the next hour;
- The use of the Cooperative DG Active Power Prediction Algorithm in the distribution network implemented in Chapter 6, in the hour considered, from a different perspective, increased the predictability of the energy delivered by the aggregation of DG's, which can be measured by the absolute average deviation and maximum deviation from the mean value indicators of Tables 6.1 and 6.2 of Chapter 6.

7.2 – Future Work

The results of the present work may be the starting point of other investigation studies. Thus, some suggestions for these studies are presented as it follows:

- Improve the meta-heuristic algorithms proposed in Chapter 4 in order to achieve PI controller gain tunings that optimize the doubly-fed induction machine performance during transient disturbances, such as grid faults;
- Evaluate the transient stability of the distribution network, presented in Chapter 6, in island operation with the integration of DG's, using the Cooperative DG Active Power Prediction Algorithm;
- Integrate other DG technologies in the distribution network presented in Chapter 6, either intermittent (photovoltaic solar, for example) and non-intermittent (fuel cells, for example), to achieve a more diversified energy production cluster;
- Evolution of the Cooperative DG Active Power Prediction Algorithm in order to also predict the reactive power flows in the distribution network;
- Creation of a package to be installed in every in-feed of the transmission network, which can be able to control all the DG power flows at the concrete distribution network;
- Creation of a package which can be able to control all the DG power flows in island operation;
- Calculate the economic feasibility, for the DG's, of the grid-connected and island operation of the distribution network presented in Chapter 6, with the packages described in the last two points.

References and Bibliography

[Ackerman et al., 2001] Ackermann, T., Andersson, G. and Soder, L., *Distributed generation: A definition,* Electric Power Systems Research no. 57, pp. 195–204, 2001

[ADENE/INETI, 2001] ADENE / INETI, *Fórum Energias Renováveis em Portugal – Relatório Síntese*, http://e-Geo.ineti.pt/geociencias/edicoes_online/ – accessed in 28/11/2007 (in Portuguese), 2001

[Akhmatov, 2000] Akhmatov, V., Nielsen, A. H. and Knudsen, H., *Electromechanical Interaction and Stability of Power Grids with Windmills*, Proceedings IASTED – International Conference on Power and Energy Systems, Marbella, Spain, September 2000

[Akhmatov, 2003] Akhmatov, V., *Analysis of Dynamic Behaviour of Electric Power Systems with Large Amount of Wind Power*, PhD. Thesis, Technical University of Denmark, April 2003

[Almeida, 2006] Almeida, R., *Contribuições para a Avaliação da Capacidade de Fornecimento de Serviços de Sistema por parte de Aerogeradores de Indução Duplamente Alimentados,* PhD. Thesis (in Portuguese), FEUP, Porto, 2006

[Anaya-Lara et al., 2006] Anaya-Lara, O., Hughes, F. M., Jenkins, N. and Strbac, G., *Rotor Flux Magnitude and Angle Control Strategy for Doubly Fed Induction Generators*, Wind Energy Magazine, Vol. 9, no. 5, pp. 479–495, June 2006

[Anderson & Bose, 1983] Anderson, P.M. and Bose, A., *Stability Simulation of Wind Turbine Systems*, IEEE Transactions on Power Apparatus and Systems, Vol. PAS-102, No. 12, pp. 3791-3795, December 1983

[Assembly of the Republic, 2007] Intervention of the Prime Minister in the monthly debate at the Assembly of the Republic about Climate Change, *Debate mensal: Alterações Climáticas*, Lisbon, January 2007

[Bhatti et al., 1995] Bhatti, T. S., Al-Ademi, A. A. F. and Bansal, N. K., *Dynamics and Control of Isolated Wind-Diesel Power Systems*, International Journal of Energy Research, Vol. 19, pp. 729–740, 1995

[Billinton & Karki, 2001] Billinton R. and Karki R., *Capacity Expansion Of Small Isolated Power Systems using PV and Wind Energy*, IEEE Transactions on Power Systems, Vol. 16, no. 4, November 2001

[Burton et al., 2001] Burton, T., Sharpe, T., Jenkins, N. and Bossanyi, E., *Wind Energy Handbook,* John Wiley & Sons, ISBN 0-471-48997-2, 2001

[Castro, 2004] Castro, R., *Condições Técnicas da Ligação de Produção Descentralizada Renovável,* Pedagogic Publication (in Portuguese), http://enerp4.ist.utl.pt/ruicastro/Pedagogia.htm – accessed in 20/11/2007, IST, Lisbon, 2004

[Castronuovo & Peças Lopes, 2004] Castronouvo, E. D. and Peças Lopes, J. A., *On The Optimization of the Daily Operation of a Wind-Hydro Power Plant,* IEEE Transactions on Power Systems, Vol. 19, no. 3, August 2004

[Chedid et al., 2002] Chedid, R., Karaki, S. and El-Chamali, C., *Adaptive Fuzzy Control for Wind-Diesel Weak Power Systems*, IEEE Transactions on Energy Conversion, Vol. 15, no. 1, March 2000

[CIRED, 1999] CIRED, *Dispersed generation: Preliminary Report of CIRED*, Working Group WG04, www.cired.be – accessed in 4/12/2007, June 1999

[Djapic et al., 2007] Djapic, P., Ramsay, C., Pudjianto, D., Strbac, G., Mutale, J., Jenkins, N. and Allan, R., *Taking an Active Approach*, IEEE Power and Energy Magazine, Vol. 5, pp. 68-77, July – August 2007

[Dondi et al., 2002] Dondi, P., Bayoumi, D., Haederli, C., Julian, D. and Suter, M., *Network integration of distributed power generation*, Journal of Power Sources, No. 106, pp. 1–9, 2002

[DTI, 2004] Department of Trade and Industry of the British Government, *Ancillary Service Provision from Distributed Generation,* http://www.dti.gov.uk/files/file15163.pdf – accessed in 17/12/2007, 2004

[EIA, 2001] Energy International Agency*, International Energy Outlook 2001,* Office of Integrated Analysis and Forecasting, U.S. Department of Energy, Washington, DC, http://www.eia.doe.gov – accessed in 15/12/2007

[**Ekanayake et al., 2003 a1**] Ekanayake, J. B., Holdsworth, L. and Jenkins, N., *Control of doubly fed induction generator (DFIG) wind turbines*, Power Engineering Journal, Vol. 17, no. 1, pp. 28-32, February 2003

[Ekanayake et al., 2003 a2] Ekanayake, J. B., Holdsworth, L., Wu, X. and Jenkins, N., *Dynamic Modeling of Doubly Fed Induction Generator Wind Turbines*, IEEE Transactions on Power Systems, Vol. 18, no. 2, May 2003

[Elgerd, 1982] Elgerd, O., *Electric Energy Systems Theory – An Introduction*, McGraw-Hill, ISBN 0-07-Y66273-8, 1982

[European Commission, 2006] European Commission, *Portugal – Folha de dados sobre energias renováveis,* http://ec.europa.eu/energy – accessed in 21/11/2007 (in Portuguese), 2006

[European Parliament, 2001] European Parliament Directive 2001/77/EC, *Promotion of the Electricity Produced from Renewable Energy Source in the Internal Electricity Market*, Official Journal of the European Community, Vol. L283, October 2001

[Fox et al., 2007] Fox, B., Flynn, D., Bryans, L., Jenkins, N., O' Malley, M., Watson, R. and Milborrow, D., *Wind Power Integration: Connection and System Operational Aspects*, IET, ISBN 0-8634-1449-4, 2007

[Gaing, 2004] Gaing, Z.-L., *A particle swarm optimization approach for optimum design of PID controller in AVR system*, IEEE Transactions on Energy Conversion, Vol. 19, no. 2, pp. 384-391, June 2004

[**Grigsby, 2007**] Grigsby, L. (editor), *Electric Power Generation, Transmission and Distribution*, Electric Power Engineering Handbook Series, CRC Press, ISBN 0-8493-9292-6, 2007

[Hedman & Sheblé, 2005] Hedman, K. and Sheblé, G., *Comparing Hedging Methods for Wind Power: Using Pumped Storage Hydro Units vs. Options Purchasing*, 9th International Conference on Probabilistic Methods Applied to Power Systems, Stockholm, Sweden, 11-15 June 2006

[IEEE, 2006] IEEE Power Engineering Society, *IEEE Recommended Practice for Excitation System Models for Power System Stability Studies*, IEEE Std. 421.5, ISBN 0-738-14786-9, 2006

[IPCC, 2001] International Panel on Climate Change, *Summary for policymakers: A report of Working Group I of the Intergovernmental Panel on Climate Change*, http://www.ipcc.ch – accessed in 15/12/2007, 2001

[Jenkins et al., 2000] Jenkins, N., Allan, R., Crossley, P., Kirschen, D. and Strbac, G., *Embedded Generation,* INSPEC Inc., ISBN 0-85296-774-8, London, 2000

[Jesus & Castro, 2004] Jesus, J. and Castro, R., *Equipamento Eléctrico dos Geradores Eólicos*, Didactic Publication (in Portuguese), http://enerp4.ist.utl.pt/ruicastro/Pedagogia.htm – accessed in 2/5/2007, IST, 2004

[Jurado & Saenz, 2002] Jurado, F. and Saenz, J., *Adaptive Control For Biomass-Based Diesel-Wind System***,** IEEE MELECON 2002, Cairo, Egypt, 7-9 May 2002

[Jurado & Saenz, 2003] Jurado, F. and Saenz, J., *Adaptive Control of a Fuel Cell-Microturbine Hybrid Power Plant*, IEEE Transactions on Energy Conversion Vol. 18, no. 2, June 2003

[Kaldellis et al., 2001] Kaldellis, J. K., Kavadias, K. A. and Christinakis, E., *Evaluation of the Wind–Hydro Energy Solution for Remote Islands*, Energy Conversion and Management Vol. 42, no. 9, pp. 1105-1120, June 2001

[Kennedy & Eberhart, 1995] Kennedy, J. and Eberhart, R. C., *Particle Swarm Optimization*, Proceedings of the 1995 IEEE International Conference on Neural Networks, pp. 1942-1948, Perth, Australia, 1995

[Kinoshita et al., 2007] Kinoshita, H., Takahashi, R., Murata, T., Tamura, J., Sugimasa, M., Komura, A., Futami, M., Ichnose, M. and Kazumasa, I., *A Cooperative Control of Doubly-Fed Adjustable Speed Wind Generator and Hydrogen Generation System*, Proceedings of the International Conference on Electrical Machines and Systems 2007, 8-11 October, Seoul, South Korea, 2007

[Korpas et al., 2002] Korpas, M., Hildrum, R. and Holen, A. T., *Operation and Sizing of Energy Storage for Wind Power Plants in a Market System*, Proc. 14th PSCC, Seville, Spain, June 2002

[Kundur, 1993] Kundur, P., *Power System Stability and Control*, McGraw-Hill, ISBN 0-07-035958-X, 1993

[Laughton & Warne, 2002] Laughton, M. A. and Warne, D. F., *Electrical Engineer's Reference Book – Sixteenth Edition*, ISBN: 978-0-7506-4637-6, 2002

[Machowski et al., 1997] Machowski, J., Bialek, J.W. and Bumby, J.R., *Power System Dynamics and Stability*, John Wiley & Sons, ISBN 0-471-95643-0, 1997

[Manitoba, 2006] Manitoba HVDC Research Center Inc., *PSCAD/EMTDC Power System Simulation Software User's Manual,* EMTDC version 4.2, Canada, 2006

[Martins de Carvalho, 1993] Martins de Carvalho, J. L., *Dynamical Systems and Automatic Control*, Prentice Hall International Series in Systems and Control Engineering, ISBN 0-132217-55-4, 1993

[Matos, 2003] Matos, M. A., *Sistema Por Unidade,* Didactic Publication (in Portuguese), http://paginas.fe.up.pt/~mam/sistemapu.pdf – accessed in 25/2/2008, 2003

[Miranda & Fonseca, 2002] Miranda, V. and Fonseca, N., *EPSO – Best-of-Two-Worlds Meta-Heuristic Applied to Power System Problems*, CEC '02 - Proceedings of the 2002 Congress on Evolutionary Computation, Vol. 2, pp. 1080-1085, Honolulu, USA, May 2002

[Miranda et al., 2007] Miranda, V., Keko, H. and Jaramillo, A., *EPSO: Evolutionary Particle Swarms*, Advances in Evolutionary Computing for System Design, Book Chapter, ISBN 978-3-540-72376-9, Volume 66/2007, Springer Berlin / Heidelberg, July 2007

[Mohan et al., 2002] Mohan, N. Undeland, T. and Robbins, W., *Power Electronics: Converters, Applications, and Design*, 3rd Edition, John Wiley & Sons, ISBN 0-471-22693-9, 2002

[Muller, 2002] Muller, S., Deicke, M. and Doncker R., *Doubly Fed Induction Generator Systems for Wind Turbines,* IEEE Industry Applications Magazine, pp 26-33, May/June 2002

[Nunes et al., 2004] Nunes, M. V. A., Peças Lopes, J. A., Zürn, H. H., Bezerra, U. H. and Almeida, R. G., *Influence of the Variable-Speed Wind Generators in Transient Stability Margin of the Conventional Generators Integrated in Electrical Grids*, IEEE Transactions on Energy Conversion, Vol. 19, no. 4, December 2004

[Papathanassiou & Papadopoulos, 2001] Papathanassiou, S. A. and Papadopoulos, M. P., *Dynamic Characteristics of Autonomous Wind Diesel Systems*, Renewable Energy, Vol. 23, No. 2, pp 293-311, 2001

[Pena et al., 1996] Pena, R., Clare, J. C. and Asher, G. M., *Doubly Fed Induction Generator using Back-To-Back PWM Converters and its Application to Variable Speed Wind Energy Generation*, IEE Proc. Electrical Power Applications, Vol. 143., no. 3, May 1996

[Pepermans et al., 2005] Pepermans, G., Driesen, J., Haeseldonckx, D., Belmans, R. and D'haeseleer, W., *Distributed generation: Definition, benefits and issues,* Energy Policy no. 33, pp. 787-798, 2005

[PNAC, 2002] PNAC, *Plano Nacional para as Alterações Climáticas,* Commission for Climate Change / Portuguese Government (in Portuguese), Lisbon, March 2002

[PNALE, 2006] PNALE, *Plano Nacional de Atribuição de Licenças de Emissão de CO_2 2008-2012,* Environment Institute / Portuguese Government (in Portuguese), Lisbon, June 2006

[Prime Mover, 1991] Working Group on Prime Mover and Energy Supply Models for System Dynamic Performance Studies, *Dynamic Models for Fossil Fueled Steam Units in Power System Studies*, IEEE Transactions on Power Systems, Vol. 6, no. 2, May 1991

[Qiao et al., 2006] Qiao, W., Venayagamoorthy, G. K. and Harley, R. G., *Design of Optimal PI Controllers for Doubly Fed Induction Generators Driven by*

Wind Turbines Using Particle Swarm Optimization, Proceedings of the IEEE International Joint Conference on Neural Networks 2006, pp. 1982-1987, Vancouver, Canada, July 2006

[Rajendiran et al., 2000] Rajendiran, K., Keerthipala, W. and Nayar, C. V., *PSCAD/EMTDC Based Simulation of a Wind-Diesel Conversion Scheme,* IEEE Power Engineering Society Winter Meeting, Vol. 1, pp. 505-510, January 2000

[Ramtharan et al., 2007] Ramtharan, G., Jenkins, N. and Anaya-Lara, O., *Modelling and Control of Synchronous Generators for Wide-Range Variable-Speed Wind Turbines*, Wind Energy Magazine, Vol. 10, no. 3, pp. 231–246, March 2007

[Saccomanno, 2003] Saccomanno, F., *Electric Power Systems: Analysis and Control*, Wiley-IEEE Press, ISBN: 978-0-471-23439-5, 2003

[Shi & Eberhart, 1999] Shi, Y. and Eberhart, R. C., *Empirical study of particle swarm optimization*, CEC 99 – Proceedings of the 1999 Congress on Evolutionary Computation, Vol. 3, pp. 1945-1950, 1999

[**Short, 2004**] Short, T., *Electric Power Distribution Handbook*, Electric Power Engineering Handbook Series, CRC Press, ISBN 0-8493-1791-6, 2004

[Svensson, 1998] Svensson, J., *Grid-Connected Voltage Source Converter – Control Principles and Wind Energy Applications*, PhD. Thesis, available at ftp://ftp.elteknik.chalmers.se/Publications/PhD/SvenssonJanPhD.pdf – accessed in 20/1/2008, Chalmers University of Technology, Goteborg, Sweden, March 1998

[Tande et al., 2004] Tande, J.O., Muljadi, E., Carlson, O., Pierik, J., Estanqueiro, A., Sørensen, P., O'Malley, M., Mullane, A., Anaya-Lara, O. and Lemstrom, B., *Dynamic Models of Wind Farms for Power System Studies –*

Status by IEA Wind R&D Annex 21, Communication at the EWEC'04 Conference, London, 22-25 November 2004

[Tang & Xu, 1992] Tang, Y. and Xu, L., *Stator Field Oriented Control of Doubly Excited Induction Machine in Wind Power Generating System*, 35th Mid-West Symposium on Circuits and Systems, pp. 1446-1449, Washington, USA, 1992

[Tapia & Otaegui, 2005] Tapia, G. and Otaegui A. T., *Optimization of the Wind Generation: Comparison between Two Algorithms,* Green Energy Contributions, Book Chapter, Springer Netherlands, ISBN 978-1-4020-2933-2, 2005

[Uhlen et al., 1994] Uhlen, K., Foss, B. A. and Gjosaeter, B., *Robust Control and Analysis of a Wind-Diesel Hybrid Power Plant*, IEEE Transactions on Energy Conversion, Vol. 9, no. 4, December 1994

[Vaz Guedes, 1993] Vaz Guedes, M., *O Motor de Indução Trifásico – Modelização*, Didactic Publication (in Portuguese), www.fe.up.pt/maquel/ – accessed in 12/2/2008, FEUP, 1993

[Vaz Guedes, 1996] Vaz Guedes, M., *O Alternador Síncrono Trifásico – Modelização*, Didactic Publication (in Portuguese), www.fe.up.pt/maquel/ – accessed in 12/2/2008, FEUP, 1996

[Vestas, 2006] Vestas Wind Systems, *Vestas V52 Datasheet*, http://www.vestas.de/pdf_ls/V52_UK.pdf – accessed in 20/10/2007, 2006

[Vianna et al., 2000 a1] Vianna, A., Vieira, L. and Nascimento, M., *Manual de Aplicação de Sistemas Descentralizados de Geração de Energia Elétrica para Projetos de Eletrificação Rural – Energia da Biomassa – versão 1*, Technical Report ADG-A / PER – 789/00 (in Portuguese), CEPEL, November 2000

[Vianna et al., 2000 a2] Vianna, A., Vieira, L. and Nascimento, M., *Manual de Aplicação de Sistemas Descentralizados de Geração de Energia Elétrica para*

Projetos de Eletrificação Rural – Energia Eólica – Versão 1, Technical Report ADG-A / PER – 785/00 (in Portuguese), CEPEL, November 2000

[Vieira et al., 2007] Vieira, J. P. A., Nunes, M. V. A., Bezerra, U. H. and Nascimento, A. C., *Controladores Fuzzy Aplicados ao Conversor de Geradores de Indução Duplamente Excitados em Sistemas Eólicos Integrados a Sistemas de Potência*, Revista Controle & Automação (in Portuguese), Vol. 18, no. 1, January/March 2007

[Yanfang et al., 2001] Yanfang, F., Yibo, W. and Qin, C., *Wind-Hydro Hybrid Power System Stability Analysis*, Proceedings of the Fifth International Conference on Electrical Machines and Systems, Shenyang, China, 2001

Appendix A – Per Unit System

The per unit system, or p.u. system, consists in the definition of base values for the fundamental quantities, followed by the substitution of variable and constant values (defined in the International System of Units) by their relation with the defined base values.

In a power system, are usually defined as independent base values the total apparent power $\mathbf{S_{base}}$ for the system and the line-to-line voltage $\mathbf{V_{base}}$ in a certain bus. These two base values conduce to the definition of other two quantities: base impedance $\mathbf{Z_{base}}$ and base current $\mathbf{I_{base}}$, for a given zone.

$$Z_{base} = \frac{(V_{base})^2}{S_{base}} \qquad \text{Eq. (A1)}$$

$$I_{base} = \frac{S_{base}}{\sqrt{3} \times V_{base}} \qquad \text{Eq. (A2)}$$

After defining the base values, all the power system parameters have to be converted to the per unit system. In what respects to machine characteristics (power transformers, generators, etc), parameters are normally given in percent values, referred to the nominal power and terminal voltage values. The compatibility of those percent values with the defined base values for the considered power system requires a base change, given by the Eq. (A3) [Matos, 2003].

$$Z_{p.u.}^{new\_base} = Z_{p.u.}^{old\_base} \times \frac{S_{base}^{new\_base}}{S_{base}^{old\_base}} \times \left(\frac{V_{base}^{old\_base}}{V_{base}^{new\_base}} \right)^2 \qquad \text{Eq. (A3)}$$

Appendix B – Software PSCAD/EMTDC®

PSCAD® and EMTDC® are a software package which allows the user to obtain a large number of simulations, essentially for electromagnetic transient studies. Actually, ETMDC® is the software that effectively does the transient analysis, while PSCAD® is a group of various software modules which are the graphical user interface of EMTDC®.

PSCAD/EMTDC® presents a wide range of power system and power electronic models such as: transmission lines and cables, power transformers, rotating electrical machines (asynchronous, synchronous, DC), turbines (hydraulic, wind, steam), converters, FACTS, relays, and many more.

One of the strongest points of PSCAD/EMTDC® is its capability of making available functions, modules and predefined modules (that can be manipulated by the user) that can be interconnected with electric or control power systems. It is also possible to create new modules using the programming language Fortran®. The operation of any module can be tested in the presence of disturbances, for the observation of its response.

PSCAD/EMTDC® is developed by the HVDC Research Centre, of Winnipeg, Canada. The current version of this software package, at the time of this thesis, is the version 4.2.1. This was the version used along this thesis. It is available in https://pscad.com/download-download.php, a free-to-trial demo version of PSCAD/EMTDC® [Manitoba, 2006].

Appendix C – Distribution Network Parameters

In Table C1 are presented the load parameters of the distribution network implemented in this work for simulation purposes in Chapters 5 and 6.

TABLE C1
LOAD PARAMETERS OF THE DISTRIBUTION NETWORK

LOAD	R_L (Ω)	L_L (H)	X_L (Ω)
1	3418	2,219	697,1194098
2	538	0,348	109,3274243
3	3522	2,276	715,026488
4	422,6	0,273	85,76547944
5	2155	1365	428827,3972
6	538	0,348	109,3274243
7	1139	0,736	231,2212193
8	3320	2,146	674,1857835
9	2834	1,832	575,5397741
10	3228	2,086	655,3362275
TOTAL	**21.114,600**	**1.377,264**	**432.680,246**

From the Eqs. (C1) and (C2), it can be obtained the active and reactive powers absorbed by each load, P_L and Q_L respectively.

$$S_L = P_L + jQ_L \qquad \text{(Eq. C1)}$$

$$P_L + jQ_L = \frac{V^2}{R_L + jX_L} \qquad \text{(Eq. C2)}$$

Where S_L is the apparent power absorbed by each load (in W); R_L and X_L are, respectively, the resistance and reactance that represent each load (in Ω) and V is the voltage in which they are subjected (in Volt).

Admitting there are no voltage drops in the network, i.e., V equals the nominal value of 15 kV among all the network, Table C2 presents the apparent, active and reactive powers absorbed by each load.

TABLE C2

APPARENT, ACTIVE AND REACTIVE POWERS ABSORBED BY EACH LOAD OF THE DISTRIBUTION NETWORK

LOAD	S_L (VA)	P_L (W)	Q_L (Var)
1	64500,10704	63199,02976	12889,78067
2	409839,1348	401630,4295	81615,65129
3	62606,98007	61355,33682	12456,18711
4	521781,3359	511356,8232	103778,4267
5	524,6800005	2,636657852	524,6733755
6	409839,1348	401630,4295	81615,65129
7	193592,9437	189723,1179	38514,49575
8	66415,54159	65087,11212	13217,11014
9	77804,8393	76248,36718	15484,81582
10	68309,11604	66943,48826	13590,61123
TOTAL	1.875.213,8132	1.837.176,7708	373.687,4033
x10^3	1.875,2138	1.837,1768	373,6874

The network behind the 60/15 kV substation of the implemented distribution network can be modelled by the following Thevenin equivalent, represented in Figure C1:

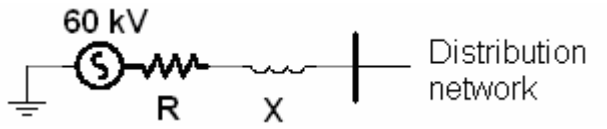

Figure C1 – Thevenin equivalent which represents the network behind 60/15 kV substation

Assuming a short-circuit equivalent power, S_{cc}, of 250 MVA and a X to R ratio of 1.5, it can be obtained the R and X values that represent the behind 60/15 kV substation.

$$S_{CC} = \frac{V^2}{\sqrt{R^2 + X^2}} \qquad \text{(Eq. C3)}$$

$$Scc = \frac{V^2}{R \times \sqrt{1 + \left(\frac{X}{R}\right)^2}} \qquad \text{(Eq. C4)}$$

To get *R* from the Eq. (C4), it is necessary to substitute S_{cc} and $\frac{X}{R}$ (*X* to *R*), to obtain:

$$R = \frac{\left(60 \times 10^3\right)^2}{250 \times 10^6 \times \sqrt{1 + \left(1{,}5\right)^2}} = 7{,}98\,\Omega$$

Being *X* to *R* equal to 1.5, X equals to:

$$X = 1{,}5 \times 7{,}98 = 11{,}98\,\Omega$$

Appendix D – Coordinate Transform Equations

The following equations refer to the coordinate transformations [Pena et al., 1993] required by the doubly-fed induction generator vector-control scheme, described in Chapter 2.

- **Clarke's Transformation**

The Eq. (D1) shows the forward (*abc* to *αβ*) and inverse (*αβ* to *abc*) Clark transformations used in this work.

Forward (*abc* to *αβ*)

$$\begin{bmatrix} \alpha \\ \beta \end{bmatrix} = \frac{2}{3} \cdot \begin{bmatrix} 1 & -1/2 & -1/2 \\ 0 & \sqrt{3}/2 & -\sqrt{3}/2 \end{bmatrix} \begin{bmatrix} a \\ b \\ c \end{bmatrix}$$

Inverse (*αβ* to *abc*)

$$\begin{bmatrix} a \\ b \\ c \end{bmatrix} = \begin{bmatrix} 1 & 0 \\ -1/2 & \sqrt{3}/2 \\ -1/2 & -\sqrt{3}/2 \end{bmatrix} \begin{bmatrix} \alpha \\ \beta \end{bmatrix} \qquad \text{Eq. (D1)}$$

- **Park's Transformation**

The Eq. (D2) shows the forward (*d-q* to *αβ*) and inverse (*αβ* to *d-q*) Park transformations used in this work.

Forward (*d-q* to *αβ*)

$$\begin{bmatrix} d \\ q \end{bmatrix} = \begin{bmatrix} \cos(\theta) & \sin(\theta) \\ -\sin(\theta) & \cos(\theta) \end{bmatrix} \begin{bmatrix} \alpha \\ \beta \end{bmatrix}$$

Inverse (*αβ* to *d-q*)

$$\begin{bmatrix} \alpha \\ \beta \end{bmatrix} = \begin{bmatrix} \cos(\theta) & -\sin(\theta) \\ \sin(\theta) & \cos(\theta) \end{bmatrix} \begin{bmatrix} d \\ q \end{bmatrix} \qquad \text{Eq. (D2)}$$

Appendix E – Meta-heuristics Applied to Power Systems: Particle Swarm Optimization and Evolutionary Particle Swarm Optimization

E.1 – Introduction

This chapter will present an overview of Particle Swarm Optimization (PSO) and Evolutionary Particle Swarm Optimization (EPSO) algorithms, both variants in the family of meta-heuristic algorithms. The purpose behind this study is to apply both meta-heuristics for tuning of the rotor side converter's PI controller gains of Doubly-Fed Induction Generators, which is detailed in Chapter 4.

At first, it will be introduced the concept behind the Evolutionary Algorithms (EA). Next, it will be presented the PSO. Afterwards, it will be explained the main lines behind the EPSO algorithm. At last, it will be discussed the similarities and differences between PSO and EPSO.

E.2 – Evolutionary Algorithms: Overview

Evolutionary Algorithms (EA) are a subset of evolutionary computation, generic population-based meta-heuristic optimization algorithms. A typical EA uses some mechanisms inspired by biological evolution: reproduction, mutation, recombination, and selection. Candidate solutions to the optimization problem play the role of individuals in a population and a user-defined fitness function determines the environment within which the solutions survive. The evolution of the population then takes place after the repeated application of the operators: reproduction, mutation, recombination, and selection.

Therefore, a general Evolutionary Algorithm may be organized in the following steps [Miranda et al., 2007]:

Procedure EA

initialize a random population P of μ elements

REPEAT

reproduction (introduce stochastic perturbations in the new population) – generate λ offspring…

…by *mutation*

…by *recombination*

evaluation - calculate the fitness of the individuals

selection - of μ survivors for the next generation, based on the fitness value

test for termination criterion (based on fitness, on number of generations, etc.)

Until test is positive

End EA

This is a general algorithm and applies to all variants of EA, whether Genetic Algorithms, Evolutionary Programming, Evolution Strategies or other of the kind.

The driving force behind any EA is the selection operator which, however, requires the action of replication or reproduction operators –

recombination and mutation – to generate new points in the search space to be evaluated.

Mutation is an operator acting on a single individual, particle or chromosome and generates a new point in the search space by modifying the coordinates of a previous point. The definition of the mutation operator may be dependent of the particular problem under analysis. In Evolution Strategies/Evolutionary Programming, where typically (not necessarily) an individual is composed of a string of real variable values, the classical mutation procedure adopts Gaussian or Lognormal random perturbations of each variable. The amplitude of mutation is governed by the variance of the distribution regulating mutations, and its square root (standard deviation) is often called learning rate.

In self-adaptive Evolution Strategies (ES), each individual is characterized by object parameters (the values of the variables describing a solution) and by strategic parameters (mutation rates for each variable, mutation correlation angles and similar) [Miranda & Fonseca, 2002].

The selection procedure has a number of variants and can be ruled by a stochastic tournament or be purely deterministic, involve elitism, etc.

E.3 – Particle Swarm Optimization

Particle Swarm Optimization (PSO), first introduced in 1995 by Kennedy and Eberhart [Kennedy & Eberhart, 1995], is part of the family of the evolutionary computation. It is inspired by the paradigm of birds flocking and schooling in fish. The method is found by the authors and their followers to be robust in solving problems featuring non-linearity and non-differentiability, multiple optima, and high dimensionality through adaption, which is derived from the social-psychological theory [Shi & Eberhart, 1999; Gaing, 2004; Qiao et al., 2006].

Particle Swarm Optimization relies on the parallel exploration of the search space by a set of solutions or alternatives called particles that are successively transformed along the process. Instead of using evolutionary operators to manipulate the particle (individual), like in other evolutionary

computational algorithms, each particle in PSO “flies” over the search space with a velocity which is dynamically adjusted according to its own “flying experience” and its companions’ “flying experience”. Thus, each particle *i* represents a potential solution, has a position in the search space represented by a position vector X_i and moves in the search space with a moving velocity V_i.

At each time step, a fitness function *f*, representing a quality measure, is calculated by using X_i as input. Each particle *i* keeps track of its individual best position, $p_{best,i}$, which is associated with the best fitness it has achieved so far. Furthermore, the best position among all the particles obtained so far in the swarm is recorded as g_{best}. This information is shared by all the particles. Then, the PSO concept consists of, at each iteration, changing the velocity of each particle *i* toward its $p_{best,i}$ and g_{best} locations.

The PSO algorithm is implemented in the following iterative procedure to search for the optimal solution [Shi & Eberhart, 1999].

$$V_i^{new} = Wi \cdot V_i + Wm \cdot (p_{best,i} - X_i) + Wc \cdot (g_{best} - X_i) \qquad \text{Eq. (E1)}$$

$$X_i^{new} = X_i + V_i^{new} \qquad \text{Eq. (E2)}$$

Where

$$\begin{cases} Wi = \omega \\ Wm = c_1 \cdot \varphi_1 \\ Wc = c_2 \cdot \varphi_2 \end{cases} \qquad \text{Eq. (E3)}$$

In Eq. (E3), c_1 and c_2 are positive constants representing the weighting of the stochastic acceleration terms that pull each particle toward $p_{best,i}$ and g_{best} positions. Low values of c_1 and c_2 allow particles to roam far from the target regions before being tugged back. On the other hand, high values result in abrupt movement toward, or past, target regions. φ_1 and φ_2 are uniformly distributed random numbers in [0, 1]. ω is a positive inertia weight developed to provide better control between global and local explorations, thus requiring less iteration on average to find a sufficiently optimal solution. As originally

developed, ω often decreases linearly from about 0.9 to 0.4 during a run. In general, the inertia weight is set according to the Eq. (E4) [Shi & Eberhart, 1999; Gaing, 2004]:

$$\omega = \omega_{\max} - \frac{\omega_{\max} - \omega_{\min}}{iter_{\max}} \times iter \qquad \text{Eq. (E4)}$$

Where $iter_{max}$ is the maximum number of iterations, and *iter* is the current iteration.

The velocity V_i is limited to the range [$-V_{max}$, V_{max}]. If the velocity V_i violates these limits, it is set to the upper or low-bound value according with the case. If V_{max} is too high, particles might fly past good solutions. If V_{max} is too small, particles may not explore sufficiently beyond local solutions.

The last two terms in Eq. (E1), *Wm* and *Wc*, named memory and cooperation weights, enable each particle to perform a local search around its individual best position $p_{best,i}$ and the swarm best position g_{best}, respectively. The first term in Eq. (E1), *Wi*, named the inertia weight, enables each particle *i* to perform a global search by exploring a new search space. Figure E1 shows the concept behind the weights *Wi*, *Wm* and *Wc* for the movement of a particle *i*. The final transformation vector of X_i to X_i^{new} is composed by the contribution of the three terms *Wi*, *Wm* and *Wc*.

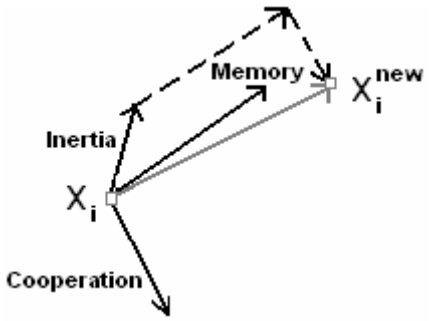

Figure E1 – Illustration of the movement of a particle from X_i to X_i^{new} in PSO, influenced by the three terms: Inertia, Memory and Cooperation [Miranda et al., 2007]

E.4 – Evolutionary Particle Swarm Optimization

The Evolutionary Particle Swarm Optimization (EPSO) was first presented in 2002 by V. Miranda and N. Fonseca [Miranda & Fonseca, 2002]. EPSO is a variant of the family of self adaptive EA, where the classical operators for recombination are replaced by a rule similar to the particle movement of PSO. Therefore, from a conceptual point of view, EPSO has an interesting feature: it allows a double interpretation on how it works, because it may be seen from two perspectives – either as a variant of PSO or as a variant of EA [Miranda & Fonseca, 2002].

In fact, the authors of EPSO see the method as a self-adaptive evolutionary algorithm where the operation recombination is replaced by a new operation called “particle movement”. This operator “particle movement” seems to be more effective than recombination to generate solutions that approach the optimum.

In terms of Particle Swarm Optimization interpretation, the authors of EPSO state they have given EPSO self-adaptive characteristics, so it no longer depends on external definition of weights or parameters. Because it is self-adaptive, EPSO seems to become more robust than PSO, according to the authors, and more insensitive to parameter initialization. In addiction, EPSO modifies slightly the PSO concept, by defining a blurred target for the global best instead of a single point, which may also improve the quality of the results.

The idea behind EPSO is to grant a PSO scheme with an explicit selection procedure and with self-adapting properties for its parameters. The variables in an EPSO formulation are divided, according to the vocabulary used in the Evolution Strategies community, in object parameters (the X variables) and strategic parameters (the weights W).

At a given iteration, is considered a set of solutions or alternatives that will be called, as in PSO, particles. A particle is a set of object and strategic parameters [X, W]. The general scheme of EPSO is presented below [Miranda et al., 2007]:

Replication - each particle is replicated *r* times

Mutation - each particle has its weights W mutated

Reproduction - each mutated particle generates an offspring according to the particle movement rule

Evaluation - each offspring has its fitness evaluated

Selection - by stochastic tournament the best particles survive to form a new generation

The particle movement rule for EPSO is the following: given particle *i* position X_i, the new particle *i* position, X_i^{new}, results from [Miranda et al., 2007]:

$$V_i^{new} = Wi^*_i \cdot V_i + Wm^*_i \cdot (p_{best,i} - X_i) + Wc^*_i \cdot (g^*_{best} - X_i) \cdot P \qquad \text{Eq. (E5)}$$

$$X_i^{new} = X_i + V_i^{new} \qquad \text{Eq. (E6)}$$

This formulation is very similar to the PSO formulation given in Eqs. (E1) and (E2), as the movement rule keeps its terms of inertia, memory and cooperation. However, the weights, taken as strategic parameters, undergo mutation, which is indicated by the symbol *. The basic mutation scheme, for any weight W, is given by the Eq. (E7) [Miranda et al., 2007].

$$W^*_{ik} = W_{ik} + \tau N(0,1) \qquad \text{Eq. (E7)}$$

Where *N(0,1)* is a random variable with Gaussian distribution with mean equal to 0 and variance equal to 1.

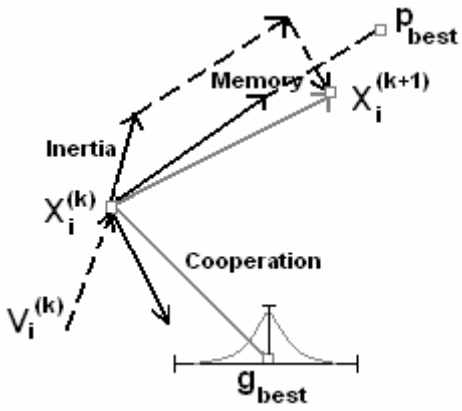

Figure E2 – Illustration of the EPSO movement rule. A particle *i* located at X_i, at an iteration *k*, origins a new descendent at iteration *k+1*, due to the terms of Inertia, Memory and Cooperation. Notice the vector associated with the cooperation factor does not point exactly to the global optimum g_{best}, but to a mutated location [Miranda et al., 2007]

In the most effective EPSO variant not only the weights affecting the components of movement are mutated but also the global best, g_{best}, is randomly disturbed to give [Miranda et al., 2007]:

$$g^*_{best} = g_{best} + \tau' N(0,1) \qquad \text{Eq. (E8)}$$

The logic behind this modification is the following: a) if the current global best is already the global optimum, it has no effect; but b) if the optimum hasn't yet been found, it may nevertheless be in the neighbourhood and so this procedure may search more accurately the current global best region - specially when the search is already focused in a certain region, at the latter stages of the process. The τ and τ' parameters are learning parameters (either fixed or treated also as strategic parameters and, thus, subject to mutation). Therefore, the EPSO scheme benefits from two "pushes" in the right direction: the Darwinist process of selection and the particle movement rule; thus, it is natural to expect that it may display advantageous convergence properties when compared to ES or PSO alone. Furthermore, EPSO can also be classified as a self-adaptive algorithm, because it relies on the mutation and selection of strategic parameters, just as any self-adaptive Evolution Strategy [Miranda & Fonseca, 2002].

Selection is modelled from the Stochastic Tournament concept: among the descendants of each particle, one compares the best one with another particle randomly sampled, and the best is selected with probability (1 – luck), where the luck parameter is defined in [0, 1] but is usually small [Miranda et al., 2007].

P, shown in Eq. (E5), is called by the authors the communication factor. The communication factor *P* induces a stochastic star topology for the communication among particles. It is a diagonal matrix affecting all dimensions of an individual, containing binary variables of value 1 with probability *p* and value 0 with probability (1-*p*); thus, the *p* value controls the passage of information within the swarm (p= 1 in the classical formulations, such as the PSO formulation).

E.5 – Particle Swarm Optimization and Evolutionary Particle Swarm Optimization: Discussion

PSO and EPSO are two variants of meta-heuristics that have some similarities but, as well, many differences between them. PSO is part of the family of the evolutionary computation, which inspiration derives from the paradigm of birds flocking and schooling in fish. EPSO is a variant of the family of self adaptive Evolutionary Algorithms, where the classical operators for recombination are replaced by a rule similar to the particle movement of PSO.

PSO has the drawback of depending on a number of parameters defined externally by the user, with values that are problem dependent. This applies for the definition of the weights W, thus a delicate work of tuning the algorithm is often necessary, in practical problems. Furthermore, the external definition of the decreasing function for the inertia weight *Wi*, given in Eq. (E1), may cause the algorithm to be trapped at some local minimum if the inertia term is eliminated at an early stage of the process. The random factors φ_1 and φ_2, while introducing a useful stochastic flavour, only have a heuristic basis and are not sensitive to the evolution of the process [Miranda & Fonseca, 2002].

EPSO relies on a self-adaptive mechanism. The weight parameters, considered as strategic, can be subject to selection and, hopefully, evolve to

values adapted to the type of landscape being searched. As EPSO adopts the movement rule of PSO, its behaviour can be regarded as a swarm whose movement is ruled by weights that self-adapt in order to produce a global drift more adjusted to the landscape. Furthermore, because these weights are subject to mutation, this may give an extra chance for the swarm to escape local minimum (i.e., having particles that still explore other regions of space, because they may gain enough speed). On the other hand, EPSO also seems to show, according to its authors, ability to focus and zoom in the optimum. This is achieved because mutations in the weights may favour the selection of the cooperation factor and then reduce the importance of inertia and memory, for example, if this strategy proves successful.

EPSO presents also a random parameter affecting communication among particles, creating a topology named by the authors as stochastic star, which may be valuable in cases where the algorithm needs to escape premature convergence, according to the authors [Miranda et al., 2007].

E.6 – Summary

This chapter presented an overview of the Particle Swarm Optimization (PSO) and the Evolutionary Particle Swarm Optimization (EPSO) algorithms, both variants in the family of meta-heuristic algorithms. This study was carried out with the objective of applying both meta-heuristics for the tuning of the DFIG rotor side converter's PI controller gains, which is detailed in Chapter 4.

After a brief presentation of the concept behind Evolutionary Algorithms, followed the PSO algorithm explanation. Next, were shown the main lines behind the EPSO algorithm, which concept relies both in Evolutionary Algorithms and PSO. At last, were discussed the similarities and differences between PSO and EPSO.

Appendix F – Parameters of the Biomass and Wind Energy Plants in the Adaptive DG Active Power Prediction Algorithm

Wind Turbine

	value	unit
Rotor Radius	22	m
Blade Angular Speed	1,904	rad/s
Air Density	1,229	kg/m^3
Number of Blades	3	
Gearbox Efficiency	97	%

Steam Turbine

Time Constant	0,2	s

Induction Wind Generator (p.u. values on base of the machine rating)

Rated Power	850	kW
Nominal Voltage	0,69	kV
Stator Resistance	0,008549	p.u.
Stator Reactance	0,09742	p.u.
Rotor Reactance	0,127074	p.u.
Magnetizing Reactance	4,50534	p.u.
Polar Moment of Inertia	0,302	s
Poles	6	
Slip	2.5	%

Synchronous Generator (p.u. values on base of the machine rating)

Rated Power	850	kW
Nominal Voltage	0,69	kV
Armature Resistance	0,0051716	p.u.
Potier Resistance	0,163	p.u.
Unsat. Direct Reactance	1,014	p.u.
Unsat. Quadrature Reactance	0,77	p.u.
Unsat. Direct Transient Reactance	0,314	p.u.
Unsat. Quadrature Transient Reactance	0,228	p.u.
Inertia Constant	2,5	s
Poles	2	

Capacitor Bank

Connected at the 0,69 kV bus

Reactive Power	360	KVar

Appendix G – Parameters of the Biomass and Wind Energy Plants in the Cooperative DG Active Power Prediction Algorithm

Wind Turbine

	value	unit
Rotor Radius	22	m
Blade Angular Speed	1,904	rad/s
Air Density	1,229	kg/m^3
Number of Blades	3	
Gearbox Efficiency	97	%

Wind Energy Plant's PI Controller Parameters

Rotor Side Converter

Proportional Gain – Kp1	1,3126	
Proportional Gain – Kp2	0,6279	
Integral Gain – Ki1	4,9954	
Integral Gain – Ki2	3,3773	

Grid Side Converter

Active Power Loop Proportional Gain	0,5	
Reactive Power Loop Proportional Gain	1	
Active Power Loop Integral Gain	0,1	
Reactive Power Loop Integral Gain	10	

Doubly-Fed Induction Generator (p.u. values on base of the machine rating)

Rated Power	850	kW
Nominal Voltage	0,69	kV
Stator Resistance	0,00488	p.u.
Stator Leakage Reactance	0,09241	p.u.
Rotor Resistance	0,00549	p.u.
Rotor Leakage Reactance	0,09955	p.u.
Magnetizing Reactance	3,95279	p.u.
Angular Moment of Inertia	3,5	s
Poles	6	
Stator / Rotor Turns Ratio	2.637687	

Steam Turbine

Time Constant	0,2	s

Steam Regulator

Speed Relay Lag Time Constant – T_1	7,5	s
Speed Relay Lead Time Constant – T_2	2,8	s
Gate Servo Time Constant – T_3	0,2	s

Wind Energy Plant's Power Converters

Power Converter Coupling Transformer

Rated Apparent Power	100	kVA
Nominal Voltage	0,69/0,2	kV
Leakage Reactance	10	(%)

DC-link

Capacitor Value	250	mF
DC-link Voltage	0,46	kV

Synchronous Generator (p.u. values on base of the machine rating)

Rated Power	850	kW
Nominal Voltage	0,69	kV
Armature Resistance	0,0051716	p.u.
Potier Resistance	0,163	p.u.
Unsat. Direct Reactance	1,014	p.u.
Unsat. Quadrature Reactance	0,77	p.u.
Unsat. Direct Transient Reactance	0,314	p.u.
Unsat. Quadrature Transient Reactance	0,228	p.u.
Inertia Constant	2,5	s
Poles	2	

Appendix H – Paper Submitted on the extent of this Dissertation

A publication entitled “Biomass and Wind Energy: Adaptive Control to Provide Predictable Active Power Output” was submitted to the *IEEE Transactions on Power Delivery* journal, at the 10th of February 2008. The paper is yet in review at the time of writing of this dissertation and is presented as follows.

Biomass and Wind Energy: Adaptive Control to Provide Predictable Active Power Output

J. Barros, H. Leite and J. A. Peças Lopes, *Senior Member, IEEE*

***Abstract* – An adaptive control of Distributed Generation (DG) to provide predictable active power output at the primary distribution substation is described. Often, distribution networks accommodate renewable energy from different energy sources and thus using different energy conversion sources. As the amount of generation that comes from intermittent renewable sources (e.g. wind energy) increases, network operators start to concern with the uncertainty of generation. However, when the power output from intermittent renewable sources is predicted, the network operators can reduce the operational costs of the network and the DG owners may go on the market. Thus, our challenge with this work was to develop an algorithm which can predict the active power output from the aggregation of wind and biomass energy at the primary distribution substation of a typical distribution network. Wind and biomass energy plant are onto the same distribution network but not necessarily onto the same feeder.**

***Index Terms* – Active Power Prediction, Adaptive Control, Distributed Generation, Distribution Network**

I. Introduction

Concern over the global climate change led the EU and the Portuguese Government to set targets to the share of electricity produced from renewable sources in 22.1% and 39% in the EU and Portugal respectively by 2010 [1]. In order to meet those targets, higher penetrations of Distributed Generation (DG) is expected to be connected to the distribution network.

In 2005, the Portuguese government tried to increase the energy that comes from biomass by increasing the prices of MWh from 72 Euros to 100 Euros [2]. With this, they intend to clean the forest and thus reduce possibility of forest fires. However, due to a low ability of transport and store of large volumes of feedstocks, the size of a biomass plant may be limited and therefore has to be connected to the distribution network.

Biomass energy is a renewable energy with the advantage of having a secure contribution to the network, assuring predictable active power output, as it uses the well-established steam turbine synchronous generation technology.

However, there are other forms of renewable energy (e.g. wind energy), produced from existing wind farms which have no facility in providing fully predictable active power output, mainly due to its character of intermittency. The increase of intermittent energy concerns the network operators because of the decrease of security and consequently leading to the increase of network operational costs.

The combining of biomass with wind farm plants may lead to a larger amount of secure renewable energy penetration on the distribution networks. Thus, it may have the advantage of increasing the availability and reliability of renewable sources and consequently the operation costs of the network can be lowered [3]. On other point of view, this larger amount of secure renewable energy penetration in the distribution networks may lead the DG owners to go in market.

With the aggregation of biomass and wind energy, the errors associated with the wind power forecast and consequent energy production can be attenuated. Thus, power systems can potentially accommodate increased levels of intermittent wind energy as the imbalances between generation and demand do not increase.

From the point of view of Distribution Network Operators (DNOs), they have then the possibility of avoiding the reinforcement of their networks and make a reconfiguration of the network as the DG will have an adaptive control. DNOs though have a localized network support as they can control DG active power output.

This paper shows the technical potential of aggregation of both biomass and wind energy to provide predictable active power output. Knowing that biomass primary energy can be stored transported whenever and where it is needed, an adaptive DG active power prediction algorithm was developed. This algorithm uses the steam turbine synchronous generation technology of the biomass energy to cover the unpredictable energy that comes from the wind. In order to present this algorithm, a typical 60/15 kV radial distribution network with the integration of distributed generators is simulated with the electromagnetic transient package PSCAD/EMTDC®. The technical performance of the adaptive DG active power prediction algorithm is analyzed and discussed.

Manuscript received ????. This work was financially supported by the Fundação para a Ciência e Tecnologia (FCT) of Portugal, under the PTDC/EEA-ENE/73829/2006 project.

The authors are with FEUP – Faculdade de Engenharia da Universidade do Porto, 4200-465 Porto, Portugal (e-mail: {jose.barros, hleite, jpl}@fe.up.pt).

II. Adaptive DG Active Power Prediction Algorithm

A. Adaptive DG Active Power Prediction Algorithm Model

The Adaptive DG Active Power Prediction Algorithm aims to predict the active power output at the primary distribution substation. The algorithm also tries to minimize the fluctuations in the active power output of the primary distribution substation. The algorithm controls the non-intermittent energy plant and, thus, predicts the active power output from both intermittent and non-intermittent energy plants. The intermittent energy plant considered in this work is a conventional wind energy plant (i.e. equipped with a conventional induction generator). The non intermittent energy plant considered in this work is a typical biomass energy plant (i.e. equipped with steam turbine synchronous generation technology).

The Adaptive DG Active Power Prediction Algorithm changes the biomass energy plant's load reference to follow the variations of the wind energy plant's active power output and, thus, minimize the fluctuations of the primary distribution substation's active power output. The Adaptive DG Active Power Prediction Algorithm changes the biomass energy plant's load reference as shown in Fig. 1 b).

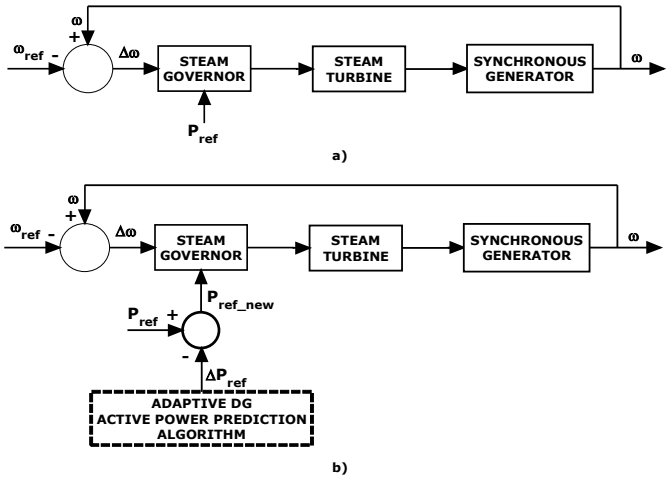

Fig. 1. a) Load Frequency Control Block Diagram of the Biomass Energy Plant; b) Load Frequency Control Block Diagram of the Biomass Energy Plant with the Adaptive DG Active Power Prediction Algorithm

As wind speed variations produce active power fluctuations at the output of the wind energy plant and, consequently, at the output of the primary substation, the Adaptive DG Active Power Prediction sets the biomass energy plant's load reference to change the biomass energy plant's active power output accordingly. Fig. 2 shows the flow chart of the Adaptive DG Active Power Prediction Algorithm.

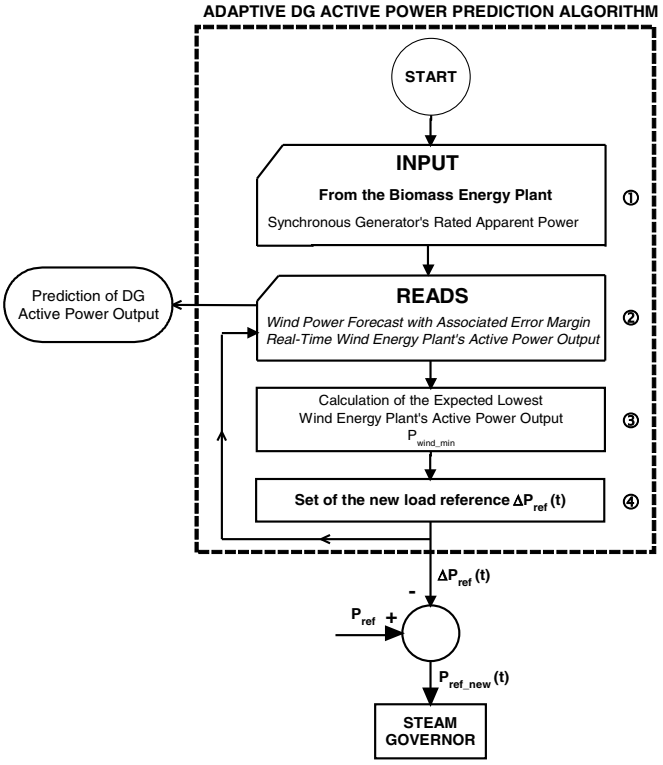

Fig. 2. Flow chart of the Adaptive DG Active Power Prediction Algorithm

Follows the detailed explanation of the Adaptive DG Active Power Prediction Algorithm. Firstly, it is necessary to input the synchronous generator's rated apparent power to enable the running of the Adaptive DG Active Power Prediction Algorithm at the specific biomass energy plant. Secondly, it starts the real-time closed loop of the Adaptive DG Active Power Prediction Algorithm. Every loop cycle, the Adaptive DG Active Power Prediction Algorithm reads the wind power forecast given by the Wind Power Forecast Centre for the wind energy plant considered. This wind power forecast is given with an associated error margin based on the wind energy plant installed capacity, dependant on the desired look-ahead time for prediction. The Adaptive DG Active Power Prediction Algorithm also reads, every loop cycle, the real-time wind energy plant's active power output, see ②.

Next, for the desired time in which DG's active power output is predicted, it is calculated the predicted lowest wind energy plant's active power output, see ③. The predicted lowest wind energy plant's active power output is obtained from the lowest wind power given by the wind power forecast, for the desired time.

Finally, the Adaptive DG Active Power Prediction Algorithm sets the biomass energy plant's load reference. The setting of the biomass energy plant's load reference consists in the subtraction from the old load reference, P_{ref}, of a real-time quantity ΔP_{ref} ($t+\Delta t$). In ④, it is indicated the setting of ΔP_{ref} ($t+\Delta t$), which is given by the Eq. (1).

$$\Delta P_{ref}(t+\Delta t) = \frac{P_{wind\_actual}(t) - P_{wind\_min}}{S_{biomass}} \text{ [p.u.]} \quad (1)$$

Where P_{wind_actual} (t) is the measured real-time active power output from the wind energy plant in W, P_{wind_min} is the predicted lowest active power output from the wind energy plant in W, $S_{biomass}$ is the rated apparent power of the biomass energy plant in VA.

B. Comments on the Adaptive DG Active Power Prediction Algorithm

The Adaptive DG Active Power Prediction Algorithm is a feedback control which, for a good performance, requires fast response capabilities of the biomass energy plant.

In conventional wind energy plants, i.e. equipped with conventional induction generators, severe wind speed fluctuations conduct to equally severe fluctuations in the wind active power delivered to the network. These severe wind active power fluctuations conduct, with the use of the Adaptive DG Active Power Prediction Algorithm, to deviations from the nominal angular speed of the biomass energy plant's synchronous generator, as shown in the Eq. (2).

$$\Delta\omega = \omega - \omega_{ref} = -\Delta P_{ref} \frac{1}{R^{-1} + D} \text{ [p.u.]} \quad (2)$$

Where $\Delta\omega$ is the angular speed deviation from the reference angular speed ω_{ref} of the synchronous generator, ω is the real-time angular speed of the synchronous generator, R is the steam governor's droop constant and D is the synchronous generator's damping constant.

The deviations from the nominal angular speed of the biomass energy plant and the consequent active power deviations should follow the wind active power fluctuations, in order to smooth the aggregated active power output. This objective is as well accomplished as faster the biomass energy plant responds to deviations from its nominal angular speed. However, it is not expected the biomass energy plant can fully respond to all the wind active power fluctuations, mainly due to the inertia constant of the synchronous generator.

III. Simulation Test of the Adaptive DG Active Power Prediction Algorithm

A. Distribution Network Modeling

Fig. 3 shows the distribution network considered on this paper to simulate and validate the Adaptive DG Active Power Prediction Algorithm.

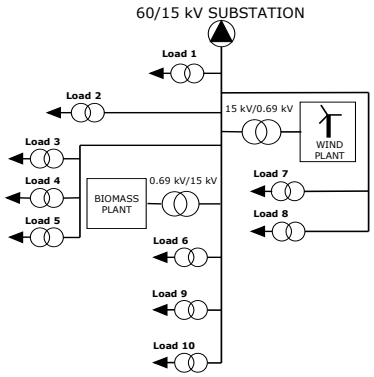

Fig. 3. Typical distribution network

The load active power demand, P_{load}, is 1.83 MW and the load reactive power demand, Q_{load}, is 0.37 MVAr, at the nominal voltage of 15 kV.

The biomass energy plant considered on this paper consists on a two pole synchronous generator [4], [5], with an IEEE Type I DC exciter [6]. The primary energy source for the biomass energy plant is the residual forest biomass. The steam governing system is of digital electro-hydraulic technology, by Westinghouse [7]. The prime mover is a non-reheat steam turbine, which can be described by a first order model. Details are available in Appendix.

The wind energy plant considered on this paper consists on a fixed-speed pitch controlled wind turbine, connected to a conventional induction generator [8 – 10]. The wind power models considered in this work, for simulation purposes, are based on a generic model for stability studies on wind turbine systems, which is fully described in [8]. A capacitor bank, for power factor correction purposes, is included on the plant. Details are also available in Appendix.

B. No-action of the Adaptive DG Active Power Prediction Algorithm

The following simulations refer to an hour of a generic day, on the distribution network shown on Fig. 3. It is assumed to be known the wind power forecast for the look-ahead time of one hour. This wind power forecast is assumed to be given with 10% error margin based on the wind energy plant's installed capacity. Thus, the predicted wind power profile for the next hour, P_{wind} (t), is shown on Fig. 4.

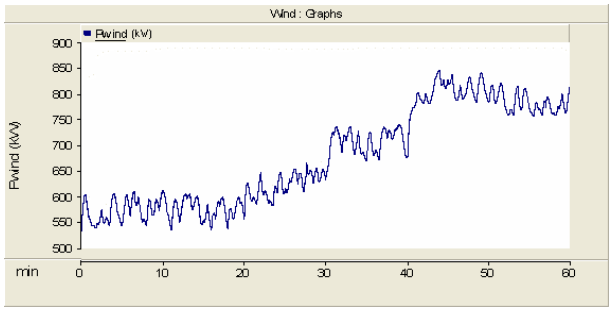

Fig. 4. Predicted wind power profile for the next hour P_{wind} (t)

Figs. 5 and 6 show, in the hour considered, the active power required to the primary distribution substation, $P_{substation}(t)$, shown on Fig. 3 ("60/15 kV Substation"). In both Figs. 5 and 6, the biomass energy plant is set to produce at full-load and the wind energy plant is set to track the maximum wind active power utilization. However, Fig. 5 shows $P_{substation}(t)$ being the wind power profile in the hour 5% higher than the wind power forecast $P_{wind}(t)$, i.e., $1.05P_{wind}(t)$. Fig. 6 shows $P_{substation}(t)$ being the wind power profile in the hour 5% lower than the wind power forecast $P_{wind}(t)$, i.e., $0.95P_{wind}(t)$. $P_{substation}(t)$ is given in kW.

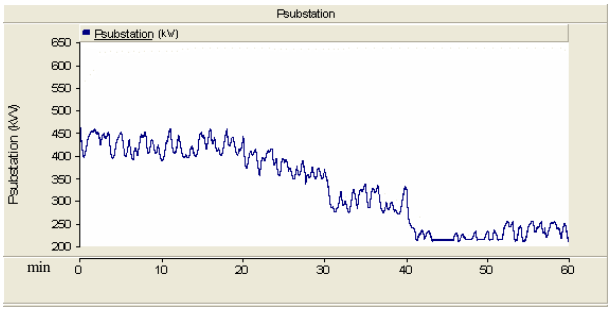

Fig. 5. $P_{substation}(t)$ in the hour considered, with $1.05P_{wind}(t)$

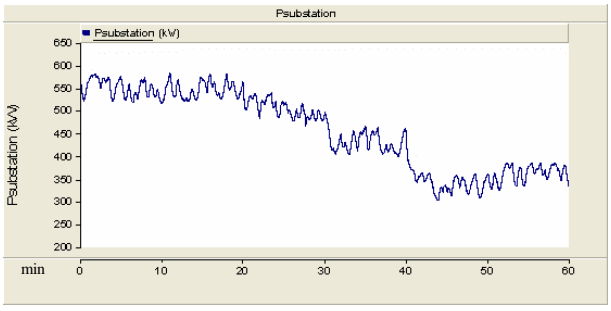

Fig. 6. $P_{substation}(t)$ in the hour considered, with $0.95P_{wind}(t)$

Table I presents statistical information on the energy delivered in the hour considered by the DG's, at the conditions described for Figs. 5 and 6.

TABLE I
$P_{biomass}(t)+P_{wind\_actual}(t)$ IN THE HOUR CONSIDERED

$P_{biomass}(t)+P_{wind\_actual}(t)$ With $1.05P_{wind}(t)$		$P_{biomass}(t)+P_{wind\_actual}(t)$ With $0.95P_{wind}(t)$	
Mean Value for the Hour (kWh)		*Mean Value for the Hour (kWh)*	
1584,1671		1445,9323	
Average Absolute Deviation From the Mean Value for the Hour		*Average Absolute Deviation From the Mean Value for the Hour*	
(kWh)	*(%)*	*(kWh)*	*(%)*
85,9764	5,9465	85,7545	5,4132
Maximum Deviation from the Mean Value for the Hour		*Maximum Deviation from the Mean Value for the Hour*	
(kWh)	*(%)*	*(kWh)*	*(%)*
168,8696	11,6789	142,6379	9,0039

Table II and Table III present the same data shown on Table I, but now considering the wind power forecast's error margin 5% and 15% of the wind energy plant's installed capacity, respectively.

TABLE II
$P_{biomass}(t)+P_{wind\_actual}(t)$ IN THE HOUR CONSIDERED

$P_{biomass}(t)+P_{wind\_actual}(t)$ With $1.025P_{wind}(t)$		$P_{biomass}(t)+P_{wind\_actual}(t)$ With $0.975P_{wind}(t)$	
Mean Value for the Hour (kWh)		*Mean Value for the Hour (kWh)*	
1551,8870		1481,9227	
Average Absolute Deviation From the Mean Value for the Hour		*Average Absolute Deviation From the Mean Value for the Hour*	
(kWh)	*(%)*	*(kWh)*	*(%)*
87,5245	5,6399	86,8815	5,8628
Maximum Deviation from the Mean Value for the Hour		*Maximum Deviation from the Mean Value for the Hour*	
(kWh)	*(%)*	*(kWh)*	*(%)*
169,5369	10,9246	160,7971	10,8506

TABLE III
$P_{biomass}(t)+P_{wind\_actual}(t)$ IN THE HOUR CONSIDERED

$P_{biomass}(t)+P_{wind\_actual}(t)$ With $1.075P_{wind}(t)$		$P_{biomass}(t)+P_{wind\_actual}(t)$ With $0.925P_{wind}(t)$	
Mean Value for the Hour (kWh)		*Mean Value for the Hour (kWh)*	
1611,2140		1409,4481	
Average Absolute Deviation From the Mean Value for the Hour		*Average Absolute Deviation From the Mean Value for the Hour*	
(kWh)	*(%)*	*(kWh)*	*(%)*
79,2696	4,9199	84,6985	6,0093
Maximum Deviation from the Mean Value for the Hour		*Maximum Deviation from the Mean Value for the Hour*	
(kWh)	*(%)*	*(kWh)*	*(%)*
136,6803	8,4831	121,2003	8,5991

C. Adaptive DG Active Power Prediction Algorithm Performance

The following simulations also refer to an hour of a generic day, on the distribution network shown on Fig. 3. It is assumed the predicted wind power profile for the next hour is $P_{wind}(t)$, which is given in Fig. 4.

With the predicted wind power profile shown on Fig. 4, it is calculated the predicted lowest wind energy plant's active power output, P_{wind_min}, for the next hour.

Figs. 7 and 8 show $P_{substation}(t)$ with the use of the Adaptive DG Active Power Prediction Algorithm, in the hour considered. Fig. 7 shows $P_{substation}(t)$, being the wind power profile in the hour 5% higher than the wind power forecast $P_{wind}(t)$, i.e., $1.05P_{wind}(t)$. Fig. 8 shows $P_{substation}(t)$, being the wind power profile in the hour 5% lower than the wind power forecast $P_{wind}(t)$, i.e., $0.95P_{wind}(t)$. $P_{substation}(t)$ is given in kW.

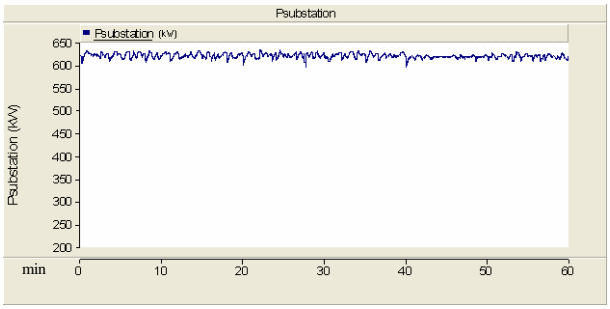

Fig. 7. $P_{substation}(t)$ with the Adaptive DG Active Power Prediction Algorithm in the hour considered, with $1.05P_{wind}(t)$

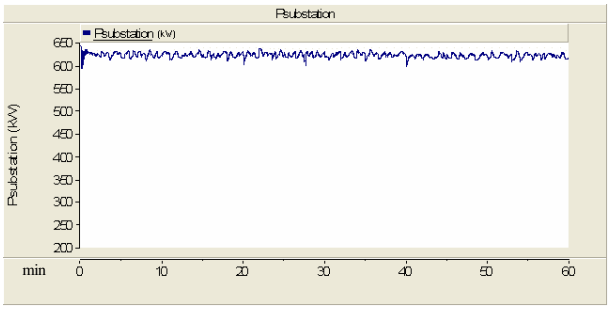

Fig. 8. $P_{substation}$ (t) with the Adaptive DG Active Power Prediction Algorithm in the hour considered, with $0.95P_{wind}$ (t)

Table IV presents statistical information on the energy delivered in the hour considered by the DG's, at the conditions described for Figs. 7 and 8, i.e., using the Adaptive DG Active Power Prediction Algorithm.

TABLE IV
$P_{biomass}$ (t)+ P_{wind_actual} (t) IN THE HOUR CONSIDERED, WITH THE ADAPTIVE DG ACTIVE POWER PREDICTION ALGORITHM

$P_{biomass}$ (t)+ P_{wind_actual} (t) With $1.05P_{wind}$ (t)		$P_{biomass}$ (t)+ P_{wind_actual} (t) With $0.95P_{wind}$ (t)	
Mean Value for the Hour (kWh)		*Mean Value for the Hour (kWh)*	
1306,4581		1307,8956	
Average Absolute Deviation From the Mean Value for the Hour		*Average Absolute Deviation From the Mean Value for the Hour*	
(kWh)	*(%)*	*(kWh)*	*(%)*
4,1301	0,3161	3,6622	0,2800
Maximum Deviation from the Mean Value for the Hour		*Maximum Deviation from the Mean Value for the Hour*	
(kWh)	*(%)*	*(kWh)*	*(%)*
23,5052	1,7972	22,5143	1,7233

Table V and Table VI present the same data shown on Table IV, but now considering the wind power forecast's error margin 5% and 15% of the wind energy plant's installed capacity, respectively.

TABLE V
$P_{biomass}$ (t)+ P_{wind_actual} (t) IN THE HOUR CONSIDERED, WITH THE ADAPTIVE DG ACTIVE POWER PREDICTION ALGORITHM

$P_{biomass}$ (t)+ P_{wind_actual} (t) With $1.025P_{wind}$ (t)		$P_{biomass}$ (t)+ P_{wind_actual} (t) With $0.975P_{wind}$ (t)	
Mean Value for the Hour (kWh)		*Mean Value for the Hour (kWh)*	
1320,9522		1321,8899	
Average Absolute Deviation From the Mean Value for the Hour		*Average Absolute Deviation From the Mean Value for the Hour*	
(kWh)	*(%)*	*(kWh)*	*(%)*
4,0381	0,3057	3,9985	0,3025
Maximum Deviation from the Mean Value for the Hour		*Maximum Deviation from the Mean Value for the Hour*	
(kWh)	*(%)*	*(kWh)*	*(%)*
23,8844	1,8081	23,7764	1,7987

TABLE VI
$P_{biomass}$ (t)+ P_{wind_actual} (t) IN THE HOUR CONSIDERED, WITH THE ADAPTIVE DG ACTIVE POWER PREDICTION ALGORITHM

$P_{biomass}$ (t)+ P_{wind_actual} (t) With $1.075P_{wind}$ (t)		$P_{biomass}$ (t)+ P_{wind_actual} (t) With $0.925P_{wind}$ (t)	
Mean Value for the Hour (kWh)		*Mean Value for the Hour (kWh)*	
1252,4582		1255,3076	
Average Absolute Deviation From the Mean Value for the Hour		*Average Absolute Deviation From the Mean Value for the Hour*	
(kWh)	*(%)*	*(kWh)*	*(%)*
3,4098	0,2723	3,8881	0,3097
Maximum Deviation from the Mean Value for the Hour		*Maximum Deviation from the Mean Value for the Hour*	
(kWh)	*(%)*	*(kWh)*	*(%)*
23,7644	1,8974	23,2511	1,8522

IV. DISCUSSION ON THE ADAPTIVE DG ACTIVE POWER PREDICTION ALGORITHM

The aggregation of biomass and wind energy done by the Adaptive DG Active Power Prediction Algorithm, can lead to an increase of secure renewable energy penetration on the distribution networks. The biomass energy's ability of storing and using the feedstocks whenever and wherever needed may represent an extra profit with the use of the Adaptive DG Active Power Prediction Algorithm, as the biomass primary energy can be saved in opposition to wind energy.

The use of the Adaptive DG Active Power Prediction Algorithm in the distribution network shown in Fig. 3, in the hour considered, led to an increased amount of not delivered energy by the DG's comparatively with the case where the adaptive DG active power prediction algorithm is not enabled. This increased not delivered energy varied, in average values, from 154 kWh to 359 kWh whether the wind power profile equaled $0.925P_{wind}$ (t) or $1.075P_{wind}$ (t) (extreme conditions) respectively, where P_{wind} (t) is the predicted wind power profile for the next hour. However, the Adaptive DG Active Power Prediction Algorithm increased the predictability of the delivered energy by the DG's, as it reduced significantly the average absolute deviation from the mean value of the delivered energy by the DG's.

The Adaptive DG Active Power Prediction Algorithm requires communication facilities for the provision of the wind power forecast and the real-time wind energy plant's active power output.

With the increase of secure renewable energy penetration on the distribution networks, the availability and reliability of the renewable sources will be improved. In consequence, network operation and expansion costs can be lowered and, in addiction, the increase of secure renewable energy penetration on distribution networks may lead the DG owners to go on the market. Thus, power systems can potentially accommodate increased levels of intermittent DG as the imbalances between generation and demand will not increase.

ACKNOWLEDGEMENTS

The authors are grateful to Prof. Fernando Lobo Pereira, from Faculty of Engineering of University of Porto, for his support and practical discussions in the conception of this

work.

APPENDIX

Wind Turbine

	value	unit
Rotor Radius	22	m
Blade Angular Speed	1,904	rad/s
Air Density	1,229	kg/m^3
Number of Blades	3	
Gearbox Efficiency	97	%

Steam Turbine

Time Constant	0,2	s

Induction Wind Generator (p.u. values on base of the machine rating)

Rated Power	850	kW
Nominal Voltage	0,69	kV
Stator Resistance	0,008549	p.u.
Stator Reactance	0,09742	p.u.
Rotor Reactance	0,127074	p.u.
Magnetizing Reactance	4,50534	p.u.
Polar Moment of Inertia	0,302	s
Poles	6	
Slip	2.5	%

Synchronous Generator (p.u. values on base of the machine rating)

Rated Power	850	kW
Nominal Voltage	0,69	kV
Armature Resistance	0,0051716	p.u.
Potier Resistance	0,163	p.u.
Unsat. Direct Reactance	1,014	p.u.
Unsat. Quadrature Reactance	0,77	p.u.
Unsat. Direct Transient Reactance	0,314	p.u.
Unsat. Quadrature Transient Reactance	0,228	p.u.
Inertia Constant	2,5	s
Poles	2	

REFERENCES

[1] European Union Directive 2001/77/EC, *On the Promotion of Electricity Produced from Renewable Energy Sources in the Internal Electricity Market*, Official J. European Community, Vol. L283, October 2001.

[2] Ministério da Economia de Portugal, *Decreto-Lei No. 33-A/2005*, Lisbon, Portugal, February 2005.

[3] P. Djapic, C. Ramsay, D. Pudjianto, G. Strbac, J. Mutale, N. Jenkins and R. Allan, *Taking an Active Approach*, IEEE Power and Energy Magazine, Vol. 5, pp. 68-77, July-August 2007.

[4] P. Kundur, *Power System Stability and Control*, ISBN 0-07-035958-X, McGraw-Hill, 1993.

[5] J. Machowski, J.W. Bialek and J.R. Bumby, *Power System Dynamics and Stability*, ISBN 0-471-95643-0, John Wiley & Sons, 1997.

[6] IEEE Power Engineering Society, *IEEE Recommended Practice for Excitation System Models for Power System Stability Studies*, ISBN 0-7381-4786-9, IEEE Std. 421.5, 2006.

[7] Working Group on Prime Mover and Energy Supply Models for System Dynamic Performance Studies, *Dynamic Models for Fossil Fueled Steam Units in Power System Studies*, IEEE Transactions on Power Systems, Vol. 6, No. 2, May 1991.

[8] P. M. Anderson and A. Bose, *Stability Simulation of Wind Turbine Systems*, IEEE Transactions on Power Apparatus and Systems, Vol. PAS-102, No. 12, pp. 3791-3795, December 1983.

[9] B. Fox, D. Flynn, L. Bryans, N. Jenkins, M. O' Malley, R. Watson and D. Milborrow, *Wind Power Integration: Connection and System Operational Aspects*, ISBN 0-8634-1449-4, IET, 2007.

[10] T. Burton, T. Sharpe, N. Jenkins and E. Bossanyi, *Wind Energy Handbook*, ISBN 0-471-48997-2, John Wiley & Sons, 2001.

J. Barros received his Electrical Engineering degree from the University of Porto, Portugal in 2007. J. Barros is currently pursuing the MSc degree in Electrical Engineering at the University of Porto.

H. Leite received his Electrical Engineering degree from the University of Porto, Portugal in 2000 and the PhD degree in Electrical Engineering from The University of Manchester, UK, in 2004. H. Leite joined University of Porto, Portugal, as a Lecturer in 2005. His research interests include Distribution Generation Integration, Electric Power Systems and Power Systems Protection.

J. A. Peças Lopes (M'80–SM'94) received the Electrical Engineering degree (five-year course), the Ph.D. degree in electrical engineering, and the Aggregation degree from the University of Porto, Porto, Portugal, in 1981, 1988, and 1996, respectively.

He is an Associate Professor of aggregation with the Department of Electrical Engineering, Faculty of Engineering, University of Porto. In 1989, he joined the staff of Instituto de Engenharia de Sistemas e Computadores do Porto (INESC) as a Senior Researcher, and he is presently Co-coordinator of the Power Systems Unit of INESC.